AMPHIPHILIC MACROMOLECULE THERAPEUTICS TO MANAGE CARDIOVASCULAR DISEASE

By

DANIEL RAIKEN LEWIS

A dissertation submitted to the

Graduate School - New Brunswick

Rutgers, The State University of New Jersey

in partial fulfillment of the requirements

for the degree of

Doctor of Philosophy

Graduate Program in Chemical and Biochemical Engineering

written under the direction of Prabhas V. Moghe

and approved by

_____

_____

_____

_____

_____

New Brunswick, New Jersey

January 2014

ABSTRACT OF THE DISSERTATION

Amphiphilic macromolecule therapeutics to manage cardiovascular disease

By

DANIEL RAIKEN LEWIS

Dissertation Director:

Prabhas V. Moghe

The hypothesis of this research is that atherosclerosis, the principal pathology underlying vascular occlusive disease, can be targeted and moderated using Amphiphilic Macromolecules (AMs). By mimicking the amphiphilicity and charge distribution of oxidized LDL, AMs can mitigate its downstream consequences by competitively blocking interaction with scavenger receptors. This work evaluated the ability of AM of various chemical compositions and architectures to reduce lipid accumulation in macrophages. Insights from these studies were used in conjunction with 3D molecular descriptors to identify the features of AM with most anti-atherogenic potency. To further develop AM as a viable therapeutic modality, these features were incorporated into kinetically fabricated nanoparticles (NPs) that are non-inflammatory and resist serum binding. An atherosclerotic animal model was established and used to examine the *in vivo* biodistribution and pharmacokinetic profile of systemically circulating AM NPs in addition to their ability to localize to lesions and stabilize plaques. Collectively, these outcomes establish AM as a multimodal nanotherapeutic platform designed to target atherosclerotic lesions and inhibit inflammation and atherogenesis.

This thesis is comprised of three principal research aims: 1) To determine quantitative structure-activity relationships between Amphiphilic Macromolecule architecture and *in vitro* reductions in oxidized LDL uptake and lipid accumulation in macrophages; 2) To develop AM into non-inflammatory serum-stable nanoparticles (AM NPs); 3) To study the *in vivo* dynamics of systemically injected AM NPs and examine their ability to target atherosclerotic lesions and mitigate plaque development.

Acknowledgements

This work is dedicated to my family and friends who have been such tremendous supports throughout my life.

Special thanks to my mother, who has continually advocated and sacrificed so that I could get the best education possible.

Sections of this thesis have been reproduced from the following publications:

- **Lewis DR**, Kamisoglu K, York AW, Moghe PV. *Polymer-based therapeutics: Nanoassemblies and nanoparticles for management of atherosclerosis*. Wiley Interdiscip Rev Nanomed Nanobiotechnol. 2011;3(4):400-420.
- **Lewis DR**, Kholodovych V, Tomasini MD, Abdelhamid D, Petersen LK, Welsh WJ, Uhrich KE and Moghe PV. *In silico design of anti-atherogenic biomaterials*. Biomaterials. 2013;34(32):7950-7959.
- York AW, Zablocki KR, **Lewis DR**, Gu L, Uhrich KE, Prud'homme RK and Moghe PV. *Kinetically assembled nanoparticles of bioactive macromolecules exhibit enhanced stability and cell-targeted biological efficacy*. Adv Mater. 2012;24(6):733-739.

Table of Contents

List of Tables

List of Figures

Chapter 1 - Introduction to atherosclerosis and the use of nanoscale assemblies to manage disease progression

Note: Sections of this chapter have been reproduced from the following publication:

Lewis DR, Kamisoglu K, York AW, Moghe PV. *Polymer-based therapeutics: Nanoassemblies and nanoparticles for management of atherosclerosis*. Wiley Interdiscip Rev Nanomed Nanobiotechnol. 2011;3(4):400-420.

Atherosclerosis

A disease with complex etiology, atherosclerosis results from the progressive long-term combination of atherogenesis, the accumulation of modified lipoproteins within blood vessel walls, along with vascular and systemic inflammatory processes. The management of atherosclerosis is challenged by the localized flare-up of several multipronged signaling interactions between activated monocytes, atherogenic macrophages and inflamed or dysfunctional endothelial cells. Atherosclerosis, resulting from systemic lipid burden, can lead to vascular occlusions including intracranial, coronary and peripheral. This thesis advances a new approach founded on multifocal, targeted therapies that seek to reverse or ameliorate the athero-inflammatory cascade within the vascular intima.

Scope and economic cost

Cardiovascular disease (CVD) is the leading cause of death in the developed world. An estimated 81 million people in the United States (more than one in three) have one or more types of CVDs. According to The American Heart Association, CVD causes nearly 50% of all deaths in westernized countries including over 800,000 American adults a year, with overall yearly costs exceeding US $440 billion [1]. Atherosclerosis, the inflammatory vascular wall disease, serves as a major trigger for coronary artery disease, a critical component of the pathologies underlying CVD. Atherosclerosis is characterized by the build-up of lipid-rich plaques within the blood vessel walls of large arteries, and manifests clinically as myocardial infarction, chronic stable angina, stroke and peripheral arterial disease [2]. Moreover, this chronic condition does not just afflict seniors, rather, atherosclerosis can be evident from 20 years of age, indicating that beyond lifestyle modification, therapy targeted at individuals with sub-acute disease could have revolutionary impact [3]. The American Heart Association (AHA) aims at a 20% reduction in deaths

caused by CVDs through the encouragement of sensible life style changes for the prevention of the disease as well as applying novel technologies for diagnosis and treatment [4].

Cellular and molecular phenomena underlying atherosclerosis

The formation of atherosclerosis is a multi-step combination of **atherogenesis** (accumulation of oxidized low density lipoprotein or LDL within the blood vessel wall) and an ensuing **inflammatory cascade**, leading to later stages of plaque development and thrombosis, which is difficult to reverse. Since atherosclerosis evolves over several years and is comprised of several complex stages, the disease can often go undetected until later stages. As a result, the treatment or management of the disease, especially at early stages, proves difficult. Despite the complexity of this disease, it offers several biomarker targets that can be exploited for directing therapeutic, diagnostic, or hybrid carriers to the lesion sites. A brief summary of the molecular and cellular events underlying atherosclerosis is discussed next.

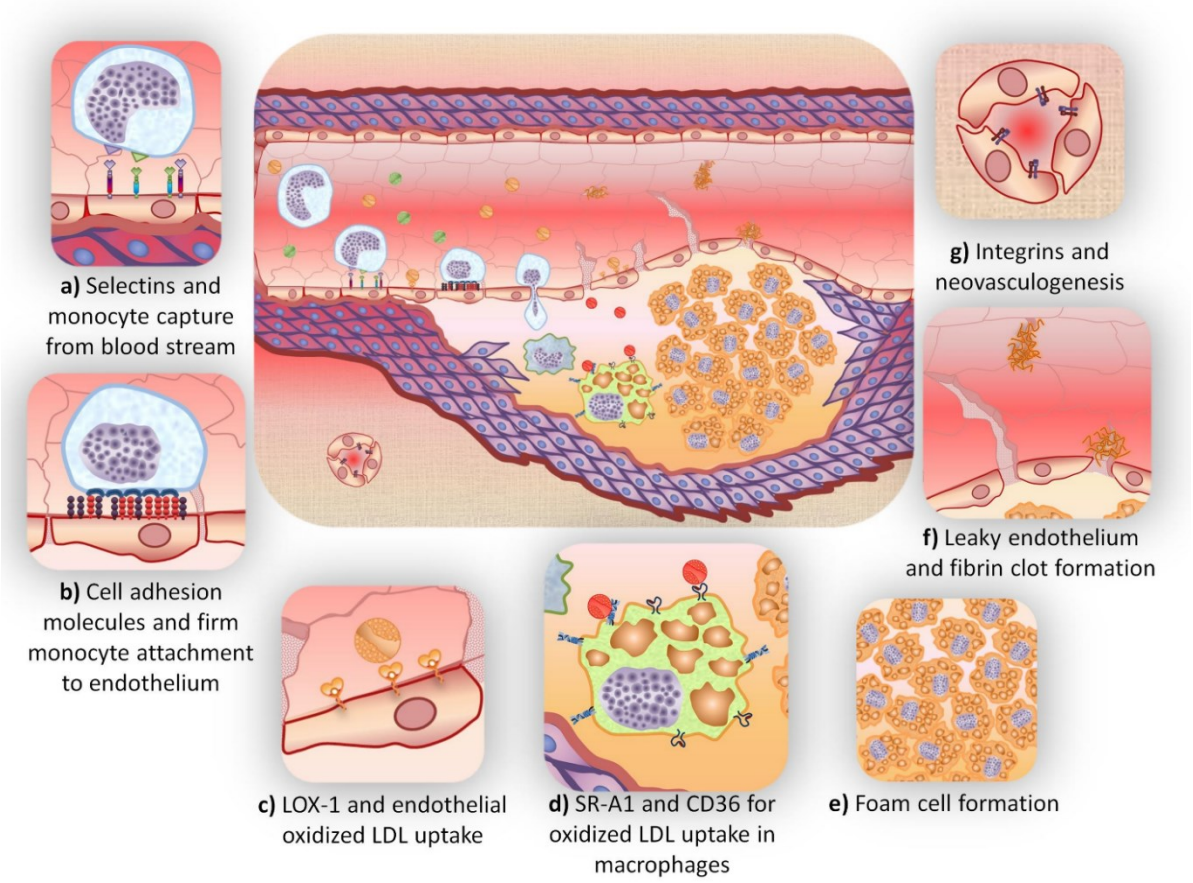

Figure 1.1. Key cellular and molecular interactions that trigger the onset of atherosclerosis. Hyperlipidemia and intimal retention of LDL within the arterial wall initiates a cascade of events leading to LDL oxidation and subsequent inflammatory response. Upregulated cell adhesion molecules [selectins (a) and IgG-type (b)] promote the recruitment of circulating monocytes and increase the permeability of endothelium facilitating more LDL transport to the extravascular space. Endothelial cells and monocytes differentiated into macrophages internalize oxLDL through scavenger receptors [LOX-1 (c), SRA-1, and CD36 (d)]. Unregulated oxLDL uptake by scavenger receptors in macrophages leads to the formation of ‘foam cells' (e). The buildup of oxidized lipids triggers the secretion of a range of cytokines and engenders a more inflammatory phenotype within all vascular cells. Compromised endothelia expose basement membrane to thrombosis, forming fibrin clots (f). Further, to fulfill the increased metabolic demand of the cells

in growing plaques, new blood vessels start to form in the media and extend into the intima (g). As the lesion progresses, the endothelium becomes dysfunctional and smooth muscle cells start to migrate, making the lesion a dynamic mass protruding inside the lumen of the vessel that reduces blood flow to vital organs downstream. From [5].

As shown in **Figure 1.1**, hyperlipidemia (excessive circulating levels of low density lipoproteins, LDL) leads to the sequestration of LDL within the arterial wall and subsequent LDL oxidation by matrix glycosoaminoglycans. Oxidized LDL (oxLDL) causes chronic injury to the endothelial cell layer, which in turn triggers an inflammatory response defined by upregulated cytokine and adhesion molecules that promote monocyte recruitment. Following recruitment, monocytes are transported through the endothelial membrane via diapedesis and differentiate into macrophages, which in turn mediate unregulated uptake of oxLDL via scavenger receptors (SR) leading to the formation of lipid-filled foam cells. Foam cells further express inflammatory cytokines continuing the cycle of inflammation and lipoprotein modification. Following the accumulation of lipid-laden macrophages, smooth muscle cells migrate into the lipid layer. Significant buildup leads to a necrotic lipid core surrounded by a fibrous cap. Degradation of the cap and subsequent rupture can lead to myocardial infarction or stroke. The inflammatory component of the disease is mediated by macrophages, primarily through scavenger receptor interactions with oxLDL [6, 7]. How the disease progresses and manifests symptoms (i.e., heart attack or stable angina) are governed by the critical relationship between atherogenesis and inflammation throughout the lifetime of the disease [8, 9].

As macrophages are crucial to continuing the inflammatory cycle and are responsible for the majority of lipid accumulation, they present an ideal target to arrest disease progression [10]. However, plaque macrophages and their progenitor monocytes are a heterogeneous population and exhibit a range of phenotypes [11]. Macrophages are generally characterized as M1

(classically activated, pro-inflammatory- high ROI, MMP, IL-1β, TNFα) or M2 (alternatively activated, anti-inflammatory - high IL-10) [12, 13]. Recent studies have expanded this distinction to encompass a gradient of expression phenotypes categorized as classically activated (pro-inflammatory), regulatory, and wound healing [14]. The balance of the different macrophage populations determines the pathogenesis of the plaque, its progression and eventual complications [15]. Although macrophages exhibit different phenotypes, they can change expression patterns in response to microenvironmental stimuli *in vivo* [16]. Activated macrophages are thought to be more deleterious to plaque stability and contribute to further monocyte recruitment [2]. Secretion of matrix metalloproteinases (MMP) by activated macrophages can degrade the structural integrity of the fibrous cap, making it more prone to rupture [17, 18]. MCP-1 and IL-8, which are highly expressed in activated macrophages, have been shown to be crucial for recruitment of new monocytes/macrophages to the lesion [19, 20]. It has been hypothesized that by transforming plaque macrophage populations from activated to regulatory, lesion growth and fibrous cap degradation will be retarded [15].

Macrophages cultured *in vitro* from human monocytes can exhibit a range of different expression profiles and phenotypes depending on the differentiation stimulus [11, 16]. Monocytes stimulated with M-CSF typically exhibit the M2 phenotype while monocytes differentiated with GM-CSF have an M1 like phenotype [21]. Gene expression studies have shown similar expression patterns with macrophages differentiated *in vitro* with M-CSF and macrophages isolated from atherosclerotic lesions in carotid arteries, while GM-CSF stimulated macrophages have similar antigen expression to non-diseased arteries [11]. Additionally, activation of the M-CSF receptor is critical for *in vivo* differentiation of monocytes to macrophages [22]. However, with pro or anti-inflammatory stimuli, macrophages can change their gene expression profile [23]. OxLDL was found to prime alternatively activated M2 macrophages for an

enhanced inflammatory response to LPS stimulation [21]. This plasticity presents the possibility of rescuing macrophages from the classically activated phenotype to a regulatory phenotype by blocking pro-inflammatory stimuli [14, 23]. As such, inflamed macrophages present an optimal target for therapeutic approaches [10].

In vivo, interactions of SR with oxLDL are one of the principal inflammatory stimuli that propagate atherogenesis [6, 22]. LDL contains a hydrophobic lipid core of cholesterol, cholesterol esters and triglycerides surrounded by an amphipathic protein monolayer consisting of one ApoB-100 with an overall size of ~22nm [24]. LDL can be extensively modified after deposition in arteries, with the most prevalent modification being oxidation, which results in a poly-anionic charge [25, 26]. This modification causes the LDL to become an inflammatory stimulus; it was shown that LDL upregulates IL-10 in macrophages, whereas oxLDL upregulates IL-12 [27].

SR are defined by their ability to recognize modified lipoproteins and have a wide variety of structures [28]. In macrophages, the SR responsible for the majority (75-90%) of oxLDL uptake are CD36 and SR-A1 [29]. Multiple studies have shown that the role of CD36 is proatherogenic and prothrombogenic [30]. Macrophages from CD36 deficient patients displayed 50% reduced oxLDL uptake and secreted significantly less IL-1β and TNFα in response [31]. When $ApoE^{-/-}$ mice (which normally develop atherosclerotic lesions when fed a Western diet) were crossed with CD36 null mice, the resulting double knockout had significantly smaller lesions than $ApoE^{-/-}$ [32]. CD36 was also shown to be required for the signaling cascade that leads to foam cell formation by activating the tyrosine Src kinases and serine/threonine MAP kinases [33]. Several mechanisms have been found for oxLDL uptake by CD36, including the dynamin-dependent pathway, a lipid raft pathway, and macopinocytosis [34-36]. Internalization of oxLDL exerts dose-dependent inflammatory effects by activation of NF-κB through PI-3K/Akt [37-39].

SR-A1 alone is thought to be responsible for up to 30% of oxLDL uptake by macrophages [29]. However, *in vivo* studies using different pro-atherosclerotic SR-A mouse models have reported contradictory results [40]. ApoE$^{-/-}$ SR-A1$^{-/-}$ double-null mice had decreased lesion size in one study, but did not in another and SR-A1 overexpression did not increase lesion size in LDL-R$^{-/-}$ mice [41-43]. SR-A1 is also involved in host-defense and SR-A1$^{-/-}$ mice are more susceptible to endotoxic shock [44]. Studies examining the mechanism of modified LDL uptake showed that JNK2 is required for SR-A1 mediated uptake and foam cell formation [45]. SR-A1 interaction with modified LDL also activates protein kinase C (PKC) and protein tyrosine kinase (PTK) to produce TNFα and urokinase-type plasminogen activator (uPA), a protease that correlates directly with more severe lesions [46-48].

In addition to serum cholesterol levels, monitoring for systemic inflammation is rapidly becoming standard practice in evaluating for therapeutic intervention in patients at risk of cardiovascular disease. The JUPITER trial found that rosuvatstatin reduced the incidence of major cardiovascular events in healthy, non-hyperlipidemic patients who had elevated C-reactive protein (CRP) [49]. CRP is an inflammatory biomarker that can independently predict vascular events, external to systemic LDL levels [50]. Although useful as a biomarker, CRP does not play a role in progressing the disease, as shown in a study of patients with genetically elevated CRP levels [51].

Cholesterol trafficking is a complex interaction that is controlled by homeostatic mechanisms. Foam cell formation is a result of imbalance of the homeostasis between cholesterol uptake and efflux. Cholesterol is absorbed from the diet or synthesized in the endoplasmic reticulum through a series of ~30 enzymatic reactions, of which HMG CoA reductase is the rate limiting step [52]. Cholesterol is transported through the blood as part of a water soluble lipoprotein, typically by LDL to peripheral tissues from the liver. Once oxLDL has been internalized

by cells, it is hydrolyzed into free cholesterol and fatty acids (FAs) in lysosomes. Free cholesterol is esterified and stored in intracellular lipid droplets, leading to the characteristic “bubbly” appearance of foam cells [53]

Removal of peripheral cholesterol via high density lipoprotein (HDL) is also known as reverse cholesterol transport [52]. HDL carries cholesterol back to the liver from peripheral tissues. In this process, cholesterol free HDL is secreted by the liver and binds free cholesterol resulting from cellular efflux, primarily via ABCA1 or ABCG1/4 on the cell surface [54]. Increasing reverse transport of cholesterol has been hypothesized as a viable way of reducing atherosclerotic plaque buildup, even when there are large amounts of crystalline cholesterol [54]

This range of observed effects opens the possibility of using a broad based approach to inhibit uptake and inflammation signaling caused by oxLDL. By engineering similarly sized nanosystems that can simulate the amphiphilicity and poly-anionic charge of oxLDL, the macrophage scavenger receptors that are key to progressing the atherosclerotic plaque can be targeted. Synthetic polymeric amphiphilic macromolecules that form micelles are of particular interest due to their size and tunability.

Therapeutic approaches to managing atherosclerosis

Conventional pharmacologic and interventional approaches

Even though treatments for clinical manifestations of atherosclerosis are available, they tend to be plagued by several inherent drawbacks. Many pharmaceutical candidates exhibit off target effects and have low efficacy at tolerated doses, which results in theoretically cardioprotective drugs falling short in a clinical setting. An example is that of the PPARγ agonists, which were thought to have anti-inflammatory and anti-atherogenic effects, but have been shown to cause weight gain, edema, fluid retention and increased risk of cardiac failure [55, 56]. Edema is primarily caused by PPARγ off-target action in the kidney nephrons causing increases in sodium and water reabsorption [57].

Of all cholesterol lowering drugs, only statins have demonstrated a reduction in mortality from coronary heart disease [58]. Statins reduce hepatic synthesis of cholesterol through the inhibition of HMG-CoA reductase, which in turn lowers circulating levels of LDL imparting cardioprotective effects. Unfortunately, statins are unable to address localized oxidative damage and inflammation that accompany atherosclerosis [59]. Alternative approaches, discussed below, have been developed to fill this need but have been met with limited success. Anti-cytokine antibodies and cytokine secretion inhibitors can reduce inflammatory responses that progress atherogenesis, but trials have not shown efficacy in reducing clinical endpoints. Additionally, the underlying cause of athero-inflammation is not addressed by these antibodies and inhibitors [60]. Anti-chemokine biologics interfere with macrophage recruitment and inflammation initiation. However, the complex interplay between chemokines and receptors has limited development of such therapeutics [61]. Lipid oxidation is a primary reason for inflammation, but antioxidants have failed clinical trials due to the difficulty in reversing decades of oxidative damage and low

accumulation at lesion sites [59, 62]. Finally, anti-platelet therapies prevent clot formation and aid clot breakup, but only address the latter stages of cardiovascular disease, when clots are more likely to form [63-65].

Liver X Receptor (LXR) agonists have also been thought to be highly cardioprotective [66, 67]. These regulate cholesterol efflux in macrophages by increasing expression of ATP-binding cassette transporter A1 (ABCA1), which exports cholesterol to HDL and Nieman-Pick C (NPC1/NPC2) which traffic cholesterol to the cell membrane [68]. The synthetic LXR ligand GW3965 inhibited the development of atherosclerosis in mice but induced lipogenesis and hypertriglyceridemia [69]. These off target effects and low bioavailability due to hydrophobicity limited clinical development.

Antioxidant therapeutics could play a role in mitigating the pro-atherogenic effects of oxidized lipids and reactive oxygen species (ROS) [70]. Preventing LDL oxidation reduces the progression of atherosclerotic lesions [71]. Vitamin E (VE), specifically its most active form α-tocopherol, has been studied extensively for the ability to reduce adverse cardiovascular outcomes. However, clinical studies have not shown a clear benefit to dietary supplementation and many offer contradictory results [72, 73]. The lack of efficacy may be due to the lack of specific localized delivery and the difference in reaction rates between superoxide and NO or VE [74]. Inhibiting NADPH oxidase may be a preferential mechanism of reducing ROS as the reaction products from tradition antioxidants may themselves be ROS [75].

The widely used interventional standard of care for patients with acute coronary syndrome (ACS) is Percutaneous Coronary Intervention (PCI), which restores blood flow by opening the artery via balloon catheter and preserving the shape with placement of a stent (1.2 million procedures/year). Two primary types of stents are currently approved for clinical use, bare

metal stents (BMS) and drug eluting stents (DES). BMS were effective at keeping arteries open immediately following intervention, but 20-30% of patients developed restenosis [76]. To combat this, drug eluting stents were developed that contained the anti-proliferative drugs sirolomus or paclitaxel [77, 78]. These stents were highly effective at reducing restenosis but experienced poor re-endothelialization, increased thrombosis, while the root cause of proliferation (inflammation) was not addressed [79]. Two 2nd generation DES have been clinically approved using sirolomus analogues with more biocompatible yet permanent coatings [80, 81]. However, there are still many issues to be addressed, indicated by the number of different stent design approaches in development.

Despite the success of PCI, stent designs have failed to target the plaques as the source of inflammation that trigger plaque growth and instability at stented lesion sites. The current generation of stents has significant drawbacks, and DES fail to address the root causes of stent thrombosis and target vessel revascularization failure. Typically, stenting causes endothelial denudation and medial dissection, stimulating an inflammatory response and platelet adhesion. Additionally, the penetration into the lipid core of the plaque releases oxidized lipids. This directly and indirectly stimulates SMC proliferation. Currently approved drug eluting stents are incapable of addressing this inflammation stimulated proliferation and indiscriminately target replicating cells. This prevents re-endothelialization and increases risk for stent thrombosis.

The suboptimal efficacy of the above atherosclerosis therapies demonstrates the need for developing alternative strategies and platforms to deliver a coordinated treatment. Nanoassemblies offer a promising option for developing novel approaches to manage the disease and have potential to transform current atherosclerotic therapies.

Nanomaterials as therapeutics for atherosclerosis

Nanomaterials, specifically molecular assemblies and organic or inorganic nanoparticles, are emerging as attractive candidates for therapeutic applications [82]. Nanosized carriers, in the range of 10 to 200 nm, are suitable for cellular level therapies as they are small enough to interact with receptor targets with high specificity and avidity, while being large enough to transport small molecule drugs and protect them from metabolic deactivation, avoid renal clearance, and provide high surface areas that can be decorated with targeting ligands [83]. In addition, these nanoassemblies can be functionalized to allow tracking their distribution and thus serve as diagnostic agents. Nanotechnology and the design of synthetic nanoassemblies have the opportunity to advance atherosclerosis therapies by 1) increasing systemic circulation time of the carrier, 2) lowering drug cytotoxicity, 3) enhancing drug solubility, 4) reducing the required dosage, 5) combining imaging and therapeutic agents for inspection of disease progression, and 6) increasing specific tissue accumulation through active or passive targeting.

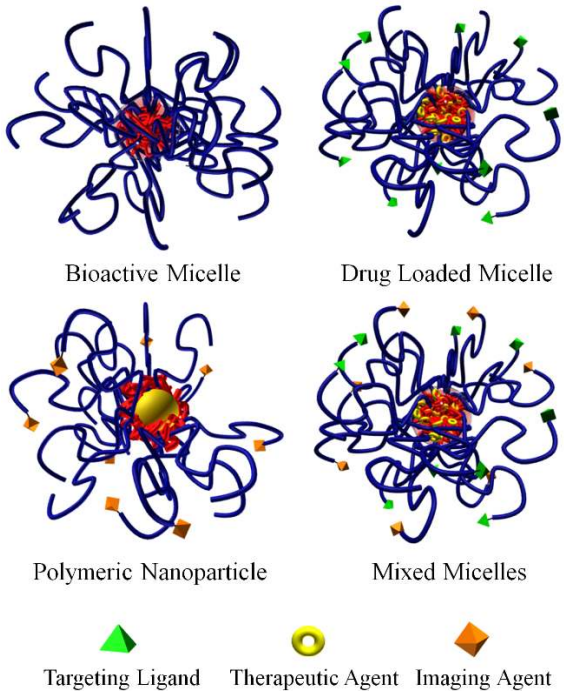

Figure 1.2. Nanoassemblies for the management or diagnosis of atherosclerosis can be classified into four broad categories: (a) Bioactive micelle with inherent therapeutic capabilities; (b) Drug loaded micelle with targeting ligands for cell-specific delivery; (c) Polymer modified nanoparticle (i.e. gold, super paramagnetic iron oxide, quantum dots, etc.) for imaging applications; (d) Mixed micelles with both therapeutic and diagnostic capabilities. Blue - hydrophilic polymer and red - hydrophobic polymer or lipid. From [5].

Molecular assemblies or nanoparticles are typically metal-, polymer- or lipid-based or a combination thereof. Several formulation methods have been employed to design such nanoassemblies. These include ligand exchange with inorganic nanoparticles with polymers or lipids, in situ reduction of metal salts in the presence of a steric stabilizer (i.e., ligands or polymer),[82, 84, 85] surface modification through non- or covalent linkages,[82, 86, 87] mini-emulsions,[83, 88] nanoprecipitation into a non-solvent,[89-91] as well as self-assembly of amphiphilic small molecules, polymers or lipids. Micelles are composed of amphiphilic molecules that self-assemble due to the energy minimization associated with hydrophobic sequestration. The modular nature of micelles allows individual amphiphilic molecules (unimers) with distinct functionalities to be assembled to address several challenges that currently plague conventional delivery methods. These challenges include, but are not limited to, poor therapeutic efficacy of tolerated dosages, adverse and unwanted side effects, lack of tissue or cell specific delivery, uncontrolled drug release, rapid drug clearance from circulation, and metabolic inactivation. The formulation of multifunctional micelles with targeting, imaging and therapeutic features is made possible by the wide range of available compositions, which in turn allows tailoring of micelle properties and/or parameters. Furthermore, the core of micelles can be exploited to solubilize hydrophobic drugs. Inorganic nanoparticle cores, necessary for *in vivo* imaging, can also be engineered by either reacting or adsorbing unimers to the particle surface. The range of molecular compositions and facile modifications to the unimer structure has made molecular assembly of polymer therapeutics a versatile platform for elucidating, benchmarking, and developing new classes of therapies and diagnostics for atherosclerosis.

The design of micellar systems is often motivated by the need to modify the pharmacokinetics and pharmacodynamics of established drugs. Optimal performance can be achieved if the therapeutic agent can be directed to a specific site requiring therapy, through

either passive or active targeting, thus reducing dose concentration and frequency. The *in vivo* performance of micellar systems is controlled by numerous factors including pathophysiological and physiochemical interactions that depend on the size distribution, shape, density, deformability, and surface properties [92]. These properties influence how the nanoassembly may flow throughout the circulatory system in addition to determining the interactions with serum proteins and cells [93]. Unfortunately, due to the complex, dynamic nature of both the nanoassembly, pharmacokinetic profiles typically cannot be represented by straightforward models.

The circulation time and tissue distribution of nanosized systems can be affected by biological effects such as phagocytotic/endocytotic recognition and ingestion, immune responsiveness, and vascular escape routes [94]. Typically, polymeric micelles exhibit slower clearance rates than solid nanoparticles due to the flexibility of the hydrophilic corona that inhibits agglomeration and protein binding [95]. However, the high sensitivity of the complement system can result in different levels of clearance for similar formulations. If the particle surface presented at the blood-particle interface is poorly designed and exhibits properties that promote plasma protein associations (i.e. opsonization) then low therapeutic efficacy will result. These binding proteins include immunoglobulins, components of the complement system, fibronectin, C-reactive protein (CRP) and the von Willebrand factor. The micelle characteristics (i.e., conjugated elements, size, steric stability), concentration, and circulation time collectively determine the degree of protein-micelle interactions [96]. These interactions play a crucial role in determining if the micelle will be rapidly removed via the mononuclear phagocyte system (MPS) or remain in circulation. Macrophages concentrated in the liver sinuses recognize and remove protein coated materials from circulation, which has clear implications on the pharmacokinetics of the system. Furthermore, if not properly protected, protein adsorption to nanoassemblies

supports *in situ* aggregation where the resulting agglomerates can become lodged in capillary beds.

Several design characteristics of polymeric micelles, as mentioned previously and detailed later, need to be considered if effective therapeutic carriers for CVDs are to be developed. One such criterion, which can dictate the rate of opsonization, is the net surface charge of the assembly. Anionic particles are usually cleared via the classical complement pathway, whereas cationically charged particles activate the alternative complement system and are subsequently cleared. In contrast, zwitterionic or neutral particles display longer circulation time and are most likely cleared via CRP binding. Although it is simple in theory to design particles that will avoid rapid MPS clearance, developing a system that is able to direct the therapy to a specific tissue/cell type is more complex.

Most delivery vehicles have been designed to focus on ways to prevent associations with blood and plasma proteins. Opsonization effects can be controlled through surface modifications, such as providing the particle with a hydrophilic corona. This coronal layer imparts steric stabilization to the micelle and thus inhibits protein adsorption by interfering with the binding of macrophage complement receptors. Masking a particle's cargo requires a simple conjugation, but the amount and length of polymer chain attached can significantly alter the *in vivo* efficacy [97]. Studies utilizing a library of various particle shapes and sizes have provided guidelines for designing delivery systems that can either enhance or avoid macrophage binding [98].

Characteristics and design criteria for polymeric micelles

Although several types of supramolecular assemblies have been utilized for the treatment and detection of various pathologies,[99-101] including atherosclerosis,[102-108] perhaps the most promising nanoassemblies are those based on synthetic polymers. Due to the wide variety

and various properties of (co)polymers, as well as the diversity and flexibility of available polymer chemistries,[109-118] multimodal nanomaterials with requisites for treating, detecting, and/or targeting cardiovascular diseases can be potentially realized. Of particular interest, is the functionalization of polymers with hydrophilic-hydrophobic motifs that promote self-assembly when introduced into an aqueous environment. The facile nature of incorporating reactive moieties to either the polymer chain ends or side chains is especially advantageous for realizing biorelevant conjugates for targeted delivery therapies or diagnostics. Polymeric architectures suited to drug or gene delivery include functional homo- or copolymers, di- or triblock, graft and star copolymers, as well as "dendrimers". Another current area of high interest, not only for atherosclerosis but other CVDs, is the use of polymer modified inorganic nanoparticles for developing novel diagnostic or imaging technologies. For more details the reader is directed to recent reviews by Broz *et al* [102]. and Fayad and coworkers [103, 104].

Since the onset and progression of atherosclerosis are consistent with the cellular uptake of natural and/or modified (i.e., oxidized) LDL,[119, 120] polymeric biomaterials for cardiovascular therapies have been designed to emulate these naturally occurring lipophilic assemblies or inhibit cellular uptake of modified LDL [102, 105, 107, 108, 121-127]. Amphiphilic polymers having the appropriate hydrophilic-hydrophobic balance can self-assemble just as small molecule amphiphiles above the critical micelle concentration (CMC) or critical aggregation concentration (CAC) [128-132]. The most common polymeric assembled structures reported are micelles, but other assemblies, including worm-like micelles and vesicles, are possible through variation of the hydrophobic to hydrophilic mass balance [129, 130, 133]. Amphiphilic polymers can be prepared through the incorporation of both hydrophobic and hydrophilic monomers in either a random or di-/triblock architecture. The latter is more widespread, whereas the former has been used to form unimolecular micelles under dilute solution [134]. The hydrophilic versus hydrophobic block

lengths (i.e. number of repeat units) or weight fractions can determine the nature of supramolecular structure formed; therefore, careful consideration should be given to this structural feature prior to polymer design. For example, tuning the length or incorporating branching of hydrophilic or hydrophobic functionalities not only dictates the assembled structure (e.g., micelle, vesicle, cylindrical micelles), but also the hydrodynamic size and steric stability of the micelle. A reduction in hydrophilic moieties may lead to unwanted aggregation and eventual precipitation, while too many may yield thermodynamically unstable assemblies due to amplified hydrophilicity, thus causing dissolution. In addition to block length, architecture and composition, other polymer characteristics to consider, in regards to developing an atherosclerosis therapy, include net ionic charge, charge type, charge and reactive functionality placement, stereochemistry, and available chemistries, all the while maintaining biocompatibility.

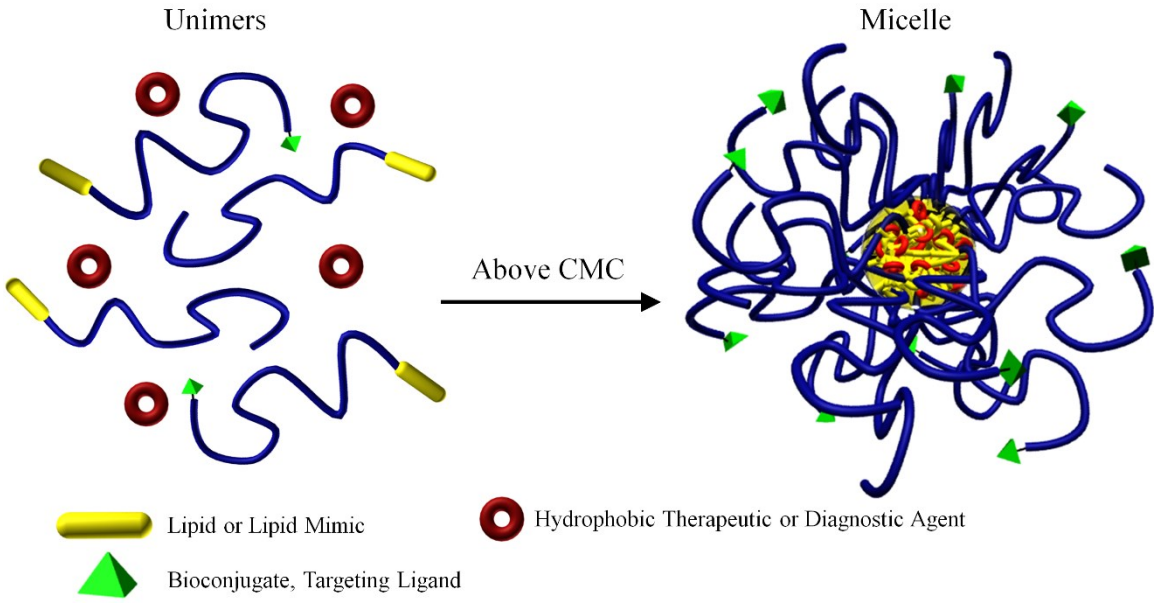

Figure 1.3. Unimer to micelle transition above the critical micelle concentration (CMC) in the presence of a therapeutic or diagnostic agent. Blue represents hydrophilic polymer. From [5]

If carefully designed, polymeric micelles or other polymer based biomaterials, used for therapeutic or diagnostic delivery, have several inherent strengths. These include 1) facile

encapsulation of aqueous insoluble therapeutics and contrast agents in the hydrophobic core, 2) retarded dissolution or enhanced thermodynamic stability in comparison to small molecular amphiphiles due to depressed CMC values (< 10^{-5} M versus ~ 10^{-3} M)[128, 131, 135, 136], 3) coronal steric stabilization that prevents inter-micellar bridging and unwanted associations with blood opsonins, thus circumventing premature circulatory clearance by the MPS,[112, 137, 138] and 4) the formation of nanosized assemblies (10-200 nm) that evade renal clearance and increase circulation half-life. In addition to these inherent strengths, the inclusion of amphiphilic polymers decorated with targeting ligands can be employed to direct the micellar assembly, along with its cargo, to a diseased site. Furthermore, in principle, the release rate of the encapsulated pharmaceutics can be further controlled by integrating reactive sites along the polymer backbone that are cross-linked following micellar assembly (i.e. shell cross-linked micelles) [117, 139-141].

Given the numerous reports and variants of (co)polymers utilized for micellar assemblies, only the essential polymeric features and notable structures are mentioned. For more detailed reports, the reader is referred to several reviews that discuss not only the polymeric structure required for micellar assemblies, but also recent advances made in stimuli-responsive block copolymers and shell cross-linked micelles with therapeutic delivery applications in mind [117, 128, 131, 134, 135, 137, 141, 142]. A wide range of hydrophilic polymers are suitable when designing amphiphilic macromolecules, but the most commonly employed are poly(ethylene glycol) (PEG) or poly(ethylene oxide) (PEO) and poly(N-(2-hydroxypropyl)methacrylamide) (PHPMA). It should be noted that PEG and PEO have identical repeat structures and are named according to polymerization method, condensation and ring-opening, respectively. The popularity of these water-soluble polymers is undoubtedly a result of the commercial availability of monofunctional or homo- and heterobifunctional derivatives, cytocompatibility, regulatory

approval, facile conjugation to biorelevant molecules, poor protein adsorptivity, and widespread knowledge of solution behavior *in vitro* as well as *in vivo*.

An important component of unimer design for micellar assembly is the chain extension of hydrophilic polymers with hydrophobic monomers or coupling to other hydrophobic motifs. Commonly studied hydrophobic macromolecules exploited for synthesizing block copolymers include, but are not limited to, poly(styrene), poly(meth)acrylates, poly(lactic acid), poly(butadiene), poly(propylene oxide) and poly(caprolactone) [132]. Amphiphilicty can also be established through the direct coupling of hydrophobes to hydrophilic polymers. For example, the laboratories of Moghe and Uhrich *et al* [105, 108, 126, 127, 143, 144], have synthesized several derivatives of PEG-hydrophobe constructs through the alkylation of mucic acid followed by PEGylation. The resulting material was able to micellize and inhibit uptake of oxLDL, which is known to exacerbate atherogenesis. Structural features for this system are displayed and discussed in the *Amphiphilic Macromolecules* section below. Micellization for hydrophilic-*block*-hydrophobic copolymers or other amphiphiles can be induced by either first dissolving the macromolecule in an organic solvent (i.e. THF, DMF, DMSO, etc.), conducive for both the hydrophilic and hydrophobic moieties, followed by dialysis against water or direct dissolution of the amphiphile into water, which promotes self-assembly.

In addition to the use of block copolymers there are several literature reports that employ micellar assemblies from polymer-lipid mimics to detect or alleviate the progression of atherosclerosis [102-104, 121, 123-125]. Generally, hydrophilic homopolymers, most notably PEG, are covalently attached to naturally occurring phospholipids, such as phosphatidylethanolamine (PE), 1,2-distearoyl-sn-glycero-3-phosphoethanolamine (DSPE) and phosphatidylcholines, or other synthetically derived lipid-mimic compounds. Just as hydrophilic-*block*-hydrophobic copolymers, polymer-lipid mimics can micellize above a CMC, solubilize

hydrophobic motifs, and be decorated with ligands for targeted therapeutic/diagnostic delivery applications (Figure 1.3). For example, Fayad and coworkers,[121, 145, 146]. in addition to other laboratories,[125] have mixed PEGylated-DSPE in conjunction with other lipid-targeting ligand and/or lipid-diagnostic/therapeutic agent conjugates to construct multimodal micelles for imaging and treating atherosclerosis. Additional highlights of these research works will be elaborated upon in subsequent sections. An alternate strategy to those discussed above would be the use of hydrophilic-*block*-stimuli responsive copolymers where one block changes hydrophilicity based on a specific stimulus (i.e. acid/base, salt or temperature) [117, 141, 147, 148]. This method provides self-assembly and reversibility in an aqueous environment allowing the transition between unimers to micelles simply by introducing and removing an external stimulus. This approach offers opportunities to design novel micellar configurations for site selective efficacy in atherosclerotic lesions.

Biological targets for management of atherosclerosis

The management of atherosclerosis is challenged by several biological barriers. Efficient targeting strategies are critically required since nonspecific nanosystems can be readily cleared by the body's inherent filters (i.e., liver, lymph nodes, and kidneys) or invoke adverse side effects systemically. Site-specific delivery through the conjugation of ligands provides routes to bypass problems associated with traditional therapeutic approaches. Knowledge of atherosclerotic markers and attachment of complementary ligands to the nanocarrier system can guide and concentrate the therapeutic agent at the site of action.

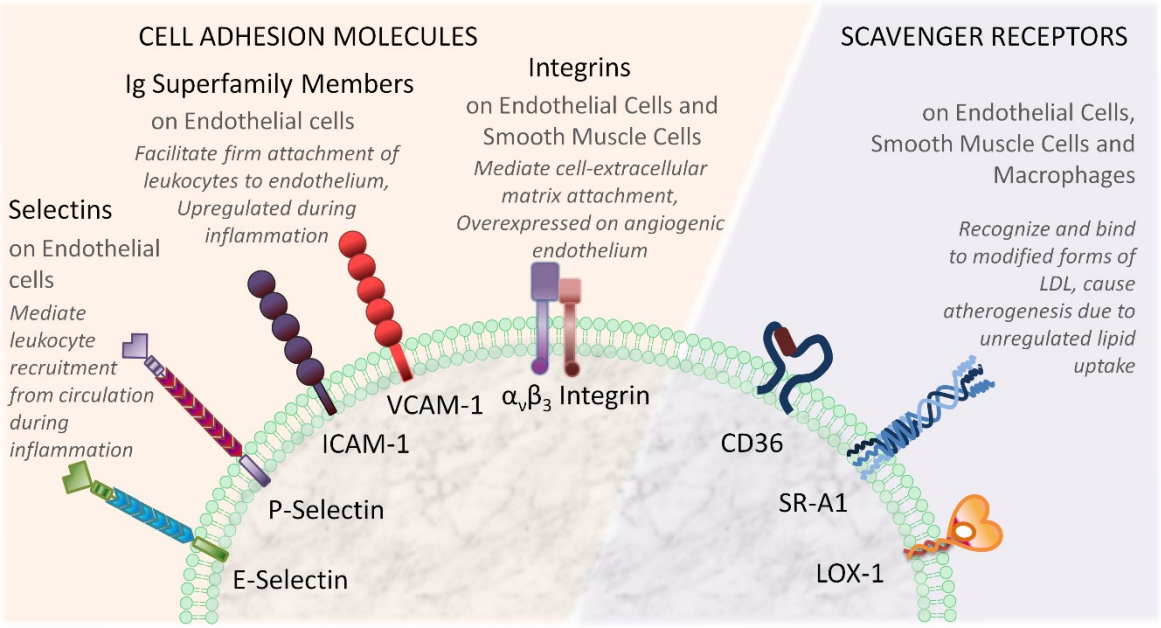

Figure 1.4. Targetable cell-surface receptors for diagnostic and therapeutic applications of atherosclerosis. Scavenger receptors in addition to ICAM-1 and VCAM-1 are of specific interest. From [5]

Propagating lesions in atherosclerosis leads to neovasculogenesis similar to that seen in cancerous tumor growth. High metabolic activity of the building plaque requires elevated nutrition and oxygen supply to the underlying cells. To fulfill this nutritional need, endothelial cells rapidly proliferate and form atypical blood vessels that are defective and immature. This state changes the dynamics of macromolecular transport to and from the lesion and is known as the EPR effect. Compromised or “leaky” vasculature allows macromolecules or nanoassemblies to pass into the interstitial tissue, while an undeveloped lymphatic drainage system promotes accumulation, and hence a higher local therapeutic concentration [103, 149]. In addition to neovascularization, tissue inflammation causes incessant leukocyte recruitment through the release of proinflammatory cytokines. This condition also increases endothelial permeability and allows for selective delivery of therapeutic carriers in the inflamed area [150]. Balloon angioplasty

of arteries can injure the endothelium and permeabilize it to systemically delivered nanoassemblies via EPR [151].

Polymeric systems that are deficient in intrinsic bioactivity may need to be modified with ligands to confer selectivity and specificity for athero-inflammatory lesions. The vascular endothelium serves as a natural candidate for targeting as it is strategically located between the circulating blood and the growing lesion, in addition to its multiple roles in pathogenesis [152]. At the early stages of the disease, the endothelium alters its cell surface protein expression from basal to proinflammatory, which in turn initiates the recruitment of inflammatory cells from the blood stream to the intima. Ligands that recognize these proinflammatory cell surface proteins may thus serve as appropriate markers for guiding novel diagnostic and therapeutic systems. For example, cell adhesion molecules (CAMs) are of special interest for targeted delivery because of their important roles in leukocyte recruitment and internalizing receptor bound ligands via CAM mediated endocytosis [152, 153].

The intercellular cell adhesion molecule-1 (ICAM-1) is a member of the CAM immunoglobulin superfamily of glycoproteins. ICAM-1 is normally expressed on the luminal side of the endothelium and is significantly (~20-50 fold [154]) upregulated following inflammation. Immunohistochemical analysis of human ex-vivo lesions showed strong ICAM-1 expression in vascular cells comprising the atheroma, thus establishing its role in the progression of the disease [155]. Antibodies [154, 156-159] and small peptide sequences [160-162] derived from endogenous ICAM-1 ligands have been employed for developing targeting strategies to treat inflammatory diseases, including atherosclerosis.

Similar to ICAM-1, vascular cell adhesion molecule (VCAM-1) is also an attractive endothelial cell surface molecule for targeted delivery applications. VCAM-1 is expressed on

endothelial surfaces under pathological conditions but also prior to the onset of visible lesions [163]. Nanoparticles conjugated to VCAM-1 targeting peptide sequences (derived from known ligands of VCAM-1 by phage display) were shown to be effective for imaging the initial progression of the disease in ApoE$^{-/-}$ knock-out mice [164, 165]. Nanosystems decorated with CAM targeted ligands offer an added benefit for atherosclerosis since such ligands can also attenuate the leukocyte-endothelium adhesion and consequently reduce athero-inflammation.

When targeting endothelial surface receptors, it becomes difficult to avoid nanocarrier localization in the pulmonary vasculature and nonspecific clearance by the reticuloendothelial system of the liver. Although low protein adsorption polymers, such as PEG, can be added to the carrier to reduce nonspecific uptake by the liver, avoiding uptake via the lungs proves difficult since the lungs represent 30% of the endothelial surface in the body and receive the entire cardiac output [159]. Therefore, careful evaluation of differential expression of cell surface molecules in other organs is required to avoid off-target accumulation when administering therapies for atherosclerosis.

In addition to endothelial cell surface proteins, macrophage specific scavenger receptors, [121, 123] are potential candidates for the development of targeting ligands. For instance, targeting endothelial (LOX-1) or macrophage (SR-A1 and CD36) scavenger receptors can block the initiation of proinflammatory signaling since these receptors mediate oxLDL uptake and establish the inflammation cascade [166]. LOX-1, an endothelial scavenger receptor, internalizes oxLDL and has been shown to cause endothelial dysfunction leading to further disease progression [167]. Nanocarriers targeting these receptors have utilized the attachment of complementary ligands,[121, 123] similar to other cell surface receptor targeted carriers, as well as utilizing electrostatic charge based interactions [105, 168, 169].

Decorating nanosystems with ligands to lesion targets while limiting unspecific protein adsorption (i.e. through PEGylation) can effectively increase the local concentration of imaging or therapeutic agents at the lesion site. Constituents used for specific targeting purposes include antibodies, peptides and polysaccharides. Antibodies, despite their high specificity and affinity towards their targets, are limited by large hydrodynamic sizes, and undesired immunogenic responses. Alternatively, antibody fragments and the even more effective small peptide sequences offer advantages over antibodies as long as *in vivo* stability is sustained [150]. For example, with the development of phage display technology, the number of small peptide sequences, that are highly selective towards their complementary receptor, has increased rapidly over recent years [170]. This technology offers immense potential to discover and subsequently utilize peptides as targeting ligands in the design of therapeutic carriers.

Table 1.1. Current targeted nanoassemblies for the treatment and/or diagnosis of atherosclerosis. From [5].

Configuration	*Composition*	*Targeting moiety*	*Therapeutic/Diagnostic modality*	*Ref.*
Nanoparticle	CLIO – crosslinked iron oxide	VCAM-1 targeting cyclic peptide CVHSPNKKC	CLIO (crosslinked iron oxide) – MRI image contrast	[164]
Nanoparticle	CLIO – crosslinked iron oxide	VCAM-1 targeting linear peptide VHPKQHR	CLIO – MRI image contrast	[165]
Micelle	PEGylated lipids	Fibrin monoclonal antibody	Gd-DTPA amphiphile – MRI signal enhancement	[171]
Micelle	PEGylated lipids	Peptidomimetic $\alpha_v\beta_3$ integrin antagonist	Gd-DTPA amphiphile – MRI signal enhancement	[172]
Micelle	PEGylated lipids	Peptidomimetic $\alpha_v\beta_3$ integrin antagonist	Fumagillin – antiangiogenic drug Gd-DTPA amphiphile – MRI signal enhancement	[173]
Micelle	PEGylated lipids	Tyrosine – for targeting lipid-rich areas of plaques	Gd-DTPA amphiphile– MRI signal enhancement	[146]
Micelle	PEGylated lipids	Clot binding peptide CREKA	Hirulog – anticoagulant drug	[125]
Polymer vesicle	PMOXA-PDMS-PMOXA	Polyguanylic acid (PolyG) – for targeting SR-A1	Pravastatin – HMG-CoA reductase inhibitor	[122]
Nanoparticle	Graft polymer with PNTBA main chain and PEG side chains	Evans blue analog recognizing endothelium dysfunction	Doxorubicin	[174]
Micelle	PEGylated lipids	SR-A1 antibody	Gd-DTPA amphiphile – MRI signal enhancement	[121]

Micelle	PEGylated lipids	SR-A1 antibody	Gd-DTPA amphiphile – MRI signal enhancement	[123]
Micelle	PEGylated lipids	Annexin A5 – for targeting PS exposed on the membrane of apoptotic cells	Gd-DTPA amphiphile – MRI signal enhancement	[124]
Nanoparticle	MION – monocrytalline iron oxide inside a dextran shell	Dextran – for macrophage targeting (specificly dextran receptor SIGNR1)	MION (monocrytalline iron oxide nanoparticle) – MRI image contrast TPC – photosensitizer for photodynamic therapy	[175]
Nanoparticle	MION – monocrytalline iron oxide inside a dextran shell	Dextran – for macrophage targeting (specifically dextran receptor SIGNR1)	MION (monocrytalline iron oxide nanoparticle) – MRI image contrast Cu^{64}-DTPA – radiotracing in PET-CT imaging	[176]
Micelle	PEGylated lipids	Antibodies for oxidation specific epitopes	Gd-DTPA amphiphile – MRI signal enhancement	[145]
Nanoparticle	PLA-Paclitaxel conjugate inside a lipid-PEGylated lipid combination corona	Collagen-IV targeting peptide KLWVLPK	Paclitaxel conjugated to PLA core – inhibition of vascular smooth muscle proliferation following percutaneous angioplasty	[177]

Micelles for drug delivery

Hydrophobic drugs, proteins and nucleic acids are excellent candidates for micelle encapsulation, conjugation, or electrostatic complexation. Receptor and extracellular matrix targeted polymeric carriers offer the added advantage of delivering an optimal concentration of therapeutics in contrast to other delivery methods. The poor aqueous solubility of numerous drugs often necessitates high dosing, which in turn results in toxicity and off target effects. On the

other hand, while free proteins or nucleic acids are aqueous soluble they are readily inactivated by metabolic degradation or cleared from the circulatory system through opsonization. Micelle encapsulation can negate many of these adverse outcomes by solubilizing, protecting and specifically delivering biologically susceptible therapeutics. The loading efficiency can vary broadly depending on the properties of the polymer, micellar assembly, and the packaged therapeutic agent.

To avoid low entrapment efficiency and allow incorporation of hydrophilic drugs, polymer-drug conjugates utilize covalent linkers, which can be synthesized prior to micellization. Ruoslahti *et al* [125] created a micellar system with polymeric unimers comprised of DSPE-PEG_{2000} and variable head groups that contained either a blood clot binding peptide (CREKA), a fluorophore or the anticoagulant synthetic peptide, hirulog. Hirulog was able to directly inhibit the clotting protein thrombin, even after binding fibrin. The micelles showed strong localization, as indicated through fluorescence techniques, to the shoulders of plaques and were able to exert antithrombin activity.

Drug eluting stents have been used to combat restenosis following angioplasty by incorporating anti-proliferatives that retard smooth muscle cell growth. However, local overdose toxicity can cause damage to the tissue surrounding the stent, while systemically administered drugs suffer from a low percentage of the initial dose reaching the site of action [79]. Several micellar systems have been developed to address these issues. Farokhzad et al. have designed multilayered polymer-lipid nanoparticles with paclitaxel conjugated to the PLA core via hydrolysable ester bonds. (105) The drug-polymer core was surrounded by a PEGylated-lipid/lipid monolayer with targeting peptides specific to collagen IV, a key basement membrane matrix protein within blood vessel walls. *In vivo* studies with balloon injured arteries showed that the targeting peptide enabled spatial distribution of the nanoparticles on the basement membrane

exposed after the percutaneous angioplasty injury. It was also seen that the hydrolysis and slow elution of paclitaxel from the core inhibited the vascular smooth muscle cell proliferation commonly seen after this procedure. As another approach to mitigate the dosage problems following stenting, Joner *et al*. developed a polymer liposome targeted to chondroitin sulfate proteoglycans that encapsulated glucocorticoid prednisolone. This nanoassembly was administered to atherosclerotic rabbits following stent injury. The drug preferentially localized at the injured arteries and was capable of reducing the degree of stenosis relative to control studies, demonstrating the utility of targeted delivery systems [178]. Ikuta *et al.* developed a polymer micelle with encapsulated Evans blue dye and doxorubicin that increased drug delivery to injured porcine aortas [174]. Rather than attaching a specific targeting ligand, some micelle systems have natural affinity to lesion sites, possibly due to increased endothelial permeability after injury. Uwatoku et al. injected untargeed micelle forming doxorubicin-polyaspartic acid-PEG conjugates after single and double balloon injury in rats [151]. Evans blue staining demonstrated increased vascular permeability and the polymer conjugates had much higher delivery compared to free doxorubicin, which resulted in reduced neointimal formation.

Perfluorocarbon nanoassemblies have been employed in several studies that combine imaging with targeted drug delivery in an attempt to mitigate drug toxicity [179]. When the water soluble formulation of the antiangiogenic drug fumagillin was administered at high doses, adverse neurocognitive effects were seen. Therefore, a surfactant emulsion was formulated to effectively deliver fumagillin and iron oxide nanoparticles for MRI [173]. These multifunctional particles enabled the imaging $\alpha_v\beta_3$ integrin expression and concurrent delivery of a hydrophobic drug at 50,000 fold lower concentration than previous studies with oral doses. Fumagillin lowered the expression of $\alpha_v\beta_3$ integrin, a key marker of angiogenic growth of the vasa vasorum. Further

studies with $\alpha_v\beta_3$ fumagillin micelles in conjunction with atorvastatin demonstrated sustained anti-angiogenic behavior over 8 weeks [180]

Polymeric carriers are also favorable as they provide an enhanced circulation half-life in comparison to free drug delivery. Extended circulation times allow the therapeutic agent to be used preferentially due to more infrequent dosing regimens. A polyamidoamine (PAMAM) dendrimer-PEG construct was developed to entrap and deliver low molecular weight heparin (LMWH), a widely used anti-thrombotic [181]. The entrapped LMWH showed significantly higher pulmonary absorption and had ~60% of the bioavailability of subcutaneous heparin. More importantly, the half-life of the dendrimer-LMWH was increased 2.4-fold relative to subcutaneous delivery in saline. This resulted in similar reductions in thrombus weight when dosed at half the frequency of subcutaneous LMWH in a rodent model. While longer circulation half-life is ideal, it is only part of the drug delivery challenge as there also needs to be cell specific delivery of the active.

Nanosystems have also been used to probe the function of composition in interactions with cells and atherosclerotic tissue. Although not directly used for therapies, these have developed mechanisms of the targeting and LDL uptake. Synthetic nanoemulsions with a structure resembling LDL were shown to have distinct fates in atherosclerotic rabbits depending on if they contain free cholesterol or cholesterol esters. Free cholesterol was cleared faster than cholesterol esters in cholesterol fed rabbits, but not healthy ones. This demonstrated the significant differences in cholesterol metabolism [182]. C-reactive protein (CRP) is involved in the aggregation and uptake of oxidized LDL. LDL mimetic polymer lipid coated nanoparticles were used to elucidate mechanisms of CRP binding to curved lipid membranes [183]. Buono *et al.* demonstrated that fluorescent PEGylated nanoparticles that were similarly sized to LDL were able

to model LDL uptake by fluid phase pinocytosis in macrophages. They found that these displayed accumulation in aortic arch atherosclerotic lesions in ApoE$^{-/-}$ mice [184]

Tracking the distribution of polymeric micelles

Many therapeutic systems are designed with a reporter to develop and track their fate [185]. The design flexibility of micelles allows for either direct conjugation of small molecules or as encapsulation and solubilization agents for hydrophobic dyes or particles. Individual imaging methods each have distinct advantages and drawbacks, but they are rarely used alone. For example, Mulder et al created a mixed micelle system that incorporated the MRI contrast agent gadolinium with flourophore or quantum dot labeled monomers [121].

Many different types of micellar formulations have been made using magnetic resonance contrast agents as the reporter molecule [103]. Gadolinium is often used as a MRI contrast agent in micellar systems due to its ability to sharply reduce T1 relaxation times. It is easily conjugated by covalent attachment of a chelator such as DTPA that reduces the inherent toxicity of free gadolinium [186]. Superparamagnetic iron oxide nanoparticles (SPIO) can also be used to image plaques, but amphiphilic surfactants are needed to stabilize the SPIO particles, leading to micelles with the particle at the core. Monocytes and macrophages have high affinity for surfactant stabilized SPIO particles and can result in T2* weighted signal loss at the site of the lesion relative to the blood-pool. Since macrophage uptake can correlate to the rate of lesion growth and its instability, it may be a particularly useful marker [187, 188].

PET and SPECT rely on radioactive isotopes and CT contrast agents rely on iodinated compounds, all of which can be conjugated within micellar systems. Hyafil et al developed an iodinated contrast agent (N1177) that showed preferential uptake by macrophages relative to

traditional contrast agent; however it needed to be solubilized with a polymer surfactant to prevent agglomeration [189].

Quantum dots and organic fluorophores offer the ability to easily visualize localization *ex vivo* or in small animals. While their utility is limited for clinical diagnostic use due to poor tissue penetration of visible light, many micellar systems incorporate a fluorophore for development and characterization. Near infrared (NIR) fluorescent quantum dots can mitigate this problem due to the increased penetration depth of NIR light [190]. Quantum dots can be encapsulated within the micelle core if coated with a hydrophobic surface or covalently conjugated to polymer monomers.

Amphiphilic macromolecules (AM)

Previous work done by this lab has utilized (co)polymers designed to mimic the amphilicity and polyanionic charge distribution seen in oxLDL [191]. The aforementioned amphiphilic macromolecules, first designed for drug delivery applications by Uhrich and coworkers,[143] comprised of a lauroyl modified mucic acid and a 5 kDa PEG chain demonstrated self-assembly behavior in water with a CMC near 10^{-7} M and a hydrodynamic diameter between 15-20 nm. The architecture of these AM allows for selective charge placement through the addition of carboxylic acids or amine functionalities. Moghe and coworkers found that AM containing a single carboxylate anion on the hydrophobic terminus, termed 1cM, yielded micelles that could sequester unmodified LDL and mildly oxLDL, but not highly oxLDL, whereas neutral polymers had no affinity towards either unmodified or oxidized forms LDL [127].

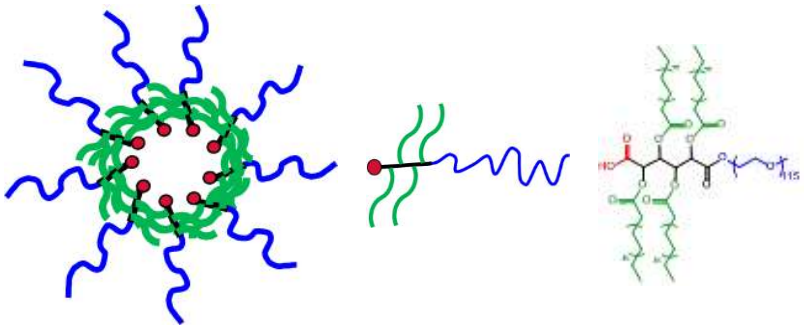

Figure 1.5: 1cM spontaneously self-assembles into micelles above the CMC of 3.2 x 10^{-7} M. At 10^{-4} M, z-average size is ~23 nm with a ζ-potential of -10.4 mV.

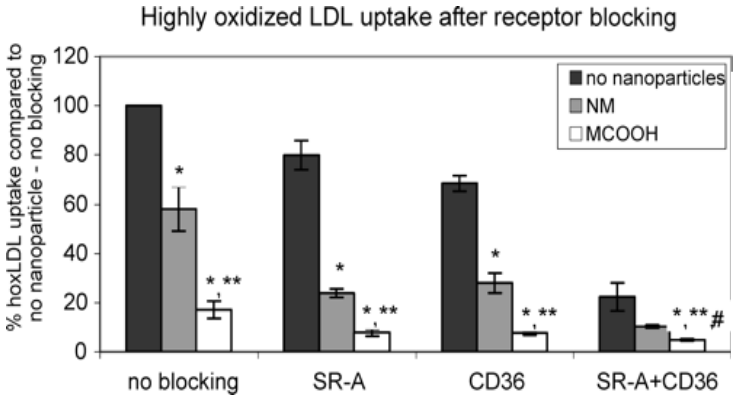

Figure 1.6: oxLDL uptake in IC21 macrophages showing the effects of AM (MCOOH = 1cM) and scavenger receptor blocking. From [119].

In vitro studies indicated high levels of polymer binding, determined via fluorolabeled AM, to IC21 macrophage scavenger receptors in contrast to endothelial and smooth muscle cells [107]. AM binding to the scavenger receptors SR-A1 and CD36 was confirmed utilizing an antibody blocking assay. Upon introducing antibodies complementary to SR-A1 or CD36, the binding affinity of the anionic AM, 1cM, **was reduced. This suggests that the oxLDL binding domain of scavenger receptors have some degree** of specificity towards 1cM. Above the CMC, the AM displayed a dose dependent effect in reducing oxLDL uptake, with the greatest decrease coming from 1cM. Controls using only the hydrophobic or hydrophilic portion of the AM functionalized with a carboxylate had no effect [144].

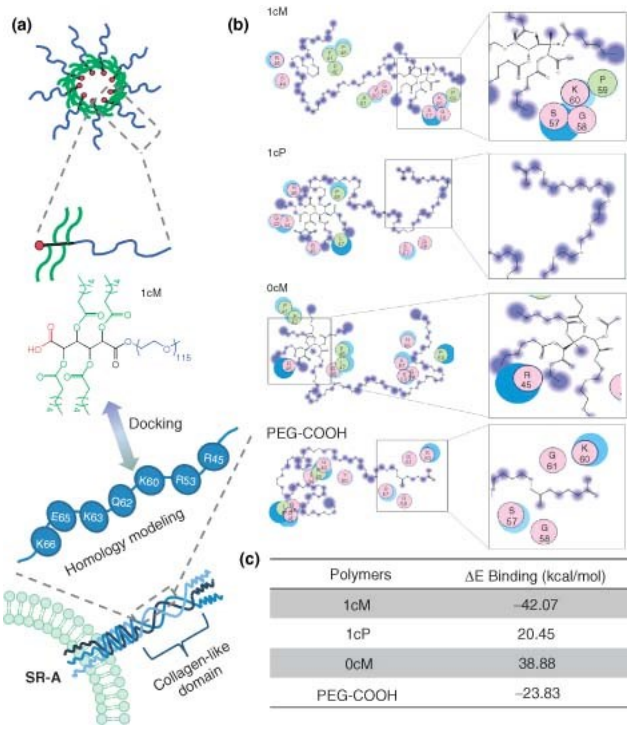

Polymers	ΔE Binding (kcal/mol)
1cM	−42.07
1cP	20.45
0cM	38.88
PEG-COOH	−23.83

Figure 1.7: AM-receptor interactions. A) Idealized representation of the structures and interactions between the amphiphilic polymer and SR-A1 receptor that were utilized in molecular modeling simulations. B) Schematic representation of the docked interactions of SR-A1 collagen-like domain homology model residues (as seen in the colored circles) with 1cM, 1cP, 0cM, and PEG-COOH. Residue characteristics are illustrated through color: purple: polar, green: hydrophobic, blue border: basic, and red border: acidic. C) Binding energy values calculated from polymer models docked to SR-A1 collagen-like domain homology model. From [105].

In a subsequent study, AM with differing charge number, placement, and/or rotational flexibility as well as various PEG lengths or architectures (i.e., linear or branched) were synthesized in order to determine the influence that polymer structure has on oxLDL uptake in macrophages [105, 168]. The highest level of uptake inhibition was seen with 1cM, an AM containing a single carboxylate anion with restricted rotational mobility. The degree of PEG branching and/or additional anionic charges did not appear to have a significant effect on oxLDL uptake.

The importance of minor structural changes for the above studied AM was previously demonstrated through computer modeling by Moghe and coworkers [169]. The use of molecular dynamics docking was utilized to determine the key features required for the most favored

interactions between the AM and the oxLDL binding domain of SR-A1. Molecular simulations on AM with various structural manipulations correlated well with the experimental findings discussed in the previous paragraph. The simulations revealed that the AM-lipid mimic 1cM had the most favorable binding energy to the modeled SR-A1 collagen-like domain. In addition, it was also found that the presence of cationic residues in the SR-A1 binding pocket (specifically Lys60, Lys63 and Lys66) were critical for AM-receptor binding efficacy.

Summary and conclusion

Polymer and polymer-lipid based micellar nanoassemblies are emerging as promising new candidates for the potential management of atherosclerosis. Intelligent design and composition flexibility in conjunction with improved targeting and tunable pharmacokinetic properties are some of the salient attributes of polymeric nanoassemblies. To date, a large portion of the systems developed have used polymers that mimic modified LDL to competitively inhibit oxLDL uptake by receptors involved in lesion lipoprotein uptake and inflammation. As a result, most of these systems employ polymer-lipid or lipid mimic constructs, thus leaving amphiphilic macromolecules relatively unexplored. This offers a unique opportunity to design novel multifunctional nanoassemblies that can rival delivery platforms currently under development.

Thesis overview and hypothesis

Macrophage foam cell formation as a response to scavenger receptor interactions with oxidized lipids aggravates atherosclerotic plaques. Finding an inhibitor for this response would create an important tool for management of the disease. To develop a molecule as a viable therapeutic, it would need to be packaged in a serum stable assembly. Finally, the biodistribution and pharmacokinetic profile would have to be characterized in addition to demonstrating the ability to target developing plaques and exert biological efficacy. In this thesis, I investigated three aims to develop novel Amphiphilic Macromolecules (AMs) as non-inflammatory, serum-stable therapeutics that can ultimately be targeted to the sites of developing atherosclerotic lesions and mitigate plaque development.

- To identify the key determinants of Amphiphilic Macromolecule architectural features that can reduce oxidized lipid uptake and foam cell formation *in vitro* in macrophages
- To develop AM into non-inflammatory serum-stable nanoparticles (AM NPs)
- To study the *in vivo* dynamics of systemically injected AM NPs and examine their ability to target atherosclerotic lesions and mitigate plaque development

Chapter 2 - *In silico* design of anti-atherogenic biomaterials

Note: Sections of this chapter have been reproduced from the following publication:

Lewis DR*, Kholodovych V*, Tomasini MD, Abdelhamid D, Petersen LK, Welsh WJ, Uhrich KE and Moghe PV. *In silico design of anti-atherogenic biomaterials*. Biomaterials. 2013;34(32):7950-7959.

* Equal lead co-authors

Abstract

Atherogenesis, the uncontrolled deposition of modified lipoproteins in inflamed arteries, serves as a focal trigger of cardiovascular disease (CVD). Polymeric biomaterials have been envisioned to counteract atherogenesis based on their ability to repress scavenger mediated uptake of oxidized lipoprotein (oxLDL) in macrophages. Following the conceptualization in our laboratories of a new library of amphiphilic macromolecules (AMs), assembled from sugar backbones, aliphatic chains and poly(ethylene glycol) tails, a more rational approach is necessary to parse the diverse features such as charge, hydrophobicity, sugar composition and stereochemistry. In this study, we advance a novel computational biomaterials design approach to screen and elucidate anti-atherogenic biomaterials with high efficacy. AMs were quantified in terms of not only 1D (molecular formula) and 2D (molecular connectivity) descriptors, but also new 3D (molecular geometry) descriptors of AMs modeled by coarse-grained molecular dynamics (MD) followed by all-atom MD simulations. Quantitative structure-activity relationship (QSAR) models for anti-atherogenic activity were then constructed by screening a total of 1164 descriptors against the corresponding, experimentally measured potency of AM inhibition of oxLDL uptake in human monocyte-derived macrophages. Five key descriptors were identified to provide a strong linear correlation between the predicted and observed anti-atherogenic activity values, and were then used to correctly forecast the efficacy of three newly designed AMs. Thus, a new ligand-based drug design framework was successfully adapted to computationally screen and design biomaterials with cardiovascular therapeutic properties.

Introduction

Inflammation is one of the key components of the atherosclerotic cascade and actively progresses the disease by recruiting more monocytes to the lesion. Continued inflammation can lead to degradation of the fibrous cap and eventual plaque rupture. Oxidized lipids, specifically oxLDL, stimulate inflammation by scavenger receptor mediated activation of pro-inflammatory pathways, which activates transcription and secretion of a wide range of cytokines. Lowering inflammation by competitively blocking this interaction could interrupt monocyte recruitment and stabilize the lesion.

Atherosclerosis is characterized as an inflammatory disease involving macrophage scavenger receptor (SR) interactions with oxidized low-density lipoproteins (oxLDL) in the vascular intima, leading to plaque initiation and growth [192]. The early stages of atherosclerosis include low density lipoproteins (LDL) sequestration and oxidation in arterial walls, followed by monocyte recruitment and differentiation into macrophages, which internalize oxLDL via SR-mediated mechanisms [6, 22]. This progression results in enhanced inflammatory signaling and lipid-laden foam cell formation [7]. The accumulation of foam cells can lead to a lipid filled necrotic core covered by a fibrous cap, which upon rupture can lead to thrombus formation and the clinical endpoints of myocardial infarction or stroke [9].

Conventional therapies are often plagued by the inability to address localized inflammation from preexisting lipid deposits [59]. Therefore, it is necessary to develop therapeutics that can address this inflammation and regulate lipid uptake. As macrophages are crucial to progressing the inflammatory cycle and responsible for the majority of lipid accumulation, they present an ideal target for therapeutics to arrest disease progression [10]. By designing nanosystems that can simulate the size, amphiphilicity and anionic charge of oxLDL, the

macrophage pathways that are key to formation of atherosclerotic plaque can be targeted. Studies from our laboratories have revealed a novel class of amphiphilic macromolecules (AM), which can competitively block oxLDL interaction with scavenger receptors, thereby mitigating downstream consequences [105, 108, 126, 127, 144, 193-195]. Previous work with first generation AM structures qualitatively studied the impact of charge placement and net charge on oxLDL uptake inhibition, but lacked the sophistication to accurately discern the key structural features that govern anti-atherogenic potency [105, 195]. More recent studies indicate that AM chemistries with similar chemical composition can elicit markedly different interactions with oxLDL when imbued with different stereochemistries [193].

However, many current methods of developing therapeutics are not amenable to AM structures (due to limits in feature space) and face several fundamental limitations. High throughput screening has an inherently high cost barrier, is often is plagued by large false negative and false positive rates [196]. Furthermore, structural optimization of early lead compounds by chemical synthesis of analogs is both time- and cost-intensive and typically based on heuristic, rather than rational drug design approaches. Computational drug discovery and optimization approaches, based on quantitative structure-activity relationship (QSAR) principles, offer an efficient and economical alternative for drug development when employed in conjunction with synthetic medicinal chemistry and experimental testing of lead compounds [197-200].

Computational (rational) drug design has made significant contributions to the discovery of new and more efficacious therapeutics. The general strategies employed today are broadly divided into ligand-based and structure-based drug design (LBDD and SBDD, respectively) [201-204]. Assuming that drug action operates through the simple mechanism of drug-target interaction, the option to use one or both strategies in a drug discovery campaign depends on the existing knowledge of biologically active ligands for LBDD and the 3D structure of the target

protein for SBDD. Modern techniques in LBDD rely heavily on *in silico* (virtual) screening of often vast chemical libraries, QSAR modeling, and pharmacophore modeling [108, 205-209]. Likewise, SBDD studies frequently employ virtual screening procedures using a process commonly known as ligand-receptor docking [193, 210-212]. LBDD and SBDD methods remain the subject of intensive research to improve their speed, accuracy, and sophistication [213, 214].

Several different approaches have been previously employed by the authors to construct QSAR models of biological activities of drugs and biomaterials [215-218]. QSAR models associate variations in the chemical structure of the subject materials, as encoded by molecular descriptors, with variations in their corresponding biological activity (e.g., inhibition of oxLDL uptake). QSAR modeling entails two key steps: 1) computing values of an ensemble of molecular descriptors, and 2) creating and validating the regression or classification models by machine learning methods and statistical analysis tools. Molecular descriptors are categorized as 1D (e.g., MW, number of rings), 2D (e.g., electro-topological/connectivity indices) whose values are conformation invariant, or 3D (e.g., dipole moment, surface area, radius of gyration) whose values are conformation dependent.

In the present study, we have taken a LBDD-based approach, using both two- and three-dimensional descriptors, to identify structure-activity relationships between the AMs and inhibition of oxLDL uptake and foam cell formation in human monocyte-derived macrophages (MDM). The QSAR models developed in this study provided the means to predict the biological activities of new AMs, thus, guiding the rational design and optimization of AMs. Of paramount importance for the current AMs, is the inclusion of 3D descriptors which uniquely encodes vital information such as stereochemistry that bears significance in determining biological activity. This research provides a framework to predict the effect of compositional changes on the inhibition of oxLDL uptake and to provide a physicochemical rationale for these biological effects.

Materials and methods

Materials

All chemicals/materials were purchased from Sigma-Aldrich (Milwaukee, WI) or Fisher Scientific (Pittsburgh, PA) and used as received unless otherwise noted. Deionized (DI) water with a resistivity of 18 MΩ·cm is obtained using PicoPure 2 UV Plus (Hydro Service and Supplies - Durham, NC). The following items were purchased from the indicated vendors: RPMI 1640 from ATCC (Manassas, VA), macrophage colony stimulating factor (M-CSF) from PeproTech (Rocky Hill, NJ), 1.077g/cm^3 Ficoll-Paque Premium from GE healthcare (Pittsburgh, PA), FBS and Hoechst 33342 from Life Technologies (Grand Island, NY), 3,3'-dioctadecyloxacarbocyanine (DiO) labeled oxLDL from Kalen Biomedical (Montgomery Village, MD), unlabeled oxidized LDL from Biomedical Technologies Inc. (Stoughton, MA), and human buffy coats from the Blood Center of New Jersey (East Orange, NJ).

AM synthesis and physicochemical property determination

Work performed by Dalia Abdelhamid and the lab of Kathryn Uhrich

AMs were synthesized as previously described [105, 108, 126, 144, 195, 219-221]. The pKa values were estimated based on ionizable functional groups. For example, aliphatic carboxylic acids have a pKa of ~ 3-5, and primary amines ~35. Attachment length was calculated by counting the number of atoms between the functional group responsible for the charge and the attachment of PEG as shown in **Figure 2.1**. In the current study, 17 different AM structures were examined, varying the overall charge, hydrophobicity, sugar structure (linear vs. cyclic) and stereochemistry. **Table 2.1** summarizes the diverse range of their physicochemical properties.

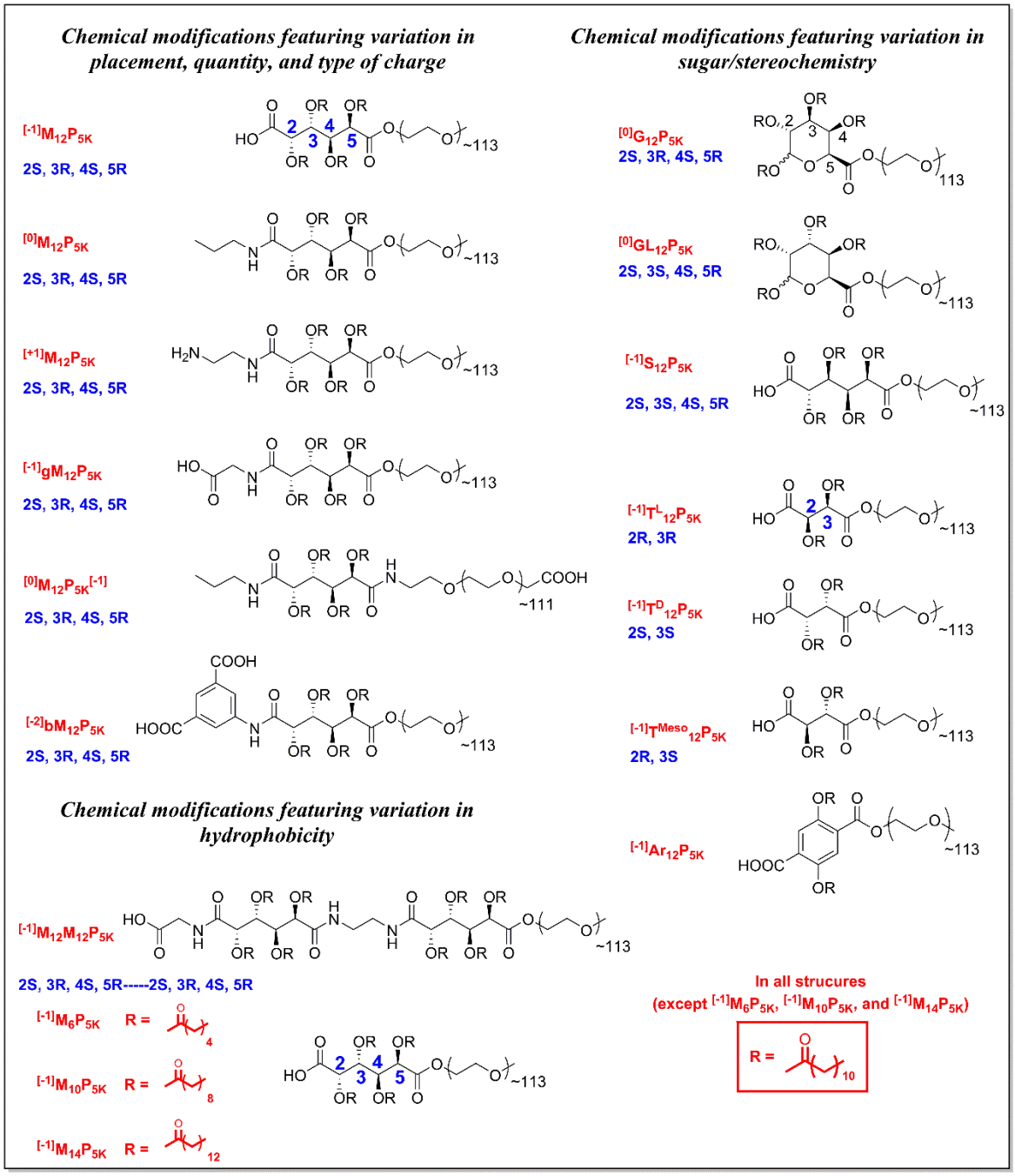

Figure 2.1: Chemical compositions, stereochemistry, and associated abbreviations for AMs in this study. Nomenclature methodology: $^{[charge]}Backbone^{Stereochemistry}{}_{chain\ length}P_{PEG\ length}$. Backbone and functional group abbreviations: M = mucic acid, S = saccharic acid, T = tartaric acid, Ar = 2,5-dihydroxyterephthalic acid, G = D-galacturonic acid, GL = D-glucuronic acid, b = benzene, g = glycine. From [222].

Table 2.1: Physiochemical properties of AM. From [222].

	M_w(kDa)	# hydrophobic chains	Hydrophobic chain length	pKa	Charge source	Charge Number	Backbone structure	Attachment length
$^{[-1]}M_{12}P_{5K}$	5.9	4	12	3-5	COOH	-1	Mucic acid	5
$^{[0]}M_{12}P_{5K}$	5.9	4	12	-		0	Ethylene-Mucic acid	-
$^{[+1]}M_{12}P_{5K}$	5.9	4	12	~35	NH2	1	Ethylene-diamine-Mucic acid	9
$^{[-1]}gM_{12}P_{5K}$	5.4	4	12	3-5	COOH	-1	Glycine-Mucic acid	8
$^{[0]}M_{12}P_{5K}{}^{[-1]}$	5.9	4	12	3-5	COOH	-1 (PEG)	Mucic acid	8
$^{[-2]}bM_{12}P_{5K}$	6.1	4	12	3-5	COOH	-2	Benzene-Mucic acid	10,10
$^{[0]}G_{12}P_{5K}$	5.9	4	12	-		0	Galacturonic Acid	-
$^{[0]}GL_{12}P_{5K}$	5.9	4	12	-		0	Glucuronic Acid	-
$^{[-1]}S_{12}P_{5K}$	5.9	4	12	3-5	COOH	-1	Saccharic Acid	5
$^{[-1]}T^{L}_{12}P_{5K}$	5.4	2	12	3-5	COOH	-1	Tartaric acid	3
$^{[-1]}T^{D}_{12}P_{5K}$	5.4	2	12	3-5	COOH	-1	Tartaric acid	3
$^{[-1]}T^{Meso}_{12}P_{5K}$	5.4	2	12	3-5	COOH	-1	Tartaric acid	3
$^{[-1]}Ar_{12}P_{5K}$	5.5	2	12	3-5	COOH	-1	2,4-Dihydroxyterephthalic Acid	5
$^{[-1]}M_{12}M_{12}P_{5K}$	6.9	8	12	3-5	COOH	-1	Glycine-Mucic-Mucic acid	18
$^{[-1]}M_{6}P_{5K}$	5.6	4	6	3-5	COOH	-1	Mucic acid	5
$^{[-1]}M_{10}P_{5K}$	5.8	4	10	3-5	COOH	-1	Mucic acid	5
$^{[-1]}M_{14}P_{5K}$	6	4	14	3-5	COOH	-1	Mucic acid	5

Isolation and culture of hMDMs

Peripheral blood mononuclear cells (PBMCs) were isolated from human buffy coats by Ficoll-Paque (1.077g/cm^3) density gradient. Red blood cells were lysed with ACK buffer and platelets were removed by centrifugation at 300g for 10 m. PBMCs were transferred to flasks containing RPMI 1640 supplemented with 10% FBS, 1% penicillin/streptomycin. Monocytes were selected from PBMCs by adherence after 24 h and then cultured for 7 days in RPMI 1640 supplemented with 10% FBS, 1% penicillin/streptomycin and 50 ng/mL M-CSF for differentiation into macrophages. After the 7 day culture, the macrophages were trypsinized and scraped from flasks, transferred into well plates at 50,000 cells/cm^2, and treatments administered after 24 h. Differentiation was characterized by phenotype and staining for macrophage markers. During the differentiation, the macrophages expanded significantly to several times their original size and have an egg/spindly morphology with a high cytoplasm/nucleus ratio. Staining for CD68, CD14, SRA1 and CD36 characterized cells as macrophages and CD1a was used as a negative control to ensure no dendritic cell differentiation.

OxLDL uptake by hMDMs

To measure AM efficacy at inhibiting oxLDL uptake, hMDMs were incubated with 1 µg/mL of DiO labeled oxLDL and 10^{-6} M AM in RPMI 1640 for 24 h. Cells were removed from plates by vigorous pipetting in cold PBS with 2mM EDTA, washed with PBS, centrifuged and fixed in 1% paraformaldehyde. DiO fluorescence (oxLDL uptake) was measured by flow cytometry on a FACScalibur (Beckton Dickenson) in the FL1 channel. A minimum of 15,000 events per sample were collected, and quantified using the geometric mean fluorescence intensity (MFI) of intact hMDMs with FloJo (Treestar). Results are the average of three independent experiments with two technical replicates per experiment. Data is presented as % oxLDL uptake inhibition, which was

calculated using the following formula: $100 - 100 * \frac{MFI\ of\ AM\ containing\ condition}{MFI\ of\ oxLDL\ control} = \%\ oxLDL\ uptake\ inhibition.$

Foam cell formation

To measure the effectiveness at preventing foam cell formation (lipid accumulation), AMs (10^{-5} M) and oxLDL (50 µg/mL) were co-incubated with hMDMs for 24 h. Cells were then washed, fixed, dehydrated with 60% isopropanol, stained with 2mg/mL Oil Red O in 60% isopropanol for 5 min, washed and the nucleus counterstained with 1 µg/mL Hoechst 33342. Brightfield and epifluorescent images were taken on a Nikon Eclipse TE2000-S and merged using ImageJ. Images shown are representative of two independent experiments with three technical replicates per experiment.

Statistical analysis

OxLDL uptake results are presented as mean ± standard error of the mean (S.E.M.) and data evaluated by one-way ANOVA and Tukey's test for post-hoc pairwise comparisons between multiple conditions. A *p*-value of 0.05 or less was considered statistically significant.

Molecular modeling

Work performed by Vladyslav Kholodovych and Michael Tomasini

AMs were constructed and minimized in Molecular Operating Environment (MOE), 2011.10 (Chemical Computing Group Inc., Canada). Initial parameterization and charge distribution calculations for AM input structures for MD simulation were performed with the antechamber program from Amber Tools package [223]. Next, a two-tier process was implemented that comprised coarse-grained molecular dynamics (CG MD) simulations on a three-dimensional model system to extract one or more representative (low energy) structures,

followed by all-atom molecular dynamics (AA MD) simulations to yield highly resolved AM conformers from which molecular descriptors were subsequently calculated. **Figure 2.2** outlines the modeling approach.

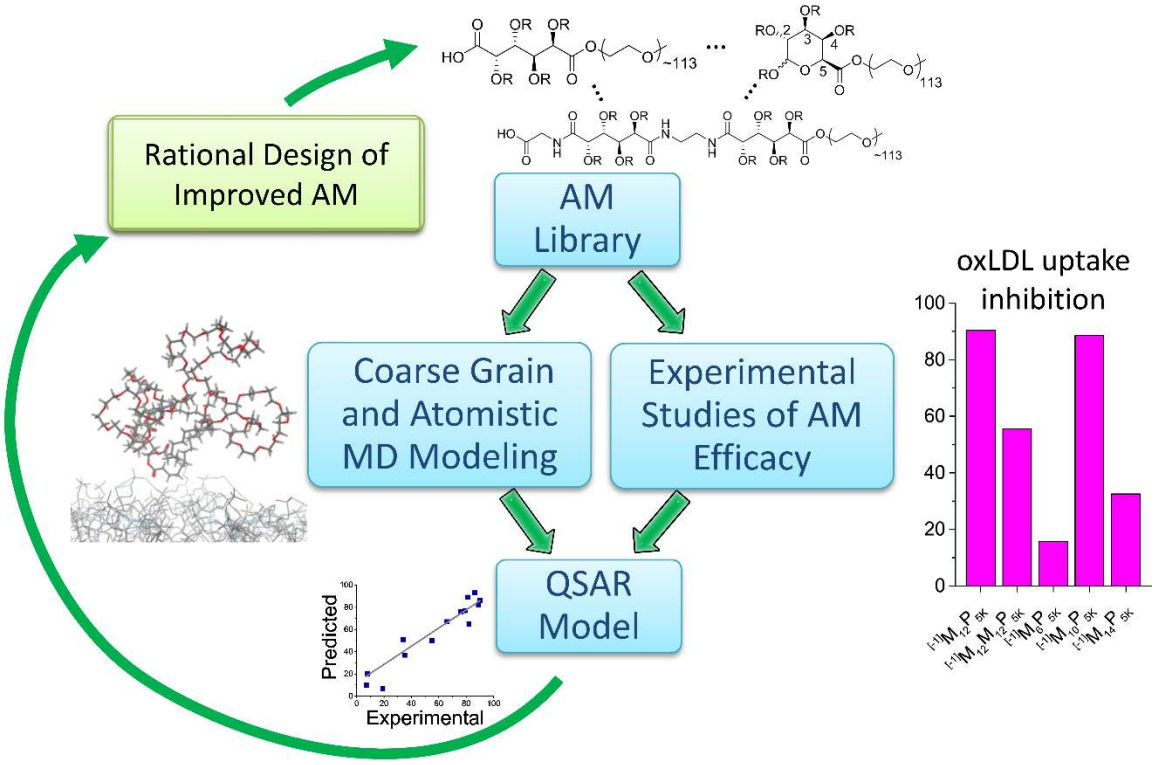

Figure 2.2: An overview of the QSAR modeling methodology employed for this study. The AM library is evaluated for experimental (oxLDL uptake inhibition) outcomes while 2D and 3D descriptors are identified with coarse grain and atomistic MD modeling. These are correlated to experimental results to develop QSAR and predictive models for new AMs. Optimal AM structures are synthesized and this process repeated. From [222]

CG MD simulations

Work performed by Michael Tomasini

To mimic a cellular environment, polymer simulations were carried out in solution in the presence of a dipalmitoylphosphatidylcholine (DPPC) bilayer. Next, the CG MARTINI force-field, which has been shown successful in the study of numerous systems including lipids, proteins, and polymers, was used [224-226]. Each AM was built by combining already parameterized functional groups such as the PEG tails from Lee et al. and aliphatic chains from Marrink et al [226, 227]. In all simulations, the length of the PEG tail was kept at 46 monomers, roughly corresponding to 2000 MW. Lipids, water, and ions were parameterized according to Marrink et al [227]. Each simulation contained 1 AM, 512 DPPC lipids, 0.1 M NaCl and 20640 CG water (82560 water molecules) and was run for 400 ns using the GROMACS software package v. 4.5.5 [228].

Representative structure from CG simulations

Work performed by Michael Tomasini

Following 400 ns of simulation time, the ensemble of generated AM structures, taken every 1 ns, was clustered with the *g _cluster* analysis program of GROMACS using the single linkage algorithm. For each AM, the root-mean-square deviation (RMSD) threshold was chosen as the minimum value such that greater than 50% of structures were members of a single cluster. The representative structure was chosen to be the median structure (in terms of RMSD) of the largest cluster.

Reverse mapping of CG structures to atomistic structures

Work performed by Michael Tomasini

The reverse transformation technique of Rzepiela et al. was applied to convert the MARTINI CG structures back to all-atom structures [229]. The Antechamber module of the Amber Tools software package was used to generate atomistic topologies for each AM and the program acpype was used to convert Amber topologies into GROMACS format [223, 230]. The GROMACS

utility g_fg2cg was used to generate an initial approximation of the all-atom structure by placing at random the underlying atoms within the volume of their corresponding CG interaction site. Simulated annealing (SA) was then used to bring the system from 1300 K to 310 K over 100 ps to allow for rearrangement of the atoms and crossing of energetic barriers. During SA, a restraining force is used such that the center of mass (COM) of atoms corresponding to a given CG interaction site align with the COM of the CG site. Following SA, the restraining force is slowly removed over a period of 10 ps. The resultant structure was then subject to energy minimization.

Atomistic MD simulations

Work performed by Vladyslav Kholodovych

Followed the long-range CG MD simulation for 400 ns, the average structures of the AMs were subjected to refinement with AA MD in aqueous solution over the surface of the membrane bilayer, constructed to mimic the macrophage cellular surface. Each reverse mapped AM was placed over the surface of the constructed membrane comprising phosphatidylcholine (PC), phosphatidylethanolamine (PE) and phosphatidylserine (PS) (courtesy of Dr. William Moyle, Department of OBGYN, RWJMS-UMDNJ), neutralized with sodium ions and solvated with *tleap* subroutine from Amber 12 software package [223]. High level AA MD simulation totaling 10 ns for each of the 17 AMs contained 1 AM, 812 lipids and 82560 water molecules in a periodic box was performed on the specifically built and dedicated high performance GPU Linux cluster.

3D molecular descriptors and QSAR analysis

Work performed by Vladyslav Kholodovych

The representative low-energy 3D structures emerging from the AA MD simulations were subjected to QSAR analysis to find correlations between polymer structural features and their effect on oxLDL uptake. Each polymer was encoded with 1664 distinct molecular descriptors using

Dragon v.5.4 software program. Sets of descriptors were limited to 3D descriptor blocks as defined in Dragon, namely Randic molecular profiles, geometrical descriptors, RDF descriptors, 3d-MoRSE, Weighted Holistic Invariant Molecular (WHIM), GEometry, Topology, and Atom-Weights AssemblY (GETAWAY) and charge descriptors (total of 735). After removing highly correlated pairs and descriptors with standard deviation below the program default threshold, the final set of descriptors was reduced to 115. Partial least squares (PLS) regression method implemented in MOE was used to model the experimental data.

Results

AMs inhibit oxLDL uptake in hMDMs

The different AM structures have demonstrated varying abilities to inhibit oxLDL uptake in MDMs. As shown in **Figure 2.3A-C** $^{[-1]}M_{12}P_{5K}$, $^{[0]}M_{12}P_{5K}$, $^{[0]}G_{12}P_{5K}$, $^{[-1]}T^{Meso}{}_{12}P_{5K}$, $^{[-1]}gM_{12}P_{5K}$, and $^{[-1]}M_{10}P_{5K}$ display the most significant reduction in oxLDL accumulation. In contrast, AM structures $^{[-1]}S_{12}P_{5K}$, $^{[-1]}Ar_{12}P_{5K}$, $^{[-1]}M_{6}P_{5K}$ did not show a statistically significant decrease in oxLDL uptake as compared to the oxLDL control.

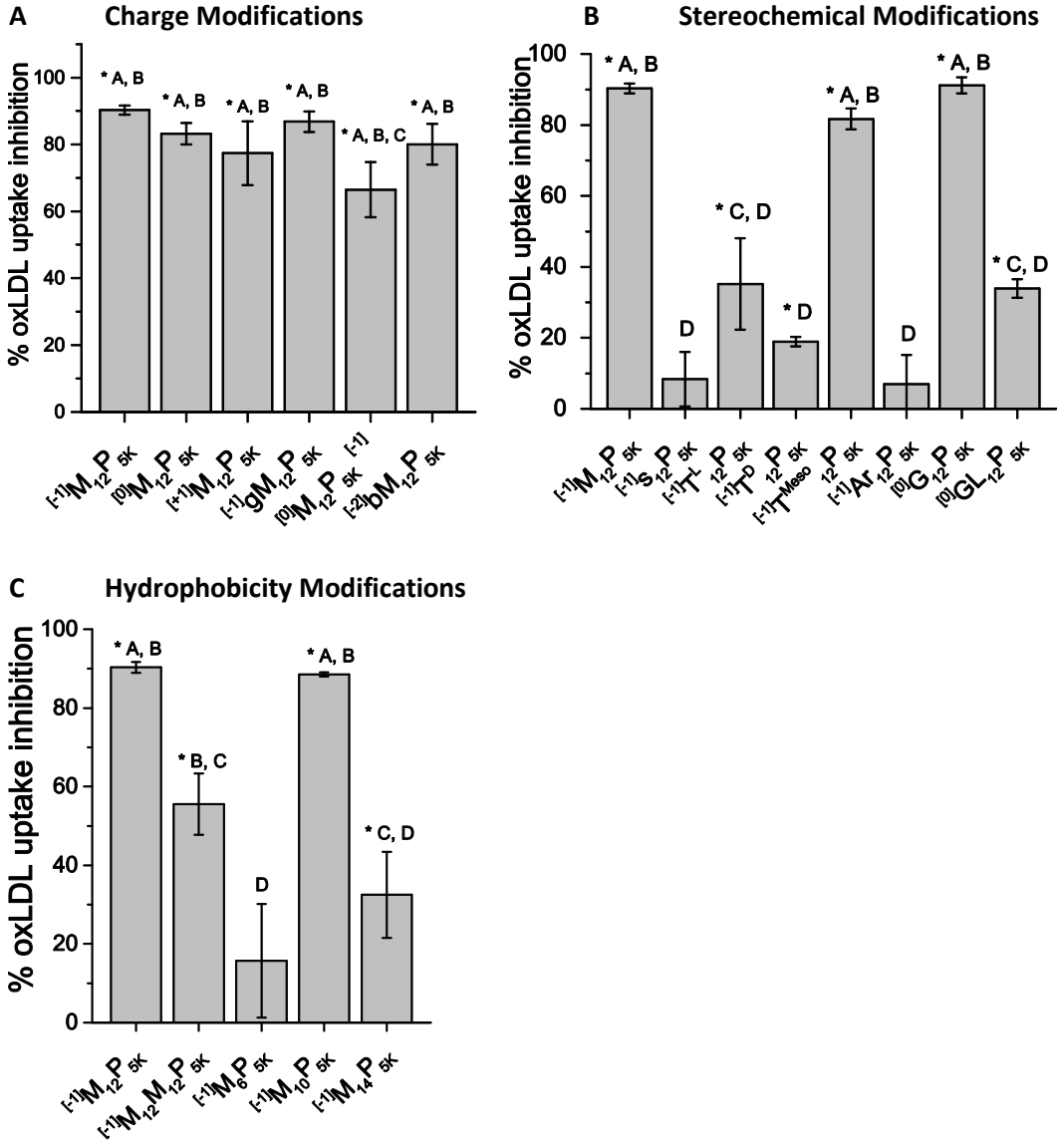

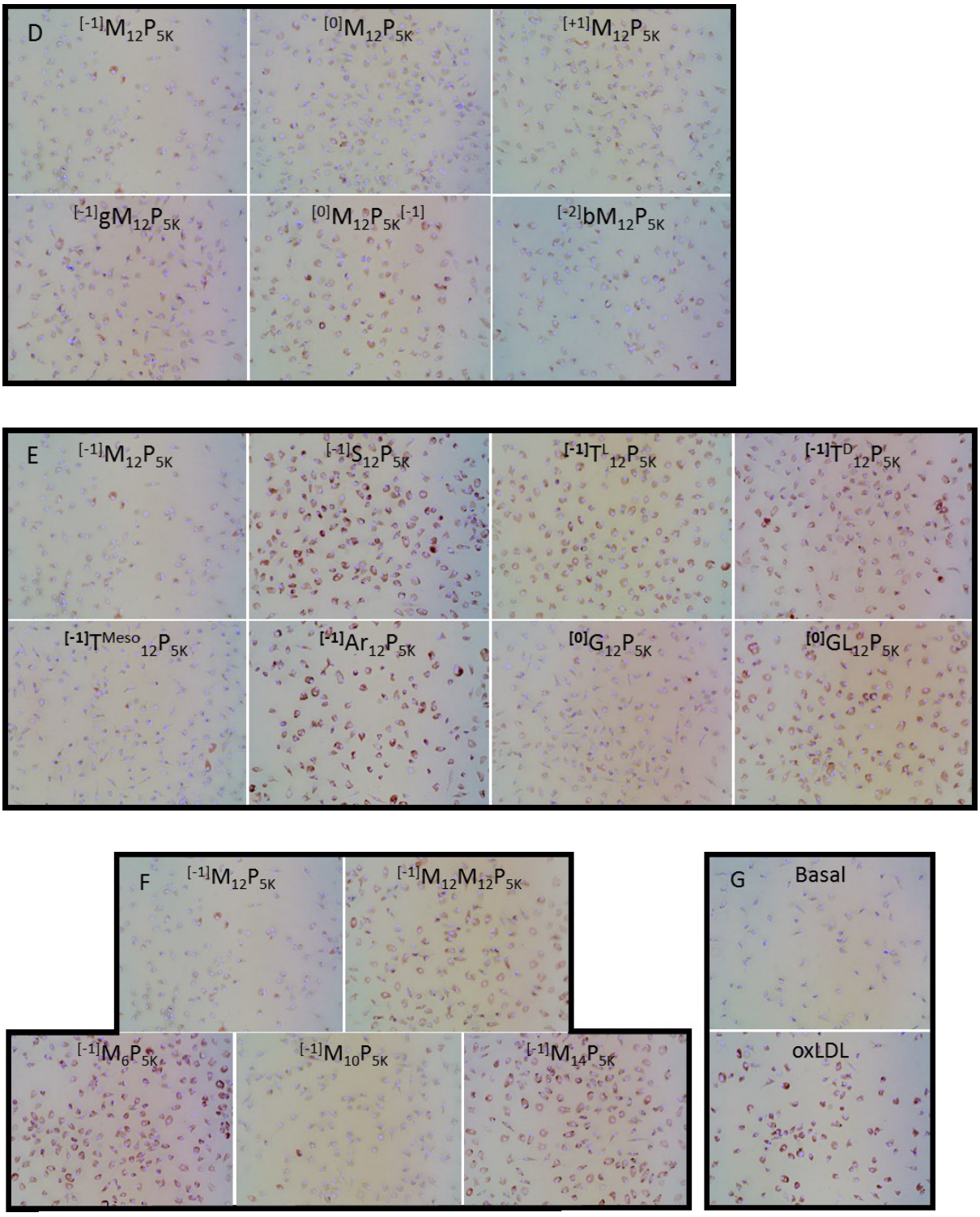

Figure 2.3: AM library shows graded efficacy of anti-atherogenesis in hMDMs A-C) The percentage of inhibition of oxLDL uptake was plotted versus nature of AM treatment in hMDMs. **D-G**) Representative micrographs showing modulation of lipid uptake and foam cell phenotype.

AM are grouped to show effects of charge (**A/D**), stereochemical (**B/E**) and hydrophobic modifications (**C/F**). Treatments with the same letter are not statistically significant from one another and the asterisk (*) indicates statistical significance ($p < .05$) from the control (no AM, oxLDL only). From [222].

Foam cell phenotype is prevented by AM

Treating hMDMs with oxLDL generated the foam cell phenotype as evidenced lipid droplet accumulation (**Figure 2.3G**). The foam cell formation results qualitatively parallel the oxLDL uptake results, and show that the AM library has differing ability to reduce lipid accumulation (**Figure 2.3D-F**). These results demonstrate the ability of AMs to mitigate actual atherosclerotic endpoints.

CGMD in conjunction with atomistic MD yield highly resolved AM conformers

The two-tiered approach used in this study provided detailed conformers for all AM structures. A schematic of an AM along with its CG representation and atomistic transformation is shown in **Figure 2.4**. Snapshots of selected AM are presented in **Figure 2.5.**

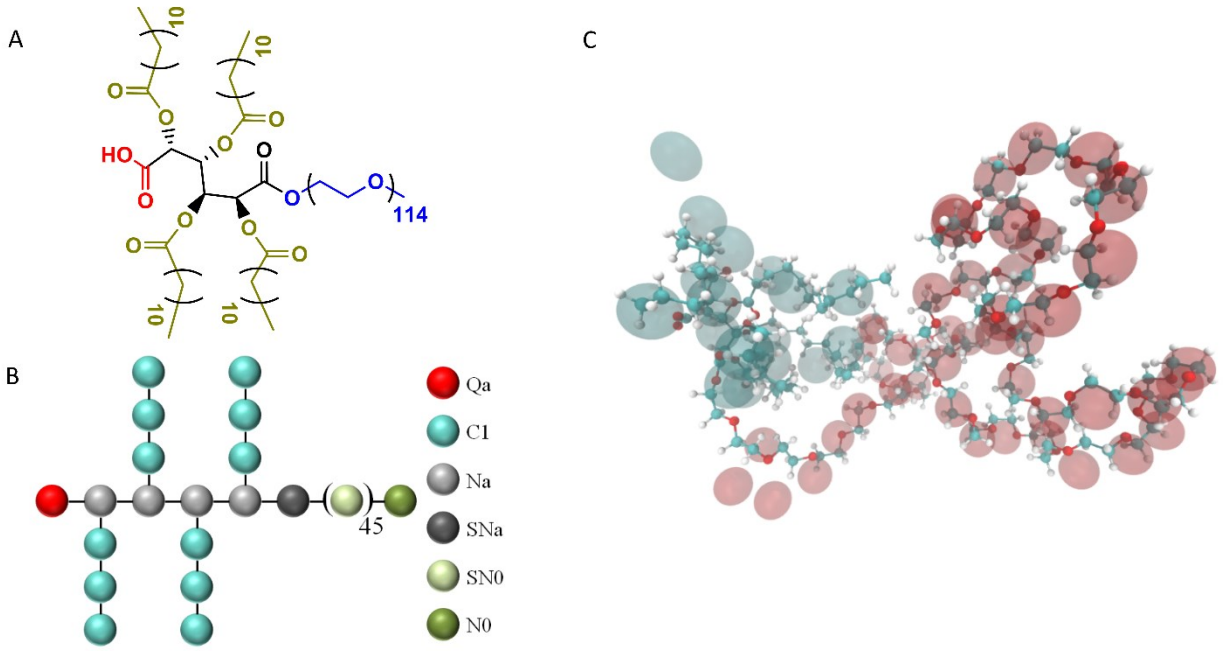

Figure 2.4: AM structures. A) The molecular and B) coarse grain structure of $^{[-1]}M_{(12)}P_{5K}$ shown in a ball-and-stick representation. **C**) The conformation of $^{[-1]}M_{(12)}P_{5K}$ along with its CG representation in the MARTINI force field where CG beads are shown as transparent spheres. From [222].

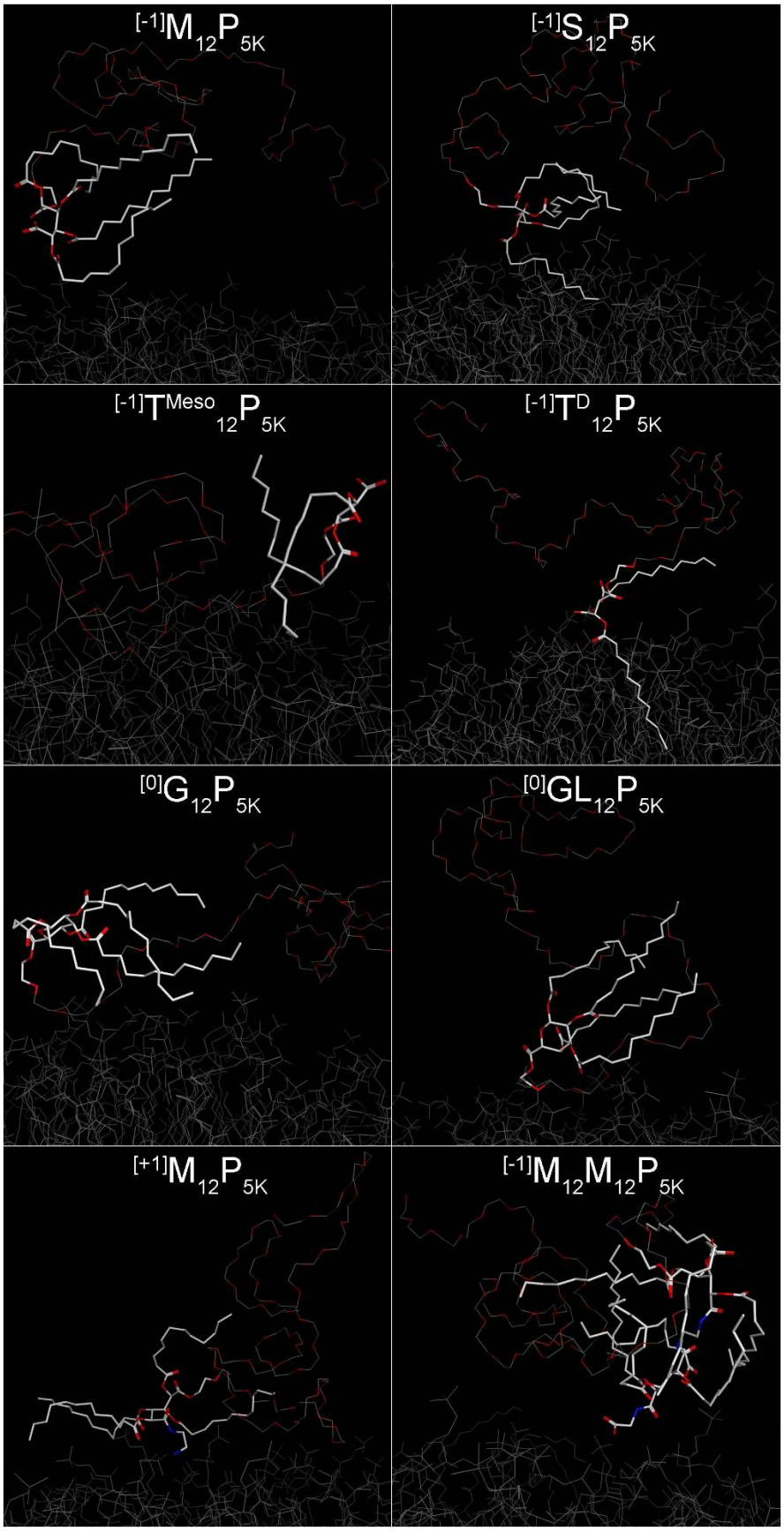
[-1]M12P5K
[-1]S12P5K
[-1]TMeso12P5K
[-1]TD12P5K
[0]G12P5K
[0]GL12P5K
[+1]M12P5K
[-1]M12M12P5K

Figure 2.5. AM conformations. AMs exhibiting high to moderate efficiency in reduction of oxLDL uptake (left column) have their aliphatic arms in an extended conformation while less effective polymers (right column) form more compact globular structures with aliphatic arms pointing in the direction opposite to the cell membrane. These snapshots of AMs were obtained after 400 ns of CG MD simulation and additional 2 ns of AA MD simulation over the surface of membrane bilayer. For simplicity, hydrogen atoms are omitted. The hydrophobic heads of the AMs are highlighted as grey sticks and the PEG tail is shown as a trace attached to the AM "head". For visual comparison, the top three rows show stereo pairs of polymers that have distinctive behavior in reduction of oxLDL uptake: $^{[-1]}M_{(12)}P_{5K}$/ $^{[-1]}S_{(12)}P_{5K}$, $^{[-1]}T^{Meso}{}_{(12)}P_{5K}$/ $^{[-1]}T^{D}{}_{(12)}P_{5K}$, and $^{[0]}G_{12}P_{5K}$/$^{[0]}GL_{12}P_{5K}$. From [222].

Effective AM maintain an extended conformation

The MD results suggest that the most effective AM at inhibiting oxLDL ($^{[-1]}M_{12}P_{5K}$, $^{[-1]}gM_{12}P_{5K}$, $^{[+1]}M_{12}P_{5K}$) tend to stay in the extended conformation during the entire MD simulation, while their less active counterparts ($^{[-1]}S_{12}P_{5K}$, $^{[0]}GL_{12}P_{5K}$, $^{[-1]}M_{12}M_{12}P_{5K}$) generally form more compact globular structures with lauryl arms pointing in the direction opposite of the cell membrane (**Figure 2.5**).

QSAR produces strong correlation with 5 descriptors

Molecular descriptors were generated to encode various physicochemical properties of the AM including spatial organization, chemical composition and stereochemistry. Following filtering and prioritization of descriptors based on their information content, QSAR models were constructed using PLS regression to predict the AM efficacy (i.e., inhibition of oxLDL uptake). Several QSAR models were built and key descriptors that explain oxLDL uptake-related behavior of AM stereo pairs were identified. A statistically strong correlation between predicted and

observed results was achieved with only five descriptors. Employing these descriptors, a QSAR model was established which exhibited a strong linear correlation (r^2=0.91, r_{cv}^2=0.77) between predicted and observed values of oxLDL uptake (**Table 2.2**).

Table 2.2: QSAR equation related oxLDL uptake inhibition and descriptors of polymers, statistical analysis of the model fit and relative influence of descriptors on the QSAR model.

$$oxLDL\ uptake\ inhibition = -617.97111 + 6528.05803 * G3p + 187.62572 * HOMA + 608.22915 * Ds - 391.41561 * R5u + 1179.44106 * G1u$$

Relative influence of descriptors		
G3p	1.000000	3rd component symmetry directional WHIM index / weighted by atomic polarizabilities
HOMA	0.329363	Harmonic Oscillator Model of Aromaticity index
Ds	0.382432	D total accessibility index / weighted by atomic electrotopological states
R5u	0.314173	R autocorrelation of lag 5 / unweighted
G1u	0.245292	1st component symmetry directional WHIM index / unweighted

QSAR fit	
Root mean square error (RMSE)	8.65491
Correlation coefficient (R^2)	0.91
Cross-validated RMSE	14.65
Cross-validated R^2	0.77

WHIM descriptors (**G3p, Ds, G1u**): (Weighted Holistic Invariant Molecular descriptors), which are geometrical descriptors based on statistical indices calculated on the projections of the atoms along principal axes
Geometrical descriptors (**HOMA**): Different kinds of conformationally dependent descriptors based on the molecular geometry.
GETAWAY descriptors (**R5u**): Descriptors calculated from the leverage matrix obtained by the centered atomic coordinates (molecular influence matrix, MIM).

QSAR model can predict efficacy of new structures

The final model was successfully applied in predicting oxLDL uptake inhibition of $^{[-1]}M_{12}P_{5K}$ analogs with variable aliphatic arms ($^{[-1]}M_6P_{5K}$, $^{[-1]}M_{10}P_{5K}$, and $^{[-1]}M_{14}P_{5K}$) (**Figure 2.6**). The predicted and experimental values for the test set, comprising three newly designed AM with varying hydrophobic moieties were correctly ranked from low to high values, thereby attesting to the prediction ability of the final QSAR model and proving its value for optimizing AM structures that mitigate adverse athero-relevant endpoints.

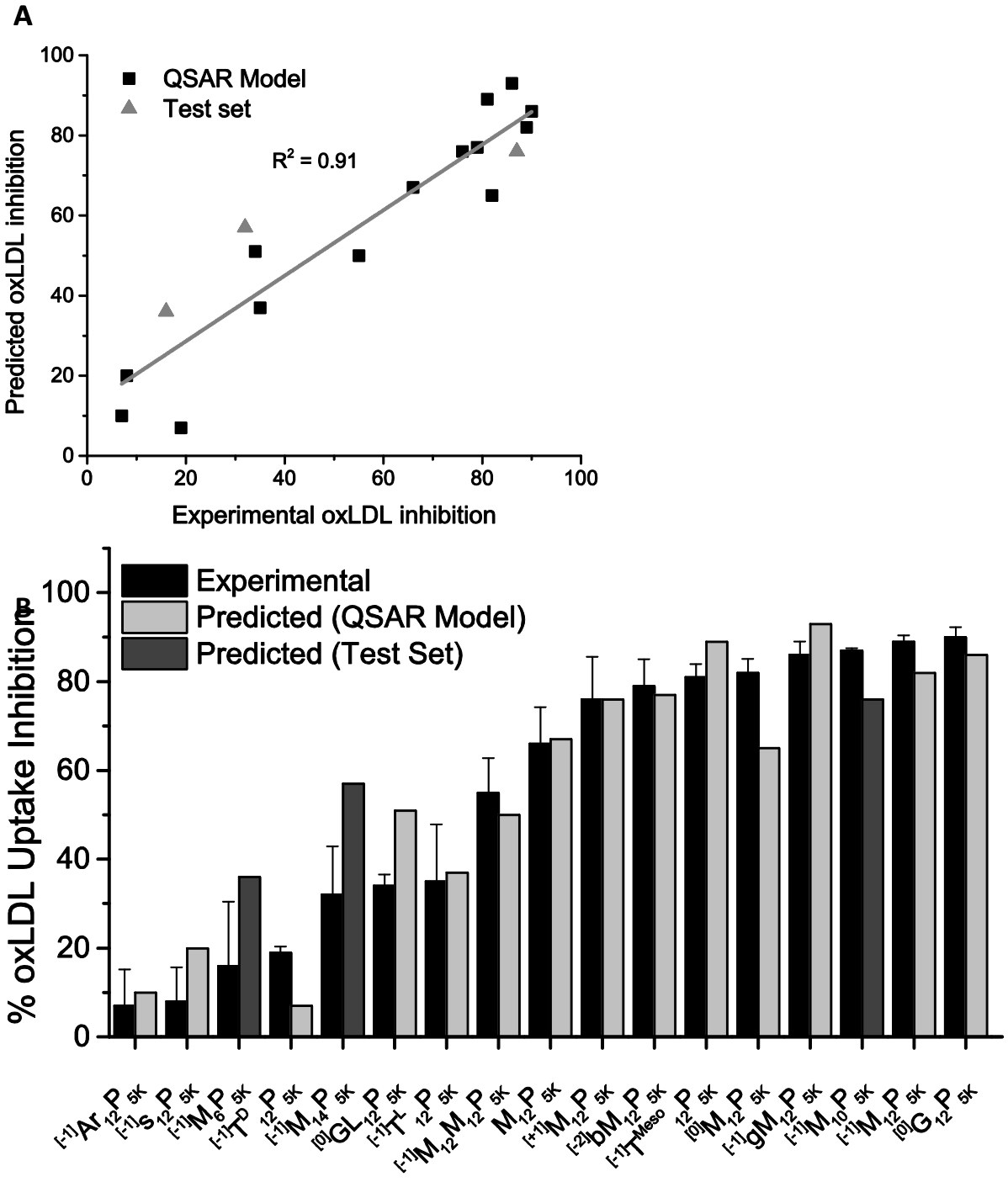

Figure 2.6: QSAR correlations. The final QSAR model was successful at predicting the bioactivity (oxLDL uptake inhibition) of the 3 member AM test set. **A**) The QSAR fit showing that the residual from simulation is often within the S.E.M. from the experimental data. **B**) The linear fit of experimental vs. predicted outcomes with $R^2 = 0.91$. From [222]

Discussion

Inhibition of the atheroinflammatory phenotype of macrophages is considered to be as a major strategic target for the management of atherosclerosis underlying cardiovascular disease [5, 13, 15, 231]. While a range of new AMs show promise in inhibiting atherogenesis in inflamed macrophages, a rational framework to designing improved AMs is currently lacking [105, 144, 169, 193, 195, 232]. In this work, a novel multiscale modeling approach was advanced by employing molecular descriptors of the AM chemical structures and geometric parameters based on conformational changes of the AMs on model lipid membranes. By correlating biological efficacy data from hMDMs with a wide range of AM descriptors, a new QSAR model was derived, which affords new insights to optimize and predict the efficacy of new AM structures.

Developing QSAR and principle component analysis (PCA) models to isolate critical molecular features is an expanding field and used in a wide array of molecular feature spaces [233, 234]. Even within a small library size, high variability in biological efficacy is observed as slight changes in AM structure produce markedly different efficacies at inhibiting oxLDL uptake and foam cell formation (**Figure 2.3**). Although this result is quite common for small molecule therapeutics, due to the large MW and the conformational flexibility, this effect was less expected for this AM library and prompted further examination.

Although previous studies found AM efficacy differences dependent on charge type and charge placement [105, 195], this work has identified that the largest differences in AM efficacy stem from stereochemical and hydrophobic modifications (**Figure 2.3A-C**). $^{[0]}M_{12}P_{5K}$ and $^{[0]}G_{12}P_{5K}$ are biologically effective despite having an overall neutral charge that should make them less effective at binding to the positive charged SR responsible for oxLDL and AM (nanoparticle and micelle formulations) uptake. This result may indicate that the folded conformation of the AM

and the presentation of hydrophobic moieties can overcome charge repulsion. Additionally, the mucic acid sugar backbone seems to provide increased efficacy as $^{[-1]}M_{12}P_{5K}$, $^{[0]}M_{12}P_{5K}$, $M_{12}P_{5K}^{[-1]}$, $^{[-2]}bM_{12}P_{5K}$, $^{[-1]}gM_{12}P_{5K}$ and $^{[+1]}M_{12}P_{5K}$ all show higher inhibition levels than tartaric and saccharic acid backbone AMs. However, changes in stereochemistry resulted in the most drastic differences in inhibition efficiency with the substitution of saccharic acid in $^{[-1]}S_{12}P_{5K}$ for mucic acid in $^{[-1]}M_{12}P_{5K}$ where the only structural difference is one stereocenter. $^{[-1]}M_{12}P_{5K}$ was the second most effective AM at inhibiting oxLDL uptake, whereas $^{[-1]}S_{12}P_{5K}$ consistently showed little inhibition.

While oxLDL uptake enables the evaluation of lipid influx, it does not consider lipid metabolism and secretion, such that alternate studies are needed to quantify total lipid accumulation [45]. Transition to the foam cell phenotype is the physiologically relevant marker of atherogenesis and defined by large lipid droplets developing within the cell. The transition to the foam cell phenotype marks the first stage in lesion development and often accompanied by increased inflammatory cytokine secretion. Although oxLDL may still be present in the artery, by blocking the cellular interaction, adverse endpoints may be avoided. Foam cell formation (**Figure 2.3D-F**) qualitatively show reduction in lipid accumulation by AMs. As these results mimic those of oxLDL uptake, they show that AM could be effective at managing atherosclerotic disease even in areas of high oxLDL concentration.

The MD results indicate that the extended conformation of alkyl arms is required for effective inhibition bioactivity and increasingly globular AMs are less effective. . This result may be caused a stronger interaction occurring between the extended lauryl arms with the membrane bilayer surface during simulation. As a result, these interactions would generate deeper and more rapid penetration of the AM into the cell membrane, suggesting that tighter AM binding leads to more effective inhibition of oxLDL uptake and foam cell formation.

The descriptors obtained from the coarse grain and atomistic MD modeling were used to establish QSAR models for predicting AM efficacy. A statistically significant model was established between predicted and experimental outcomes using only five AM descriptors. The descriptor set, although not easily transferable into simple chemical terms, encompasses a wide range of AM descriptors such as aromatic rings and unsaturated bonds (HOMA descriptor), molecular geometry, size, shape and stereochemistry. Among the prominent 3D descriptors are the WHIM descriptors, which are geometrical descriptors based on statistical indices calculated on the projections of the atoms along principal axes and the GETAWAY descriptors (**Table 2.2**) [235-238]. WHIM descriptors encode 3D information on molecular size, shape, symmetry and atom distribution with respect to invariant reference frames, while the GETAWAY descriptors encode atomic properties such as atomic mass, atomic polarizability, atomic electronegativity, van der Waals atomic volume, and the unit weight. This QSAR model was successful at predicting the efficacy of $^{[-1]}M_{12}P_{5K}$ analogs with variable hydrophobicity ($^{[-1]}M_{6}P_{5K}$, $^{[-1]}M_{10}P_{5K}$, and $^{[-1]}M_{14}P_{5K}$) (**Figure 2.6**).

Implementation of the validated QSAR model, together with insights into structure-activity relationships gained from analyzing the leading molecular descriptors, will guide optimization of AM structures that mitigate adverse athero-relevant endpoints. Moreover, the QSAR models will gain in predictive performance and statistical robustness as more experimental results are obtained for model building.

Conclusion

Developing predictive models of drug behavior to optimize therapeutics can speed drug development. However, different therapeutic classes require distinct predictive models and structural feature knowledge. AMs offer a novel approach to managing cardiovascular disease but their structure-function relationships were not fully understood until this study. An expanded AM library modulating key molecular features was created that displayed high variability in the reduction of oxLDL uptake and foam cell formation. As 2D molecular parameters cannot adequately describe a large 3D structure, MD simulations were used to generate 3D structures in solution. These 2D and 3D molecular models yielded several descriptors, which were correlated to biological activity using QSAR. This model based upon five key descriptors was then implemented to successfully predict the efficacy of novel AM structures. This work demonstrates the unique interplay of 2D and 3D computational approaches combined with powerful bioactivity prediction models that can be used for the rational design and optimization of novel macromolecular therapeutics.

Supplementary Data

AM cytotoxicity

MDMs were plated at 50,000 cells/well and treated with 10^{-5}M AM in RPMI media for 24 hours before Live/Dead staining. The assay was performed by incubating cells with 2µM Calcein AM and 1 µM Propidium Iodide (PI) solution for 30 minutes before quantification by flow cytometry using a Beckman Coulter FC500 Analyzer. Live cells were counted as those that exhibited Calcein (FL1) fluorescence and dead cells were counted as those that were Calcein negative and PI positive.

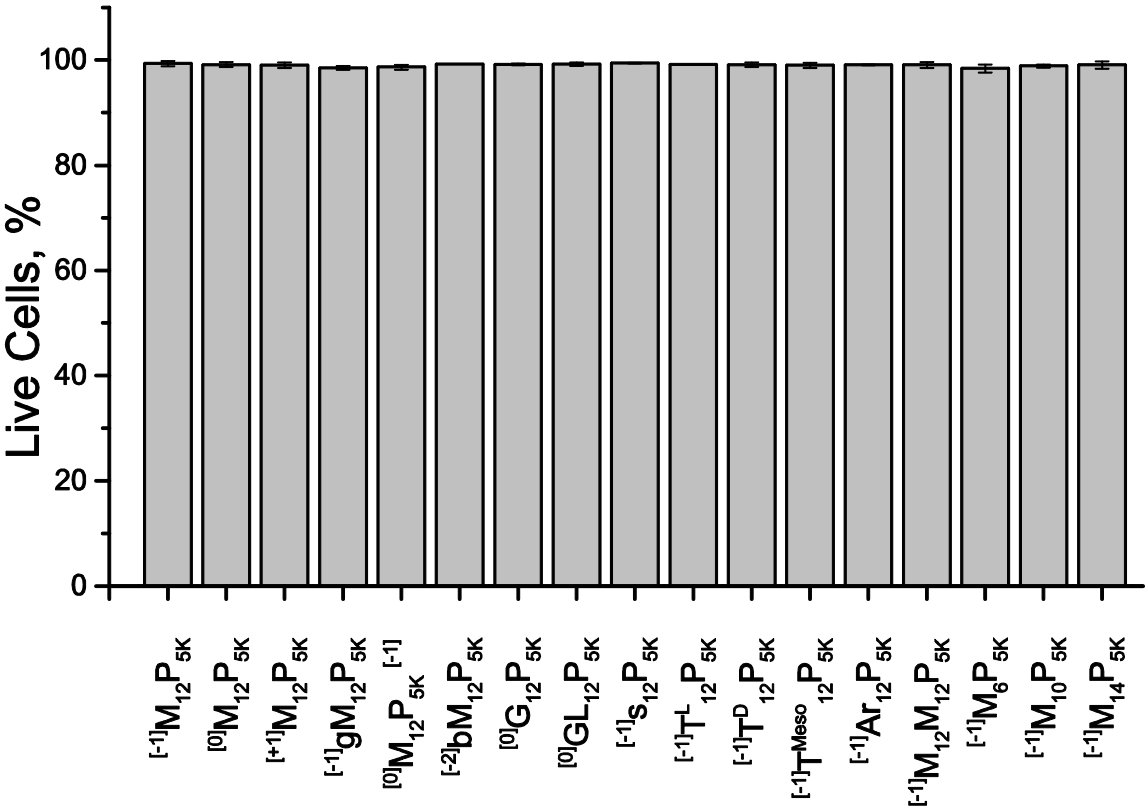

Figure S2.1 Cytotoxicity studies confirmed that the various AMs displayed minimal toxicity to human macrophages over 24 h and thus were highly cyto-compatible. This was expected as AM are constructed from biocompatible moieties. From [222].

AM conformations

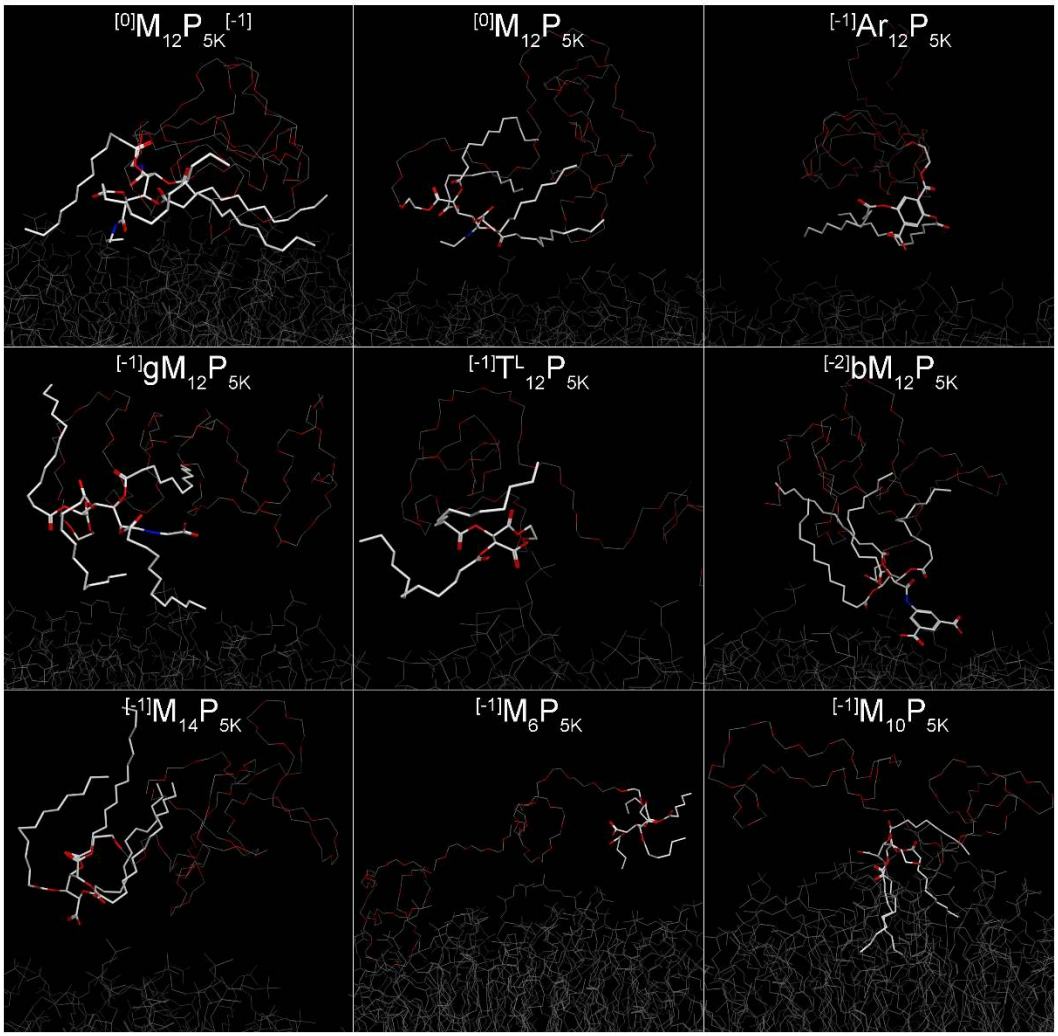

Figure S2.2 AM conformations for all the structures follows the trend. Highly bioactive AM maintain an extended conformation while less efficacious AM form globular masses by sequestering the alkyl arms. From [222].

Chapter 3 – Non-inflammatory nanoparticles fabricated from amphiphilic macromolecules

Note: Sections of this chapter have been reproduced from the following manuscript:

York AW, Zablocki KR, **Lewis DR**, Gu L, Uhrich KE, Prud'homme RK and Moghe PV. *Kinetically assembled nanoparticles of bioactive macromolecules exhibit enhanced stability and cell-targeted biological efficacy*. Adv Mater. 2012;24(6):733-739.

Abstract

Atherosclerosis is an inflammatory disease that is characterized by the buildup of lipid rich plaques in arterial walls. Amphiphilic macromolecules (AMs) have been designed to mitigate key disease endpoints, namely the prevention of lipid accumulation within macrophages. These have further been fabricated into a core-shell configuration within a kinetically assembled nanoparticle (NP) formulation with superior serum stability. Such nanoparticles exhibit high levels of inhibition of atherogenesis in macrophages, however, due to their size and anionic charge display, these nanoparticles may also trigger inflammatory signaling in macrophages. In this study, we have developed a 2nd generation of AM NPs designed to be non-inflammatory, enabling more effective treatment of athero-inflammation. To this end, the antioxidant vitamin E was incorporated into the core of nanoparticles, which were then tested for anti-oxidized lipid accumulation bioactivity and inflammatory signaling. Substitution of the hydrophobic core of the AM NPs with vitamin E caused pronounced reduction in the inflammatory signaling by macrophages relative to 1st generation AM NPs, while maintaining high levels anti-atherogenic efficacy. Thus, this non-inflammatory, lipid-reducing AM NP composition would be well suited as an *in vivo* therapeutic.

Introduction

Atherosclerosis, the buildup of lipid laden plaques within arterial walls, is one of the principal initiators of cardiovascular disease (CVD). Responsible for ~50% of deaths in western countries, CVD remains a multifocal disease in need of novel management strategies [4]. Atherosclerosis is principally understood to be an inflammatory disease that self-aggravates. High levels of circulating low density lipoproteins (LDL) result in LDL deposition in the arterial wall, where it is modified to oxidized low density lipoproteins (oxLDL) [7]. This initiates inflammatory cytokine secretion and adhesion molecule upregulation, which signals enhanced recruitment of leukocytes, specifically monocytes. These undergo diapedesis and differentiation into macrophages, at which point they have unregulated uptake of oxLDL via scavenger receptors [239]. The macrophages in turn exacerbate the inflammatory signaling, leading to plaque growth and narrowing of the artery [240].

In the absence of inflammation, plaque development is severely restricted. Studies using atherosclerotic mice models have shown that pro-inflammatory cytokines, MCP-1 and IL-8, are required for advanced lesion development. [19, 20]. Additional studies have found that scavenger receptors play a critical role in foam cell formation and plaque buildup [32, 42]. Foam cell formation can lead to increased susceptibility to the inflammatory phenotype [21]. By limiting foam cell development, the lipid burden and cytokine secretion could be reduced [37].

Amphiphilic macromolecules (AM), designed to competitively bind scavenger receptors, could arrest lipid accumulation and the ensuing inflammation [5]. Previous studies have shown that AMs could significantly reduce oxLDL uptake and foam cell formation [105, 222]. Recently, it has been identified that the AM architecture, specifically the 3D conformation (stereochemistry),

has a marked effect on its bioactivity [222]. In this work the AM, $^{[-1]}M_{12}P_{5K}$, showed the highest level of reduction of oxLDL uptake and foam cell formation.

PEGylated micelles are an attractive nanoscale assembly for *in vivo* applications due to the natural shielding that PEG provides. However, micelles exist in dynamic equilibrium, with individual unimers continually partitioning in and out of the assembly. (**Figure 3.1 A**) In simple environments, this process is not a concern due to the lack of hydrophobic sinks. However, in a complex setting, such as circulating blood, many serum proteins act as hydrophobic sinks that can drive the equilibrium away from micelle formation. Once a unimer separates from the micelle, it can partition into the hydrophobic domain of a protein and is then removed from contributing toward the critical mass of unimeric assemblies.

To overcome the challenges associated with micelle stability, nanoparticles fabricated from the bioactive AMs using a flash nanoprecipitation process (FNP) have been shown to exhibit significantly higher stability in serum conditions relative to micelles [232]. FNP utilizes the rapid, confined mixing of an amphiphile and hydrophobe dissolved in an water miscible organic solvent with excess of water, which results in rapid nucleation of the hydrophobe and stabilization into nanoparticles (NPs) by the amphiphile (**Figure 3.1 C**) [90, 241, 242]. The hydrophobic core of the NP traps the amphiphile and prevents thermodynamic dissociation (**Figure 3.1 B**). Since the amphiphilic unimers do not dissociate, lipid sink containing environments do not adversely impact their bioactivity.

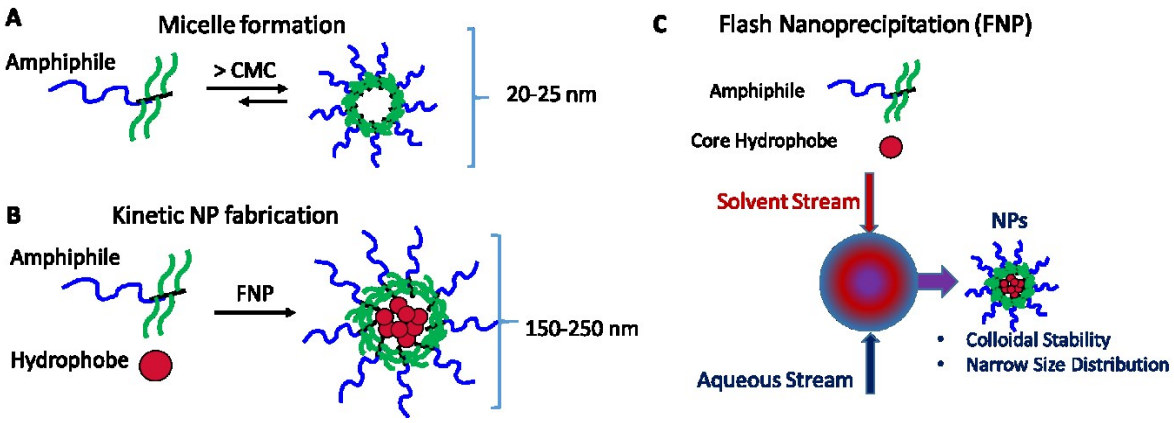

Figure 3.1: Comparison of thermodynamic micelles to kinetically assembled nanoparticles (A/B). C) Flash NanoPrecipition method of assembling nanoparticles.

Previous studies showed that AM NPs exhibited much slower release of AM unimers in serum containing PBS relative to AM micelles [232]. In this work, increased stability of NPs translated to increased efficacy in preventing oxLDL uptake and lipid accumulation in hMDMs in serum-containing media as compared to thermodynamically stabilized micelles. When hMDMs were co-treated with oxLDL and AM NPs or micelles at various serum concentrations, the efficacy of micellar formulations decreased with increasing serum. AM NPs showed a slight decline in efficacy at higher serum concentrations, yet still maintained an ability to block atherogenic oxLDL accumulation [232].

One potential concern for using AM NPs is the inherent pro-inflammatory nature of nanosized materials [243]. Macrophages are part of the innate immune system and recognize a wide variety of foreign objects that induce a foreign-body inflammatory response. The size and surface chemistry of NPs plays a critical role in this recognition, most likely due to the high surface area to volume ratio [244, 245]. Two imaging nanosystems exploited this selective association/internalization by monocytes/macrophages for the visualization of plaques using PET and MRI [246, 247]. Nanoparticles in particular can stimulate inflammatory pathways that could

exacerbate the signaling cascade that leads to atherogenesis [248]. Ensuring that NPs do not cause cellular or systemic inflammatory responses is a major consideration in the design of implantable or injectable nanosystems [249].

Long circulation half-life is a fundamental goal in pharmaceutical development, which should be reconciled with long term NP accumulation in tissues for the sustained treatment of vascular occlusive regions [94, 244]. If particles are able to fully evade systemic clearance, they can potentially cause tissue damage in off-target areas where they may accumulate excessively over time [250]. Features that imbue particles with preferential targeting and slow clearance as opposed to uncontrolled tissue accumulation (for example in the liver or reticuloendothelial system) need to be identified and integrated in the design of improved nanosystems [92]. AM NPs offer an attractive alternative to solid NPs as they will eventually break down into their component amphiphiles and hydrophobes. These in turn are synthesized from biocompatible building blocks, such as linear sugars, lauryl chains and PEG.

As LDL oxidation and inflammation is critical to the progression of atherosclerosis, it would be optimal to have antioxidant therapeutic incorporated within AM NPs. Vitamin E (VE), specifically α-tocopherol, has been studied extensively as a potential cardioprotective antioxidant [72]. *In vitro* and rodent studies demonstrated elevated resistance to oxidation of LDL and decreased plaque development with VE treatment [251]. Intracellularly, VE inhibits cyclooxygenase (COX) activity and expression of prostaglandin E2 in macrophages, resulting in lower peroxynitrite levels [252]. VE also has been shown to reduce adhesion molecule expression in endothelial cells [253]. Incorporating VE into AM NPs could provide a mechanism for enhanced cellular delivery where the anti-oxidant effect could be amplified and mitigate inflammation.

In this work, we have used FNP to fabricate AM NPs incorporating the anti-oxidant vitamin E and the bioactive M_{12} and evaluated their atheroprotective capabilities in cultured primary human macrophages. We hypothesize that the vitamin E-containing formulations combined with M_{12} hydrophobes will achieve a two-fold amelioration in athero-inflammation, namely facilitate a reduction in inflammation while preventing oxLDL uptake in the macrophages. This combination-therapeutic formulation could provide a new approach for the treatment and management of atherosclerosis.

Materials and methods

Materials

All chemicals/materials were purchased from Sigma-Aldrich (Milwaukee, WI) or Fisher Scientific (Pittsburgh, PA) unless otherwise noted. 18 MΩ·cm resistivity deionized (DI) water was obtained using PicoPure 2 UV Plus (Hydro Service and Supplies - Durham, NC). The following items were purchased from the indicated vendors: 1.077g/cm^3 Ficoll-Paque Premium from GE healthcare (Pittsburgh, PA), RPMI 1640 from ATCC (Manassas, VA), macrophage colony stimulating factor (M-CSF) from PeproTech (Rocky Hill, NJ), FBS and AlexaFluor 680 carboxylic acid succinimidyl ester from Life Technologies (Grand Island, NY), unlabeled oxLDL from Biomedical Technologies Inc. (Stoughton, MA), 3,3'-dioctadecyloxacarbocyanine (DiO) labeled oxLDL from Kalen Biomedical (Montgomery Village, MD), and human buffy coats from the Blood Center of New Jersey (East Orange, NJ).

AM synthesis

Work performed by the lab of Kathryn Uhrich

AMs were synthesized as previously described [219]. Briefly, the hydroxyl groups of mucic acid were acylated with dodecanoyl chloride in the presence of zinc chloride, then 5000 Da monohydroxyl-substituted PEG was coupled using 1,3-dicyclohexylcarbodiimide (DCC) and DPTS as catalyst. The product was precipitated from CH_2Cl_2 and diethyl ether yielding AM as a white solid. After precipitation and application of a high pressure vacuum to remove residual organic, the AM were dissolved in 50:50 DMSO/H_2O to release any hydrophobic impurities and dialyzed into DI H_2O using a 3500MW membrane before lyophilization. The structures of the AM were confirmed by ^{1}H and ^{13}C NMR with $CDCl_3$-*d* solvent on Varian 400 MHz spectrometers.

Fluorescent AM synthesis

To track cellular association, amine terminated $^{[-1]}M_{12}P_{5K}$, and polystyrene-*block*-poly(ethylene glycol) (PS-*b*-PEG) were prepared as previously described and fluorescently labeled with AlexaFluor680 carboxylic acid succinimidyl ester (AF680) [232]. Following deprotection and isolation, the amine terminated, bioactive AM (26 mg, 4.3 μmol) was dissolved in 400 μL of anhydrous DMSO and AF680 carboxylic acid succinimidyl ester (5 mg, 4.3 μmol) was dissolved in 600 μL of anhydrous DMSO. 5.0 μmol of triethylamine was added to the AM solution as catalyst. The AM solution was added to the AF680 solution over a 3 h period to give a final AM and activated AF680 concentration of 4.3 mM and was allowed to react in the dark for 18 h at room temperature. The resulting fluorophore labeled AM was purified by dialysis, lyophilized and characterized by UV-vis spectroscopy using a NanoDrop 2000C (Thermo Scientific) with an extinction coefficient of 184,000 M^{-1} cm^{-1}.

Nanoparticle fabrication

Kinetically assembled nanoparticles (NPs) were prepared via flash nanoprecipitation [90, 232, 254]. All fabrication equipment was sterilized in an autoclave, 0.5M NaOH + 1M NaCl solution or 70% ethanol for 30 minutes and flushed with sterile DI H_2O prior to use. Shell and core materials (shown in **Figure 3.3**) were dissolved in tetrahydrofuran (THF) and filtered with a 0.22 μm sterile nylon syringe filter. A confined impinging jet mixer was utilized to mix 500 μL of an aqueous stream with 500 μL of a THF stream containing 40 mg mL^{-1} shell (AM) and 20 mg mL^{-1} core. After mixing, the exit stream was immediately introduced into 4.5 mL of sterile DI H_2O (H_2O:THF volume ratio of 9:1) and subsequently dialyzed against sterile PBS. For AM NPs, $^{[-1]}M_{12}P_{5K}$ (hereafter referred to as AM) was used as the NP shell. The core was composed of mucic acid acylated with lauroyl groups (M_{12}), α-tocopherol (VE) or 50:50 weight ratio of M_{12} to VE (M_{12}/VE). Control NPs

were synthesized using PS-*b*-PEG as the shell and polystyrene (PS) as the core. To track NP fate and cellular association, some experiments had 1.5 mol % of the shell amphiphile labeled with AF680. NP size and poly dispersity index (PDI) was determined by dynamic light scattering (DLS) using a Zetasizer Nano (Malvern).

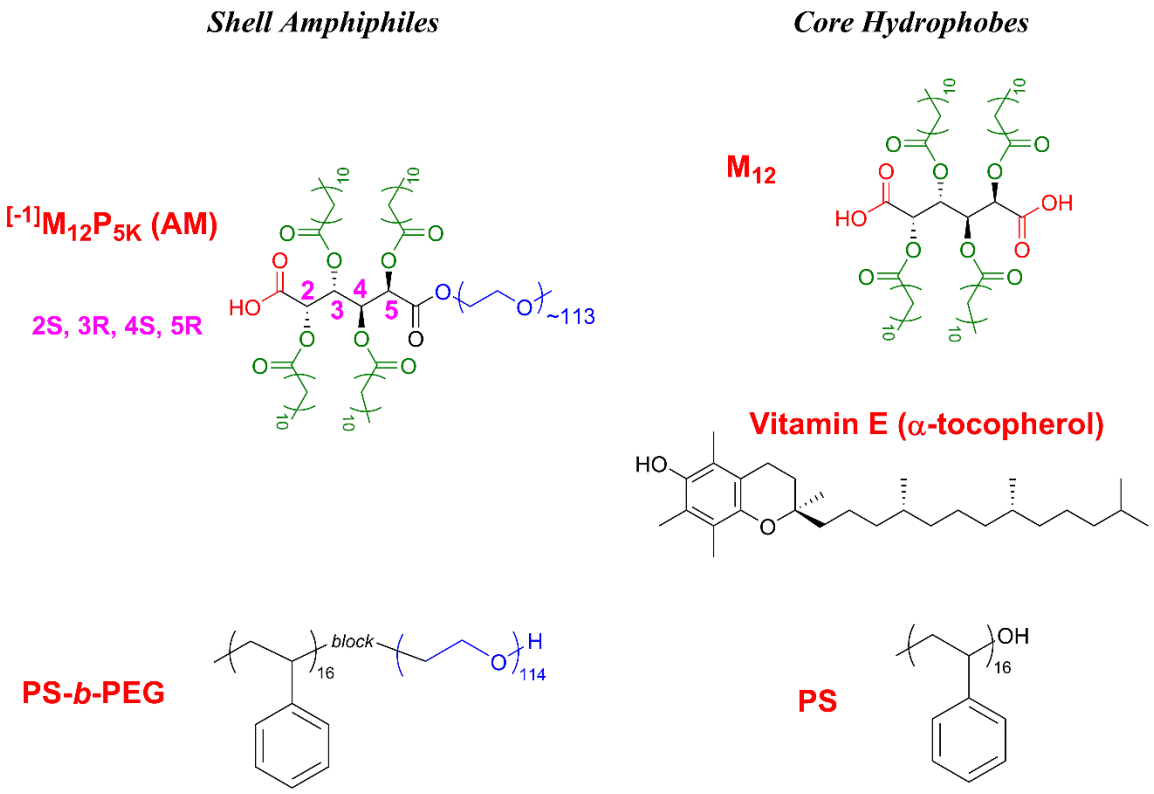

Figure 3.2. Chemical structures of amphiphiles and hydrophobic cores.

Isolation and culture of human monocyte derived macrophages (hMDMs)

Peripheral blood mononuclear cells (PBMCs) were isolated from human buffy coats and differentiated into macrophages as previously described [222]. After differentiation, macrophages were trypsinized, scraped from flasks and transferred into well plates at 50,000 cells/cm^2. Treatments were administered after 24 h to allow for macrophage adherence.

OxLDL uptake by hMDMs and NP cellular association

To measure AM NP efficacy at inhibiting oxLDL uptake, hMDMs were incubated with 5 μg/mL oxLDL (1 μg/mL DiO labeled, 4 μg/mL unlabeled) and 10^{-6} M or 10^{-5} M AM NPs in RPMI 1640 with 10% FBS for 24 h. To measure cellular association of NPs, hMDMs were incubated with 10^{-6} M NPs with 1.5% shell amphiphile labeled with AF680 in RPMI 1640 with 10% FBS for 24 h. hMDMs were removed from plates by vigorous pipetting in cold PBS with 2mM EDTA, washed with PBS, centrifuged and fixed in 1% paraformaldehyde. To measure foam cell formation, hMDMs were incubated with 50 μg/mL oxLDL and 10^{-5} M AM NPs in RPMI 1640 with 10% FBS for 24 h before fixation in 4% paraformaldehyde. Cells were washed with 60% isopropanol and stained with 3mg/mL Oil Red O in 60% isopropanol and counterstained with Hoechst 33342.

Flow cytometry

Uptake of fluorescently labeled oxLDL (DiO) and cellular association with fluorescently labeled NPs (AF680) were quantified using a Gallios flow cytometer (Beckman Coulter). A minimum of 10,000 macrophages per sample were collected, and quantified using the geometric mean fluorescence intensity (MFI) of either NP or oxLDL fluorescence associated with the hMDMs using FloJo software (Treestar). Results are the mean of three independent experiments with two technical replicates per experiment. Data is presented as % oxLDL uptake inhibition, which was calculated using the following formula: $\%\ oxLDL\ uptake\ inhibition = 100 - 100 * \frac{MFI\ of\ AM\ containing\ condition}{MFI\ of\ oxLDL\ control}$.

Microscopy

After treatment with fluorescently labeled oxLDL and NPs, hMDMs were fixed and counterstained with Hoechst 33342 in a Labtek slide chamber. Cells were imaged on a Leica TCS

SP2 confocal microscope using a 63x oil immersion objective. Oil Red O stained hMDMs were imaged on a Nikon Eclipse TE2000S using a 40x objective.

NP inflammatory response

To measure the inflammatory response to AM NPs, hMDMs were incubated with 10^{-5} M AM NP in RPMI 1640 with 10% FBS for 24 h. Cell culture supernatant was collected for IL-8 cytokine quantification using ELISA (Biolegend) and RNA was isolated for quantitative gene expression studies.

Gene expression studies using quantitative real-time PCR (qRT-PCR)

RNA was extracted by RNeasy Plus Mini Kit with Qiashredder columns (Qiagen) following the kit instructions. RNA concentrations were determined on a Nanodrop 2000c and brought to equivalent concentrations with nuclease free water. RNA was reverse transcribed to cDNA with High Capacity cDNA Kit (Life Technologies) using a RapidCycler thermal cycler (Idaho Technology). Real-Time PCR was performed on a Lightcycler 480 (Roche) with Fast SYBR Green Master Mix (Life Technologies) for 40 cycles and a melting curve. Fold change was analyzed using the ΔΔCt method with endogenous controls (ACTB and GAPDH) relative to a basal condition. Primer sequences are available in supplementary materials.

Cytokine secretion quantification

Sandwich enzyme linked immunosorbant assays (ELISAs) were used to quantify protein secretion from hMDMs. IL-8 ELISA kits were purchased from Biolegend and the protocol followed accordingly.

Statistical analysis

Results are presented as mean ± standard error of the mean (S.E.M.) and data evaluated by one-way ANOVA and post-hoc Tukey's test for comparisons between multiple conditions. A *p*-value of 0.05 or less was considered statistically significant.

Results

NP Compositions

NPs were fabricated from AM with variable cores, modifying the amount of vitamin E. Control NPs, with no expected bioactivity, were created from PS-*b*-PEG shells and PS cores (PS-PEG[PS]). AM NPs created with flash nanoprecipitation have a larger size than AM micelles. AM micelles have an average hydrodynamic diameter (D_h) of 22 nm while AM NPs have an average D_h of 230nm and exhibit narrow size distributions (PDI). PS-PEG[PS] NPs are significantly smaller than AM NP due to the increased hydrophobicity of PS relative to M_{12} and VE. NP composition, sizes and PDI are listed in **Table 3.1**. AF680 labeling of 1cM and PS-*b*-PEG was found to be quantitative and incorporation of AF680 amphiphiles into NPs did not significantly alter their size or PDI.

Table 3.1. NP composition, size and PDI as determined by DLS. The naming convention used for NPs is shell[core].

Nanoparticle	Shell	Core	Size (D_h)	PDI
AM[M_{12}]	$^{[-1]}M_{12}P_{5K}$	M_{12}	246 ± 8 nm	0.159 ± 0.023
AM[M_{12}/VE]	$^{[-1]}M_{12}P_{5K}$	50:50 M_{12}:Vitamin E	236 ± 5 nm	0.108 ± 0.027
AM[VE]	$^{[-1]}M_{12}P_{5K}$	Vitamin E	227 ± 4 nm	0.098 ± 0.020
PS-PEG[PS]	PS-*b*-PEG	PS	138 ± 2 nm	0.208 ± 0.010

NP bioactivity

Figure 3.4 shows the uptake inhibition potential of the NP formulations. Variation in the core material of the AM NPs did not significantly affect their ability to reduce oxLDL uptake at 10^{-5}M as there was no statistical difference between M_{12}, VE and M_{12}/VE core AM NPs. AM NP were

able to inhibit approximately 80% of oxLDL uptake, even in the presence of 10% serum. However, at 10^{-6}M NP concentration, the 100% VE core NPs had a significant reduction in bioactivity and oxLDL inhibition potential. PS NPs minimally inhibited oxLDL uptake at both concentrations and were found to not be significantly different than cells treated only with oxLDL.

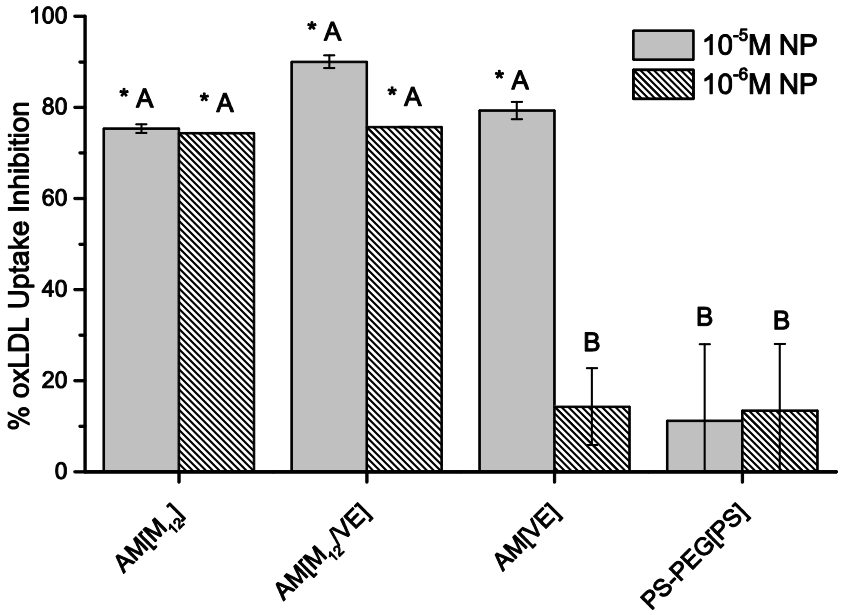

Figure 3.3. OxLDL uptake inhibition by NPs in hMDMs. AM NPs with M_{12} cores were most effective at preventing oxLDL uptake while AM[VE] lost efficacy at lower concentrations. hMDMs were co-incubated with 5 µg/mL oxLDL and 10^{-5}M or 10^{-6}M NPs for 24 h. Treatments with the same letter are not statistically significant from one another and the asterisk (*) indicates statistical significance ($p < .05$) from the control (no AM, oxLDL only).

NP cellular association

AM NPs with M_{12} in the core displayed high levels of association with hMDMs and were readily internalized. AM NPs with 100% VE in the core were internalized to a lesser extent. PS-PEG[PS] NPs were not significantly internalized by the cells. Even cells that did interact with PS-PEG[PS] NPs exhibited high levels of oxLDL uptake. The quantification of cellular internalization of

NPs in all hMDMs is shown in **Figure 3.5A**. Cells that internalized M_{12} core NPs had minimal oxLDL uptake while cells that internalized AM[VE] or PS-PEG[PS] had similar high levels of oxLDL uptake (**Figure 3.5 B**). Representative images of hMDMs treated with oxLDL and NPs are shown in **Figure 3.5 C and D**.

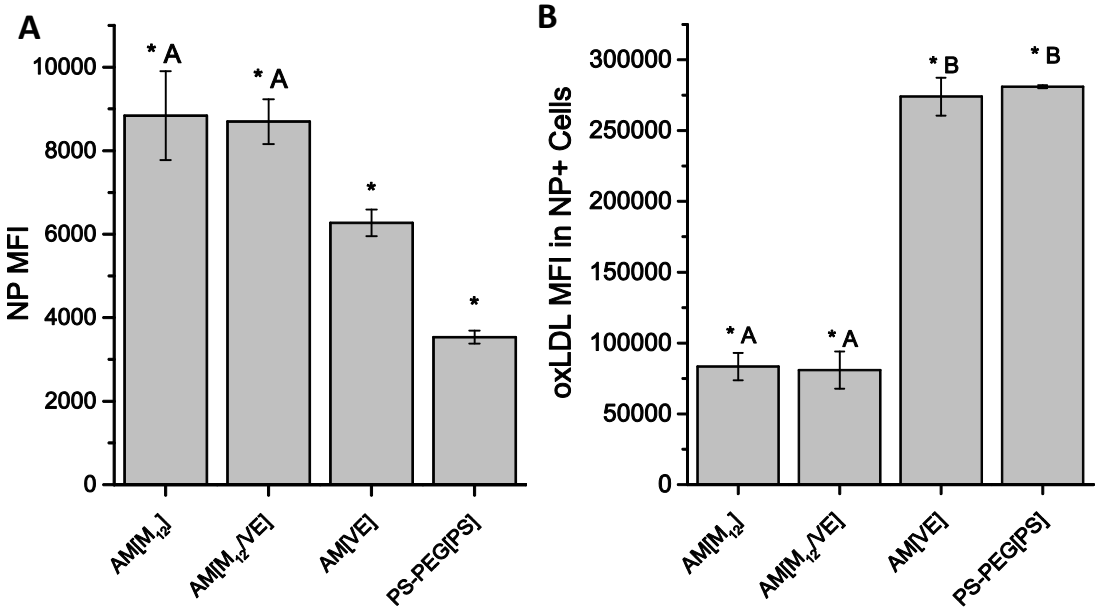

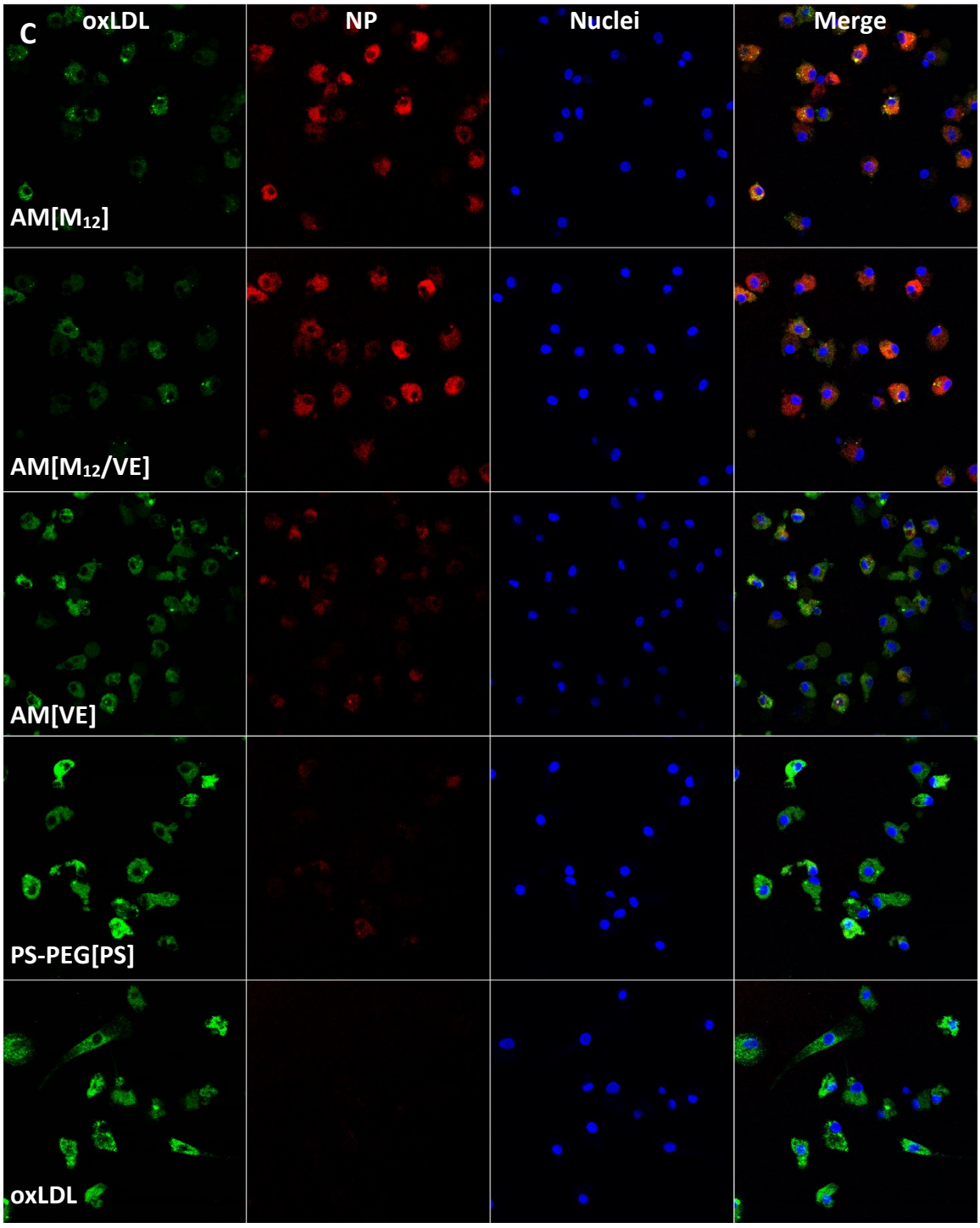
C
oxLDL
NP
Nuclei
Merge
AM[M12]
AM[M12/VE]
AM[VE]
PS-PEG[PS]
oxLDL

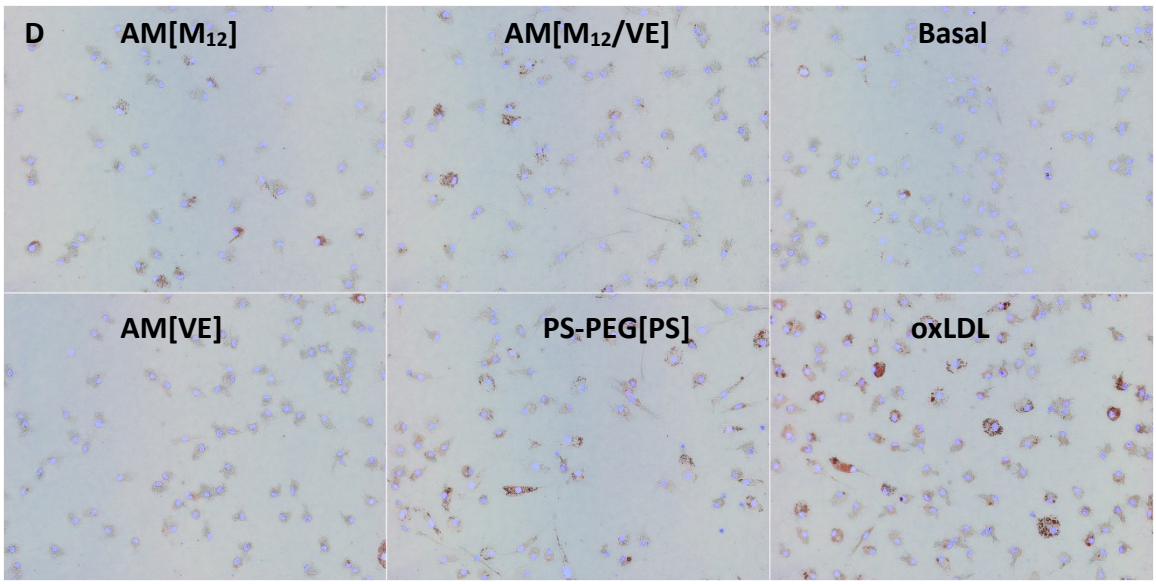

Figure 3.4. Cellular association of NP with hMDMs and oxLDL uptake inhibition. A) AM NPs had significantly higher levels of cellular internalization relative to PS-PEG[PS] NPs. M_{12} in the core of the NP led to more cellular association than VE core NPs. B) oxLDL uptake in cells that internalized NPs. Cells positive for NP with M_{12} in the core had much lower levels of oxLDL uptake than AM[VE] and PS-PEG[PS] NP positive cells. C) Representative images of hMDMs after treatment with oxLDL (green) and AF680 labeled NPs (red). Nuclei were counterstained with Hoechst 33342 (blue). hMDMs were co-incubated with 5 μg/mL oxLDL and 10^{-6}M NPs for 24 h. D) hMDMs stained with Oil Red O to indicate transition to the foam cell phenotype. Foam cell development mirrors levels of oxLDL uptake for different treatments. hMDMs were co-incubated with 50 μg/mL oxLDL and 10^{-5}M NPs for 24 h then stained with Oil Red O. Treatments with the same letter are not statistically significant from one another and the asterisk (*) indicates statistical significance ($p < .05$) from the control (no AM).

Gene regulation

Inflammation was evaluated in hMDMs by assessing gene expression and cytokine secretion following treatment with the NPs with different bioactive cores. qRT-PCR was used to

measure expression changes in hMDMs treated with NPs for an array of genes that modulate inflammation (IL-1β, IL-6, IL-8, IL-10, TNFα, NFκB1, MCP-1, MMP9), oxLDL uptake (CD36, SRA1) and lipid trafficking (NR1H3, PPARγ, ABCA1). The fold change in mRNA levels is shown in **Figure 3.6**.

NPs with M_{12} in the core exhibited higher levels of pro-inflammatory gene upgregulation, notably IL-1β, IL-6 and IL-8. M_{12} cores also had the effect of downregulating scavenger receptor expression for CD36 and SR-A1. oxLDL had a similar gene regulation profile to M_{12} containing NPs with the 100% M12 core NPs causing the greatest downregulation. PS[PS] NPs did not exhibit any significant gene changes. Vitamin E core NPs elicited basal, low levels of inflammatory gene expression whereas the M_{12}/VitE core NPs had the same gene regulation pattern as the 100% M_{12} core NPs.

		AM[M_{12}]	AM[M_{12}/VE]	AM[VE]	PS-PEG[PS]
Inflammation markers	**IL-1β**	642	631	5	-1
	IL-6	30	42	16	2
	IL-8	79	96	2	-1
	IL-10	-1	-1	-1	1
	TNFα	4	4	3	1
	NFκB1	2	1	1	1
	MCP-1	2	4	4	2
	MMP9	5	7	1	1
Scavenger receptors	**CD36**	-10	-7	-2	-2
	SRA1	-14	-8	-2	-2
Lipid transport	**NR1H3**	-3	-2	-1	1
	PPARγ	1	1	-3	-2
	ABCA1	-5	-3	-3	-2

Figure 3.5. Gene expression changes after treatment of hMDMs with NPs. M_{12} core NPs highly increased inflammatory gene expression while downregulating scavenger receptors. hMDMs were incubated with 10^{-5}M NP for 24 h. Data is presented as fold change relative to untreated cells and was normalized using GAPDH and β-actin as endogenous controls. Positive numbers (green) represent gene upregulation and negative (red) represent gene downregulation.

Cytokine secretion

While qRT-PCR is highly sensitive to changes in gene expression and allows for parallel assay of numerous genes, mRNA translation does not always correlate to protein transcription.

To evaluate the correlation between qRT-PCR expression patterns and protein secretion, ELISAs were used to quantitatively measure cytokine secretion. IL-8 was chosen as a representative protein as it was consistently highly upregulated and is necessary for monocyte recruitment [19]. The secretion profile of the inflammatory cytokine, IL-8, following differential treatment of hMDMs with the NP conditions is graphed in **Figure 3.7**. The AM NPs with M_{12} in the core significantly increased secretion of the inflammatory cytokine. While the 50% M12 and 50% VE co-core NPs caused lower levels of IL-8 secretion than the 100% M12 core NPs, these were not significant from one another. VE core NPs did not have an increase in IL-8 secretion that is significant relative to basal cells. PS-PEG[PS] NPs also do not have an effect on IL-8 production.

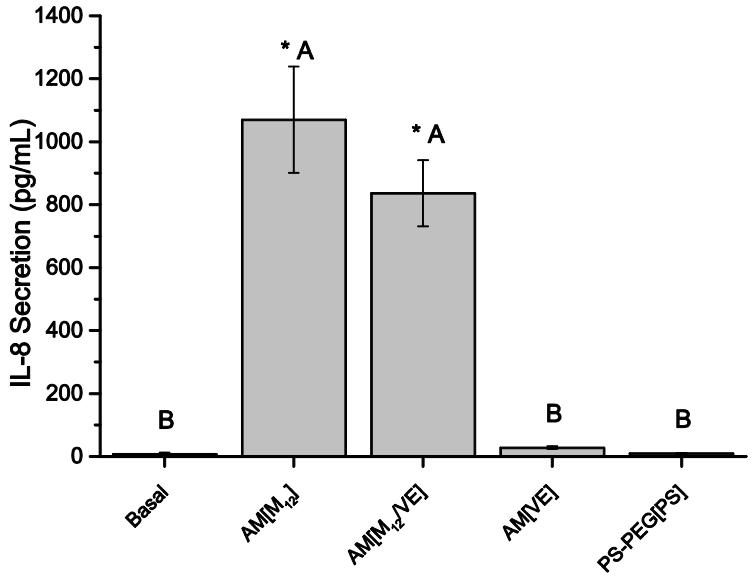

Figure 3.6. IL-8 secretion from hMDMs after treatment with NPs. Trends mirror qRT-PCR results with AM[M_{12}] and AM[M_{12}/VE] highly increasing IL-8 secretion. hMDMs were incubated with 10^{-5}M NP for 24 h. Treatments with the same letter are not statistically significant from one another and the asterisk (*) indicates statistical significance ($p < .05$) from the control (basal cells).

Discussion

Molecular interventions to block lipid uptake and the ensuing inflammatory phenotype are among the possible strategies for the inhibition of plaque development in atherosclerosis [5, 10, 13, 15, 231]. While the AM micelle formulation has been demonstrated to inhibit oxLDL uptake *in vitro*, it is not ideal for *in vivo* applications as micelles often exhibit relatively short half-lives due to the natural thermodynamic dissolution and hydrophobic partitioning [125]. Using flash nanoprecipitation, the Moghe laboratory and collaborators have created serum-stable anti-atherogenic NPs from AMs, which can further enhance *the* therapeutic utility of AMs *in vivo*. The primary NP formulation is able to stabilize the AMs with a hydrophobic core thereby extending the circulation half-life of AMs. In this work, a 2nd generation of NPs was envisioned to enhance anti-atherogenic activity of these serum-stable particles by minimizing inflammation and maximizing bioactivity (inhibition of oxLDL uptake).

The development of non-inflammatory AM NPs is critical to their success as a viable therapeutic. FNP remains an attractive way of synthesizing NPs due to the consistent size of NPs generated and the narrow, unimodal size distribution (**Table 1**). As size is a critical factor for internalization by macrophages, being able to generate consistently sized materials with a narrow size distribution is important for process scale up and clinical studies. Increasingly hydrophobic molecules used for the core can lead to smaller NPs due to reaching supersaturation faster and having more nucleation sites. It can also lead to more stable NPs, with individual unimers having slower release kinetics from the particle to a binding domain. The larger size of nanoparticles relative to micelles protects them from renal filtration, which has a size cutoff of ~8 nm, enabling longer circulation times [255]. However, the NP formulation may also trigger an immune response from the macrophages they are designed to target, making inflammation a critical aspect to consider in the design and development of nanoscale therapeutics [244, 245].

AMs alone were found to be highly tolerated in a maximum tolerated dose study, with an LD_{50} of >2000 mg/kg (supplementary data). This translates to an approximate serum concentration of $5*10^{-3}$ M immediately after dosing, 500 fold higher than used for *in vitro* tests. The high cytocompatibility of the AMs is most likely due to synthesis from non-cytotoxic, biocompatible building blocks: linear sugar, lauryl groups and PEG. The high upper dosing limit can enable concentrated dosing, but incorporation into a NP can drastically change the systemic response.

In this work an array of NPs were fabricated with different core and shell materials to evaluate both the anti-atherogenic and anti-inflammatory capabilities of the NPs. Anti-atherogenic inhibition of oxLDL uptake was evaluated and demonstrated that the core of the NP is important for bioactivity. NPs with 100% VE cores lost a significant portion of bioactivity when tested at the lower concentration (10^{-6} M), while NPs containing M_{12} in the core were effective at inhibiting ~80% of oxLDL uptake at both concentrations. M_{12} was originally chosen for incorporation into the NP core as it was the hydrophobic portion of the bioactive AM, $^{[-1]}M_{12}P_5$, and had increased miscibility when formulated in this way. It is hypothesized that the M_{12} hydrophobic core partially contributes to the blockage of the scavenger receptor interaction with oxLDL which may explain why the 100% vitamin E NPs are less efficacious at the lower concentration [256]. The PS [PS] NP formulation contains neither the anti-atherogenic or anti-oxidant molecules in the shell or core and, as expected, does not contribute to inhibition of oxLDL uptake.

The cellular association of AM NPs with hMDMs appears to be directly correlated to oxLDL inhibition. AM NPs with M_{12} had high levels of internalization by hMDMs) whereas VE core NPs were internalized less. This is consistent with previous work which suggests that M_{12} core NPs bind more readily to hMDMs through scavenger receptor SR-A1 [256]. Control PS-PEG[PS] particles were both ineffective at inhibiting oxLDL uptake and cellular internalization. Furthermore, even

cells with internalized PS-PEG[PS] NPs did not exhibit any oxLDL uptake. Despite the PEG shell surrounding the bioactive AM NPs, these elicit strong uptake behaviors in macrophages as demonstrated in this work and previous studies [232, 256]. Thus, specific cellular delivery of other therapeutic drugs that have limited targeting capability (lipid efflux enhancers, antioxidants, or anti-inflammatory agents) to cells with high levels of lipid accumulation could be achieved with the AM NP formulation with the goal of further reducing their atherogenic phenotype.

Most plaque macrophages have the anti-inflammatory (M2) phenotype, yet inflammatory signaling is required for disease progression [10, 11]. Reducing this signaling or preventing further exacerbation of it remains a therapeutic challenge. In this work 1st generation AM NPs utilizing M_{12} for the hydrophobic core were found to induce the inflammatory phenotype in human macrophages. IL-1β, IL-6 and IL-8, which are classical markers of macrophage activation were upregulated as was secretion of IL-8, indicating a potential transition from the alternative M2 to a more M1-like activated phenotype [12]. This could then lead to further monocyte recruitment and macrophage differentiation. The high charge density of the M_{12} in NPs may be the stimulus for this inflammation and 50% vitamin E in the core was not able to mitigate inflammatory gene upregulation and subsequent cytokine secretion caused by the M_{12}. Interestingly, the scavenger receptors responsible for oxLDL uptake, CD36 and SR-A1, were downregulated by the M_{12} core NPs. This is consistent with previous work which revealed the AM NPs ability to downregulate surface expression of scavenger receptors on hMDMs [256]. As expected, the 100% vitamin E core AM NPs were able to reduce inflammatory gene expression back to basal levels and minimize secretion of IL-8; however, they lack the ability to downregulate scavenger receptor expression. While the M_{12} core may contribute to inflammation it also plays a key role in scavenger receptor down regulation, thought to prevent oxLDL uptake. Thus a

combination particle with smaller fraction of M_{12} and larger fraction of vitamin E or M_{12} with a more potent anti-inflammatory agent can be envisioned.

Future studies could examine the relationship between structure of the amphiphile or core hydrophobe and the resulting inflammatory phenotype. Quantitative structure activity relationships were previously developed to determine AM molecular features that contributed to bioactivity [222]. A similar approach could be envisioned based on a NP library that modulates core materials and properties. Additionally, the intracellular signaling mediators of the inflammatory response could be investigated to expose the precise pathways being triggered, enabling a new generation of rationally designed non-inflammatory NPs or a novel target for anti-inflammatory therapeutics.

Conclusion

To more effectively treat atherosclerosis, anti-atherogenic therapeutics must be able to not only minimized lipid accumulation but also minimize inflammation. A 2nd generation of AM NPs was fabricated, incorporating the antioxidant vitamin E into the core. oxLDL uptake, cellular association and intrinsic ability to stimulate inflammation were found to be dependent on NP core composition. While vitamin E core NPs were less efficacious at inhibiting oxLDL uptake at lower concentrations, they were much less inflammatory than their M_{12} counterpart NPs. AM NPs utilizing M_{12} for the hydrophobic core were more effective at inhibiting oxLDL uptake lower concentrations and downregulating scavenger receptor gene expression but induced cellular inflammation. A combination core NP composed of a small fraction of M_{12} and larger fraction of vitamin E may be the most effective anti-athrogenic therapeutic option encompassing both the oxLDL inhibiting/scavenger receptor downregulating potential of the M_{12} with the anti-inflammatory capabilities of vitamin E. These studies provide a NP optimized framework for future

in vivo studies to better elucidate the most effective NP compositions and determine biological efficacy.

Supplementary data

Primer sequences

Primer sequences were designed by Harvard Primer Bank or Primer-BLAST and synthesized by Integrated DNA Technology. Primer efficiency was calculated using 4x dilution series of cDNA from hMDMs. All primers used exhibited >95% efficiency with a single melting peak corresponding to a unique amplicon. Genomic DNA contamination was monitored by including a reverse transcription reaction without reverse transcriptase.

Table S3.1. Primer sequences used for qRT-PCR

Gene	Forward Primer	Reverse Primer
Human MMP9	GTC CAC CCT TGT GCT CTT CCC TG	CGC AGG CCC CAG AGA TTT CGA CT
Human ACTB	CACAGAGCCTCGCCTTTGCCGATC	ACGAGCGCGGCGATATCATCATC
Human GAPDH	ATGGGGAAGGTGAAGGTCG	GGGGTCATTGATGGCAACAATA
Human PPARG	CATTACGGAGAGATCCACGG	CCAGAAAGCGATTCCTTCAC
Human SR-A1	GCA GTG GGA TCA CTT TCA CAA	AGC TGT CAT TGA GCG AGC ATC
Human CD36	GCC AAG GAA AAT GTA ACC CAG G	GCC TCT GTT CCA ACT GAT AGT GA
Human IL-10	CTC ATG GCT TTG TAG ATG CCT	GCT GTC ATC GAT TTC TTC CC
Human IL-6	AAC CTG AAC CTT CCA AAG ATG G	TCT GGC TTG TTC CTC ACT ACT
Human NR1H3	CAT GGC ACC AGA TCC CCA TAG	GGG TAG CTG TTT AGC AAA GTC AA
Human TNFα	ATG AGC ACT GAA AGC ATG ATC C	GAG GGC TGA TTA GAG AGA GGT C
Human Il-1B	CTC GCC AGT GAA ATG ATG GCT	GTC GGA GAT TCG TAG CTG GAT
Human MCP-1	CAG CCA GAT GCA ATC AAT GCC	TGG AAT CCT GAA CCC ACT TCT
Human IL-8	ACT GAG AGT GAT TGA GAG TGG AC	AAC CCT CTG CAC CCA GTT TTC
Human ABCA1	AACTCTACATCTCCCTTCCCG	CTCCTGTCGCATGTCACTCC

Systemic toxicity methods

To determine the maximum tolerated dose (MTD) of AM, a limit test was used for the highest dose possible, 2000mg/kg. Five male BALB/c mice, 12 weeks old, with an average weight of 25 g and approximately 1.8 mL blood volume were used for the initial limit test. Mice were dosed intraperitoneally once with 2000 mg/kg AM, $^{[-1]}M_{12}P_{5k}$, at 30 mg/mL in 0.9% sterile buffered saline. Injections were staggered at 48 h intervals to monitor health. Saline controls were also injected due to the large bolus (1.7 mL) injection. After administration, mice were monitored every 3-6 h for signs of morbidity for the first 48 h and twice per day thereafter until day 14. Monitoring was performed according to the FDA guidance on Single Dose Acute Toxicity Testing for Pharmaceuticals [257]. At 14 days post-injection, all mice were sacrificed by cardiac puncture and examined by gross necropsy.

Systemic toxicity results

AMs exhibited minimal systemic toxicity in mice. Saline mice exhibited normal behavior after 2 h and AM treated mice displayed signs of mild peritonitis 2 h post injection. Peritonitis was diagnosed by hunched posture, lethargic behavior, and lack of nesting. AM treated mice all had full recovery after ~72 h and had no observable physical differences from saline controls: they were active, groomed, and chewed nestlets to form bedding.

Upon necropsy, there were no visible differences between AM treated mice and saline controls. During dissection, no signs of tissue damage were observed as evidenced by necrosis or connective tissue growths. Thus, the LD_{50} of $^{[-1]}M_{12}P_{5k}$ is classified as >2000mg/kg.

Chapter 4 - Amphiphilic macromolecule nanoparticles mitigate atherosclerosis and inflammation in ApoE$^{-/-}$ mice

Abstract

Atherosclerosis is triggered by the progressive buildup of lipid rich plaques within arterial walls, and is further escalated by the coupled cascade of atherogenesis and inflammation. Amphiphilic macromolecules (AMs) formulated into serum-stable nanoparticles (NPs) were conceived to inhibit oxidized lipid uptake by macrophages, minimizing inflammatory signaling and plaque progression. In this study, we evaluated a second generation of nanoparticles, incorporating cores comprised of atheroprotective bioactive macromolecules and antioxidant molecules, within an atherosclerotic mouse model *in vivo*. ApoE$^{-/-}$ mice, fed a high fat diet for 16 weeks were dosed repeatedly with AM NPs. The ability of AM NPs to localize to atherosclerotic lesions was examined with live and *ex vivo* fluorescent imaging. AM NPs exhibited long circulation half-lives of ~27 h and localized to areas of plaque growth in the aortic arch. Lesion-specific binding of the AM NPs principally occurred through activated endothelial cells and caused a downregulation of their activated phenotype in treated mice. Additionally, the ability of AM NPs to inhibit plaque progression was determined by examining occlusion, lipid accumulation and inflammation. AM NPs were effective at reducing inflammatory signaling and plaque formation in the neointimal lining of the artery, which correlated with a decrease in plaque size and lipid burden. Taken together, these findings highlight the promise of AMs as a molecular tool for tracking and therapeutic management of lipid rich lesions *in vivo*.

Introduction

Cardiovascular disease is responsible for 1 out of every 3 deaths in the US [258]. Atherosclerosis, the primary pathology leading to this condition, is a disease defined by the buildup of lipid filled plaques within arterial walls. Chronically high LDL cholesterol levels in circulation result in LDL deposition and oxidation (oxLDL) within arterial walls where it stimulates endothelial inflammation, which results in the recruitment of circulating monocytes by upregulating the expression of monocyte-specific adhesion molecules on the endothelia. These monocytes differentiate into macrophages that exhibit unregulated uptake of oxLDL [6, 22]. Inflammation is crucial to the progression of this disease as inflammatory signaling through cytokines and surface molecules from macrophages in response to oxidized lipid burden further exacerbates both endothelial inflammation and monocyte recruitment [192]. Accumulation of the lipid laden macrophages result in plaques that progressively assume necrotic cores protected by neointimal fibrous caps. Rupture of these caps causes thrombi that can occlude arteries leading to MI or stroke.

Statins (HMG CoA reductase inhibitors) are effective at reducing these endpoints through reduction in LDL cholesterol levels, however they do not have direct effect on the atherosclerotic lesions and thus are unable to address locally deposited lipids in arteries [58]. A targeted system to mitigate local vascular inflammation and lipid uptake at the lesion site could be an important part of a treatment strategy. Micelles have been used previously to target atherosclerosis, but suffered from rapid clearance [125]. Nonspecific micelles can be readily cleared by the body's inherent filters (renal and hepatic) and may have problems associated with off-target bioactivity [5]. Designing a nanosystem that incorporates preferential targeting with long circulation times could allow for more efficient therapeutic delivery.

Our lab has previously developed amphiphilic macromolecules (AM) as a therapeutic to inhibit oxLDL uptake in macrophages [105, 108, 126, 127, 144, 193-195]. Studies examining receptor binding demonstrated that the nanoassemblies have inherent affinity for the scavenger receptors responsible for oxLDL uptake [169, 193]. In an attempt to overcome limitations of micellar systems, AM were incorporated into kinetically stabilized nanoparticles (NPs) that displayed resistance to AM release and instability in serum-rich environments [232]. This process used flash nanoprecipitation, which involves the rapid mixing of an AM shell and a hydrophobic core molecule dissolved in an organic solvent with an aqueous stream through a confined chamber. This initiates nucleation of the hydrophobe followed by immediate stabilization of the core with a corona AM [90, 241, 259]. The hydrophobic core entraps the AM, preventing rapid dissolution caused by thermodynamic instabilities and thus limits sequestration within external hydrophobic moieties such as those in blood plasma proteins *in vivo*, thus extending the stability and residence times of AM NPs in circulation. Thus, in a physiologic environment, this could result in higher effective concentrations.

The AMs also possess scavenger receptor-binding affinity, which further enhances their retention at prospective inflammatory lesions that are rich in activated macrophages [232]. Recent work has found that the bioactive hydrophobe M_{12} is primarily responsible for this specific binding and has the ability to downregulate expression of scavenger receptors [256]. The development of M_{12} core AM NPs invites the possibility of a targeted nanosystem for site-specific localization and treatment of plaques. As ligands for scavenger receptors can also trigger basal inflammatory signaling upon occupancy and endocytosis, we hypothesized that high concentration nanoassemblies of M_{12} cores can elevate the intrinsic inflammatory profile of the AM nanoparticles [6]. *In vitro* studies support this premise as was presented in Chapter 3. Thus, the incorporation of other anti-inflammatory, anti-oxidant molecules into the bioactive AM NP

formulation can provide another avenue to tune the inflammatory profile of AM NPs while maintaining their anti-atherogenic potency.

Fortuitously, flash nanoprecipitation allows for the incorporation of multiple hydrophobic molecules into the core of NPs. Because lipid oxidation and the reactive oxygen species are a major initiator of inflammatory signaling, antioxidants are an attractive therapeutic candidate. The hydrophobic antioxidant Vitamin E (VE), has been theorized to be highly cardioprotective [72]. However, clinical studies using Vitamin E (VE) failed to show improvement in morbidity and mortality outcomes [72]. The lack of enhanced outcomes may have been possibly due to the barriers underlying specific delivery to lesion sites. To be efficacious at preventing LDL oxidation and reducing cellular activation, high concentrations of VE would need to be localized to areas of plaque formation. Thus, the incorporation of VE into AM NPs could provide a mechanism for enhanced delivery to lesions. We hypothesize that the anti-oxidant effect could be effective in at least two complementary ways: first by preventing the progressive oxidation of LDL (mildly oxidized LDL is sequestered by the matrix glycosaminoglycans of the vascular intima and released only upon extensive modifications and oxidation) and, second, by mitigating the inflammation that promotes further monocyte recruitment and macrophage differentiation [260]. The additional possibility exists that the VE could stabilize the inflammatory activation of existing or nascent lesions.

In vitro assays cannot reproduce the complex cellular signaling and inflammatory cascade that occurs in atherogenesis. To develop AM NPs as a viable therapeutic, an atherosclerotic animal model is necessary to determine their ability to target lesions and validate their anti-atherogenic and anti-inflammatory effects. The transgenic $ApoE^{-/-}$ mouse model is widely used for atherosclerosis research due to the rapid, spontaneous development of atherosclerotic lesions along the aortic tree with a high fat diet [261-263]. ApoE is critical for lipid metabolism and its

absence results in high plasma cholesterol levels due to impaired clearance of LDL and VLDL by LDLR and related receptors, leading to this pathology [264]. Lesions typically develop in regions of turbulent blood flow that results in high pressure vessel wall strain and low flow shear stress, predominantly the aortic arch at the bifurcation of the carotid arteries [265-269].

In the present study, AM NPs were fabricated with bioactive M_{12} and the anti-oxidant vitamin E. Atherosclerotic $ApoE^{-/-}$ mice were dosed intravenously with fluorescently labeled AM NPs over the course of 5 weeks. The biodistribution, pharmacokinetics and lesion-binding and retention of NPs were examined. The effect of AM NPs on atherogenesis, specifically neointima formation, inflammation signaling, lipid accumulation, and lesion morphology was evaluated. Specific cellular association and gene expression at the site of the lesions were monitored to understand the AM NP mechanisms of action and assess their therapeutic potential for atherosclerosis. Insights from this study will facilitate our understanding of *in vivo* AM behavior in a model of human disease and guide further development of AM nanomaterials as a translational therapeutic.

Materials and methods

Materials

All chemicals/materials were purchased from Sigma-Aldrich (Milwaukee, WI) or Fisher Scientific (Pittsburgh, PA) and used as received unless otherwise noted. 18 MΩ·cm resistivity deionized (DI) water was obtained using PicoPure 2 UV Plus (Hydro Service and Supplies - Durham, NC). The following items were purchased from the indicated vendors: 1.077g/cm^3 Ficoll-Paque Premium from GE healthcare (Pittsburgh, PA), RPMI 1640 from ATCC (Manassas, VA), macrophage colony stimulating factor (M-CSF) from PeproTech (Rocky Hill, NJ), FBS and AlexaFluor 680 carboxylic acid succinimidyl ester from Life Technologies (Grand Island, NY), unlabeled oxLDL from Biomedical Technologies Inc. (Stoughton, MA), 3,3'-dioctadecyloxacarbocyanine (DiO) labeled oxLDL from Kalen Biomedical (Montgomery Village, MD), and human buffy coats from the Blood Center of New Jersey (East Orange, NJ).

NP fabrication and characterization

AMs were synthesized as previously described [219]. Amphiphiles were fluorescently labeled by conjugating AlexaFluor 680 (AF680) carboxylic acid succinimidyl ester with amine terminated AM as previously described [232]. Kinetically assembled nanoparticles (NPs) were fabricated via flash nanoprecipitation [90, 232, 254]. Briefly, the amphiphile (with 5 mol % AF680 labeled) and the corresponding core hydrophobe were dissolved in tetrahydrafuran (THF) before being rapidly mixed with an aqueous stream in a confined chamber (Figure 4.1). NPs that were assembled were were then dialyzed into PBS for 24 h to remove residual THF and sterile filtered with a 0.45μm nylon filter. For AM NPs, $^{[-1]}M_{12}P_{5K}$ (hereafter referred to as AM) was used as the NP shell. The core was composed of mucic acid acylated with lauroyl groups (M_{12}), or M_{12} combined with α-tocopherol (VE) (50:50 weight ratio, M_{12}/VE). Control NPs were synthesized

using PS-*b*-PEG as the shell and polystyrene (PS) as the core. NP size and poly dispersity index (PDI) was determined by dynamic light scattering (DLS) using a Zetasizer Nano ZS (Malvern).

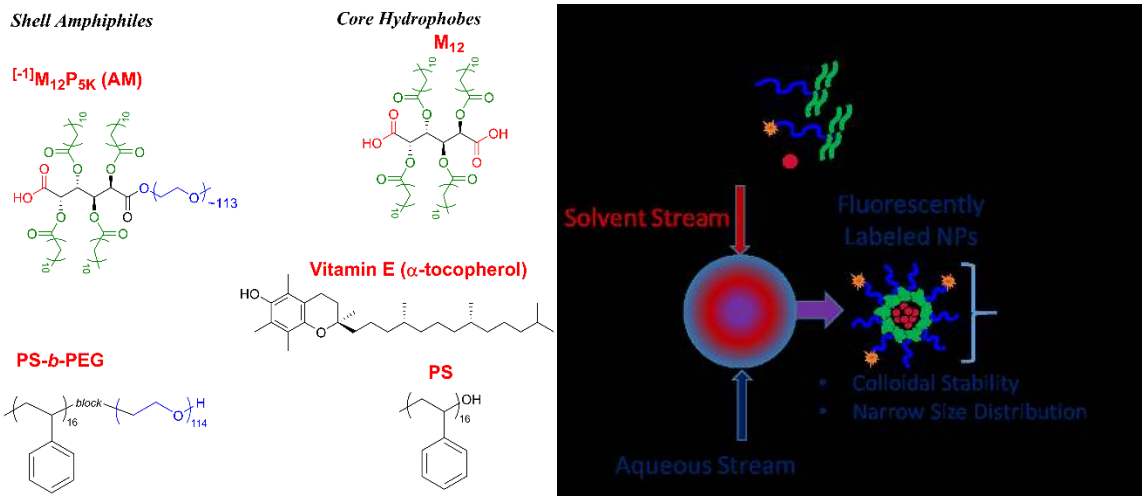

Figure 4.1. Materials for and method of NP fabrication. A) Structures of the amphiphilic shell molecules and core hydrophobes fabricated for the NP treatment groups. B) Flash nanoprecipitation process used to fabricate the nanoparticles.

In vitro validation of NPs

NP were evaluated for efficacy by measurement of oxLDL uptake inhibition and cellular association. Human monocyte derived macrophages (hMDMs) were cultured and exposed to oxLDL (5 µg/mL) and NPs (10^{-5} M) for 24 hours as previously described [222]. OxLDL uptake and NP cellular association were quantified using a Gallios flow cytometer (Beckman Coulter).

Animal care

4 week old B6.129P2-*Apoe*^{tm1Unc} (ApoE$^{-/-}$) and C57B/L6 mice purchased from Taconic were given free access to food and water. The Institutional Committees on Animal Care and Use at Rutgers University approved all procedures involving animals (protocol # 06-016). ApoE$^{-/-}$ mice were fed Harlan Teklad diet TD.88137, a Western diet (21% fat, 34% sucrose, and 0.2%

cholesterol), that results in rapid lesion development and atherosclerosis disease progression [270]. C57B/L6 mice were given standard chow diet.

Administration of NPs

For NP administration, mice were anesthetized with isoflurane and given tail vein injections (5 µL/g body weight) of NPs at $7.5*10^{-4}$ M. Mice were dosed a total of 4 times in 8 day intervals, beginning at 8 weeks after initiation of the high fat diet. (**Figure 4.2**). $ApoE^{-/-}$ treatment and no treatment groups had n=5, C57B/L6 had n=3.

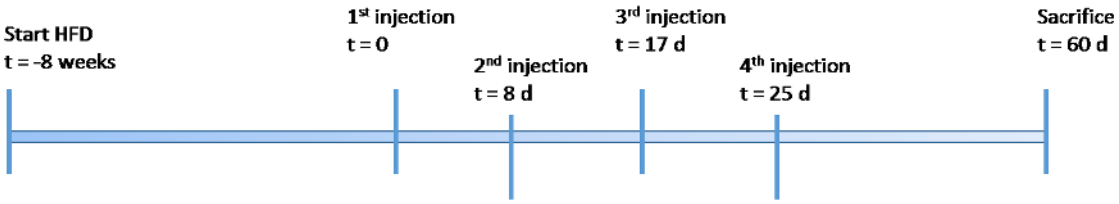

Figure 4.2. Administration regimen for NPs in $ApoE^{-/-}$ mice.

Animal imaging and blood collection

To determine biodistribution over time, mice were imaged live. For this, mice were anesthetized with 2.5% isoflurane by inhalation and imaged using a MultiSpectral FX Pro In Vivo Imager (Carestream) before NP administration and at 1, 2, 4, 8, 10, 18 and 26 days after the initial NP administration. Fluorescence images were taken with the following settings: Ex 650, Em 700, 30 s exposure with 10 s X-Ray exposure to visualize anatomy. Blood samples were withdrawn through the saphenous vein in heparinized capillary tubes prior to administration and at 1, 2, 4, 8, 10 and 18 d post initial injection. After collection, plasma was separated by centrifugation and frozen at -20°C for analysis. For measurements prior to the terminal timepoint, plasma was pooled for all animals within a given treatment group.

Animal euthanasia

At 8.5 weeks after initiation of treatment, mice were anesthetized with 2.5% isoflurane by inhalation and sacrificed by cardiac puncture and perfusion with phosphate buffered saline (PBS). The aorta, heart, liver, kidneys, lungs, intestines and adipose were excised and immediately imaged using a MultiSpectral FX Pro. The tissues were then preserved in RNALater (for gene expression analysis), preserved in formalin (for immunohistochemistry) or homogenized, strained, and stained (for flow cytometry). The aorta was divided into three sections for analysis; ascending aorta and aortic arch for immunohistochemistry, thoracic aorta for PCR and abdominal aorta for flow cytometry (**Figure 4.3**). Blood was allowed to clot for 30 minutes at room temp, and serum was separated by centrifugation before freezing at -20°C until quantification.

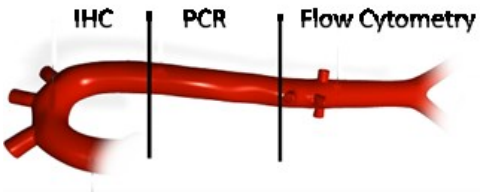

Figure 4.3. Dissection of aortas for *ex vivo* analysis. The ascending aorta and aortic arch were sectioned for immunohistochemistry, RNA was extracted from thoracic aorta for qRT-PCR and the abdominal aorta was homogenized for flow cytometry.

Gene expression

RNA was extracted from RNALater preserved tissues using the RNeasy Plus Mini Kit (Qiagen). Tissues were homogenized in lysis buffer with a TissueLyser LT bead mill followed by centrifugation through Qiashredder tubes before RNA isolation following the manufacturers protocol. RNA concentrations were normalized and cDNA was synthesized with the High Capacity RT kit (Life Technologies). Primer sequences (in supplementary methods) were obtained from Harvard Primer Bank, synthesized by Integrated DNA Technology. qRT-PCR was performed on a

Lightcycler 480 using Fast SYBR Green Master Mix (Life Technologies) for 40 cycles. C_t values were obtained by 2nd derivative maxima and fold change was calculated with ΔΔCt. GAPDH and B2m were used as endogenous controls and untreated $ApoE^{-/-}$ mice as the control basal condition for normalization.

NP cellular association and receptor expression using flow cytometry

Tissues were homogenized (Tissue Tearor) and then passed through a 40 µm cell strainer and washed with PBS. Solids were allowed to settle for 2 min and the cell suspension removed. Cells were blocked with PBS buffer containing 0.5% bovine serum albumin, 0.1% sodium azide, and 1% normal goat serum for 30 min. Following blocking they were incubated with labeled antibodies against CD68, VCAM1 and α-smooth muscle actin (Biolegend) for 1 hour at 4°C. After the incubation they were washed twice with PBS, incubated with CyTRAK Orange (eBioscience) for 30 min, fixed in 200 µL of 1% paraformaldehyde, and then quantified (10,000 cellular events per sample) using a Gallios flow cytometer (Bekman Coulter). Samples were quantified using the geometric mean fluorescence intensity (MFI) of intact cells with FloJo (Treestar).

NP pharmacokinetcs

To determine circulating NP levels, serum was measured for AF680 fluorescence at Ex 679/Em 705nm on a Tecan M200 Pro and normalized using a NP standard curve. For pharmacokinetic parameter determination, the half-life was calculated assuming a one-compartment model.

Aorta tissue preparation for imaging and immunohistochemistry

The ascending aorta and aortic arch were sectioned serially to examine plaque morphology and binding of AM NPs to lesions via microscopy. Aortas from treated mice were fixed in formalin and prepared for cryosectioning by immersion in 30% sucrose. Tissue was

embedded in OCT media (Tissue Tek), frozen and sectioned into 10 μm serial sections on a cryostat (Thermo Electron). Slides were imaged with an Olympus VS120. NP accumulation was evaluated on a Leica TCS SP2 confocal microscope using a 63x oil immersion objective following counterstaining with ProLong Gold with DAPI (Life Technologies).

Aortic cross sections were analyzed for lipid accumulation and markers of neointimal formation and inflammation. To visualize areas of lipid deposits, sections were washed in 60% isopropyl alcohol before staining with 3 mg/mL Oil Red O in 60% isopropyl alcohol and counterstaining with hematoxylin. To determine neointimal formation and levels of inflammation in tissue, sections were stained with rabbit polyclonal COX-2 and α-smooth muscle actin antibodies (Abcam). Briefly, sections were delipidized in xylene (9 min) and a decreasing series of alcohol (2 min each) for before neutralization with 3% H_2O_2, followed by blocking with goat serum (100% and 25% respectively) and streptavidin (Vector Labs) for 2 h at room temp. Sections were incubated with primary antibodies (1μg/mL COX-2, 0.4μg/mL α-SMA) in blocking buffer with biotin (Vector Labs) overnight at 4°C, then washed before secondary incubation with Vectastain Elite anti-rabbit IgG (Vector Labs). Staining was visualized with DAB peroxidase (Vector Labs) and counterstained with Mayers Hematoxalin for 3 m. Sections were imaged with an Olympus VS120.

Image analysis

Fluorescence images (mouse whole body and *ex vivo* organs) were quantified using ImageJ. The background (rolling ball radius = 50) from non-treated groups was subtracted from total fluorescence intensity, which was then normalized to area. Aortic cross sections were quantified for area using VS-AFW software (Olympus).

Statistical analysis

Results are presented as mean ± standard error of the mean (S.E.M.) and were evaluated by one-way ANOVA with post-hoc Tukey's test for comparisons between multiple conditions or Student's t test for individual comparisons. A *p*-value of 0.05 or less was considered statistically significant.

Results

AM NP characterization and *in vitro* validation

AM NPs were fabricated using FNP and exhibited monodisperse size distributions. AM NP composition, size and PDI are listed in **Table 4.1**. AM NPs were initially evaluated *in vitro* for cellular association and their ability to inhibit oxLDL uptake in hMDMs. Both the M_{12} and M_{12}/VE core AM NPs demonstrated the ability to inhibit oxLDL uptake (86-81%) and displayed strong association with the hMDMs, while PS-PEG[PS] NPs minimally inhibited oxLDL uptake and were not internalized by the majority of cells (supplementary **Figure S4.1 A and C**). Interestingly, even the cells with internalized non-bioactive PS-PEG[PS] NPs had high levels of oxLDL whereas those with the M_{12} containing core AM NPs exhibited very low oxLDL levels (**Figure S4.1 B**). This observation indicates that the AM NP anti-atherogenic bioactivity is not correlated with the degree or fate of NP internalization.

Table 4.1. AM NP treatments with dosing, AM NP composition, size and polydispersity index (PDI).

Mouse Strain	Treatment	Dosage	Shell	Core	Size (nm)	PDI
ApoE$^{-/-}$	AM[M_{12}]	5 µL/g	$^{[-1]}M_{12}P_{5K}$	M_{12}	310	0.248
ApoE$^{-/-}$	AM[M_{12}/VE]	5 µL/g	$^{[-1]}M_{12}P_{5K}$	50:50 M_{12}:Vitamin E	376	0.316
ApoE$^{-/-}$	PS-PEG[PS]	5 µL/g	PS-*b*-PEG	PS	177	0.258
ApoE$^{-/-}$	non-treated					
C57B/L6	non-treated					

NP biodistribution and pharmacokinetics

Post injection, AM and PS NPs exhibit homogenous body distribution and do not rapidly localize to specific organs (**Figure 4.4A-C**). A dilution series of AF680 labeled NPs was evaluated and exhibited fluorescence linearity over an AM NP 10^{-4}-10^{-9} M range and was used to quantify NP concentration in serum samples (**Figure 4.4D**). AM NP half-lives calculated from the first 8 days of serum concentrations are displayed in **Table 4.2**. PS NPs display significantly slower clearance than AM NPs, which is reflected in higher terminal serum NP concentrations (**Figure 4.4E**).

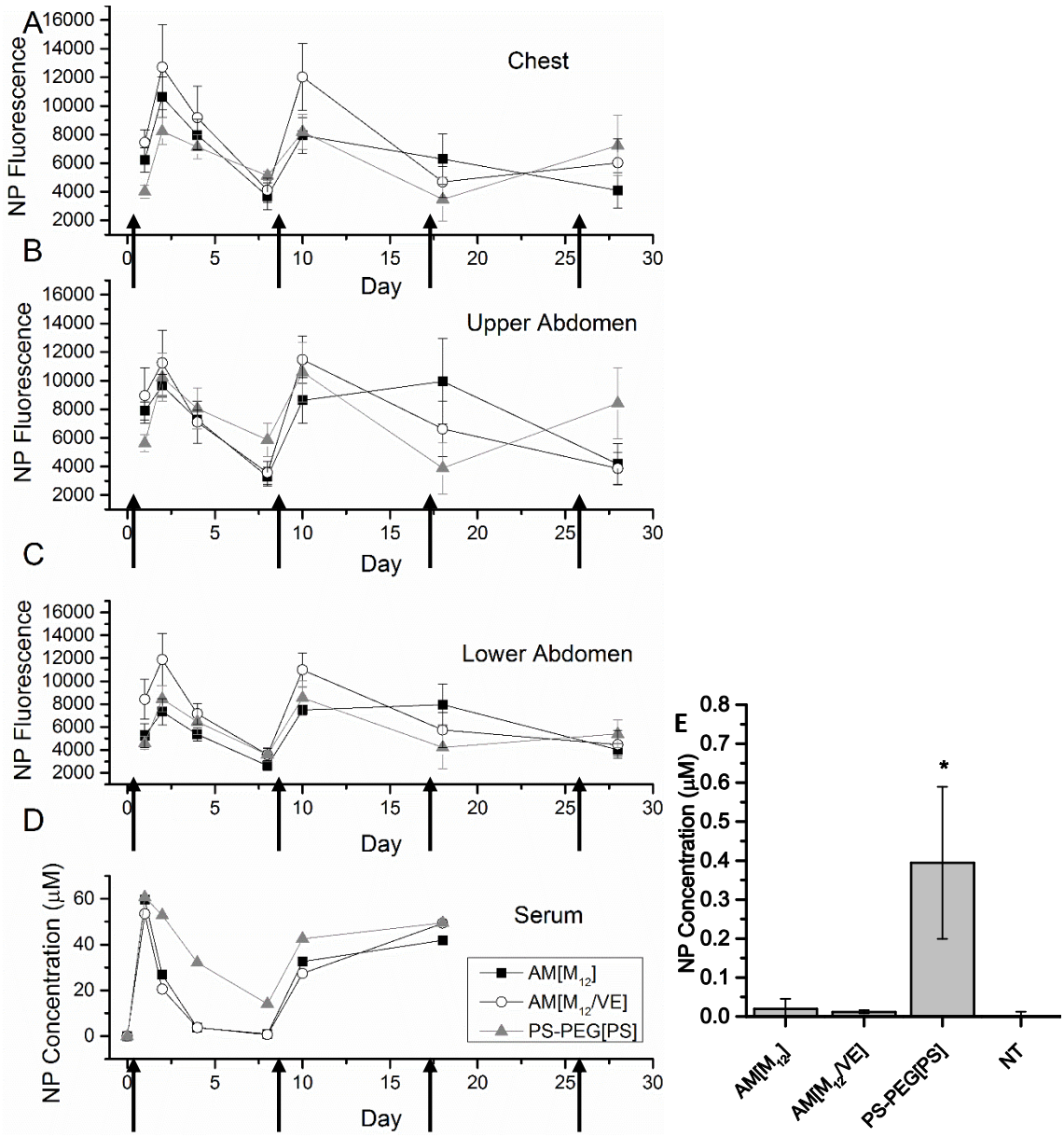

Figure 4.4. Biodistribution and pharmacokinetics. Tissue fluorescence from whole body images on days post-injection for A) chest, B) upper abdomen and C) lower abdomen. D) NP concentration in serum. A-D) Y-axis arrows indicate injection timepoints. E) Terminal (60 d post initial injection) serum NP concentrations indicating total clearance of AM NPs and residual PS NPs in circulation. Error bars represent standard error of the mean (S.E.M.). Asterisk (*) indicates statistical significance ($p < .05$) from the control (NT).

Table 4.2. Serum half-lives for NP formulations. PS NPs had significantly slower clearance from circulation.

Treatment	T1/2 (h)	R2
AM[M12]	29	0.93
AM[M12/VE]	27	0.97
PS-PEG[PS]	78	0.99

NP organ association

At the terminal timepoint (60 d post initial injection), organs were excised and imaged whole. Representative organ images are presented in **Figure 4.5A** and quantification of NP fluorescence is presented in **Figure 4.5B**. PS NP had significantly elevated levels of fluorescence accumulation compared to the AM NPs in most organs, especially the liver, spleen and kidneys. AM NPs showed low basal levels of accumulation in all organs quantified, with most of the fluorescence associated with AM NPs retained in the liver.

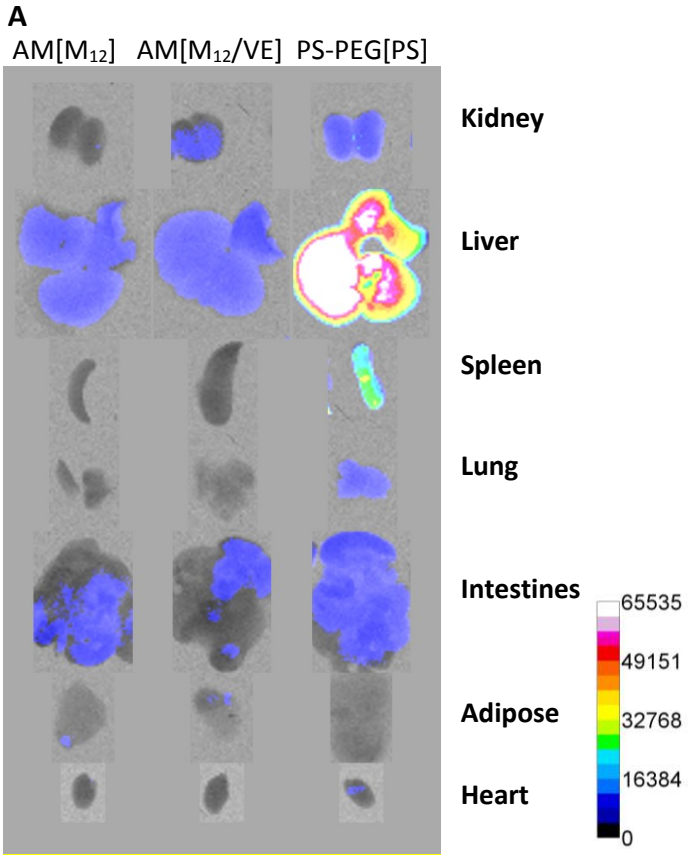
A
AM[M12]
AM[M12/VE]
PS-PEG[PS]
Kidney
Liver
Spleen
Lung
Intestines
Adipose
Heart
65535
49151
32768
16384
0

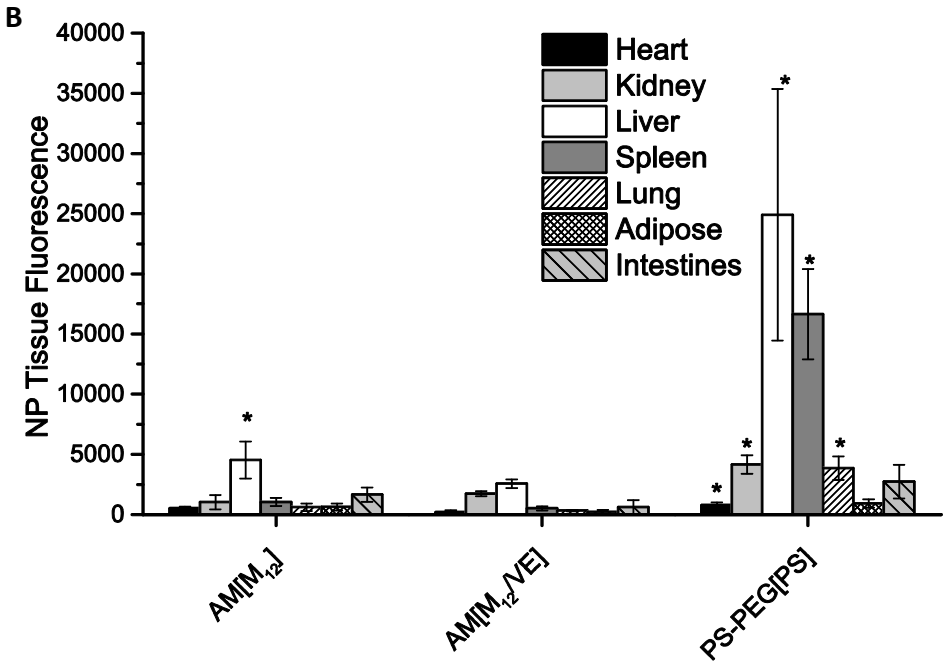
B
NP Tissue Fluorescence
40000
35000
30000
25000
20000
15000
10000
5000
0
Heart
Kidney
Liver
Spleen
Lung
Adipose
Intestines
AM[M12]
AM[M12/VE]
PS-PEG[PS]

Figure 4.5. Organ biodistribution. A) Representative organ images for each treatment group showing NP fluorescence overlayed on X-ray images. B) Quantification of the NP fluorescence associated with whole organ images with background subtraction (error bars represent standard error of the mean (S.E.M.). Asterisk (*) indicates statistical significance ($p < .05$) from the control (NT) for each organ.

NP association with aortic plaques

AM NPs were found to preferentially localize to areas of aorta with atherosclerotic plaque development. *Ex vivo* fluorescence images are shown in **Figure 4.6A**. The aortic arch and carotid branch points are areas of largest plaque development in the $ApoE^{-/-}$ mice and exhibit the highest concentration of AM NPs throughout the aortic tree (**Figure 4.6B**). AM[M_{12}] had the highest level of NP binding to the aorta as well as the aortic arch region.

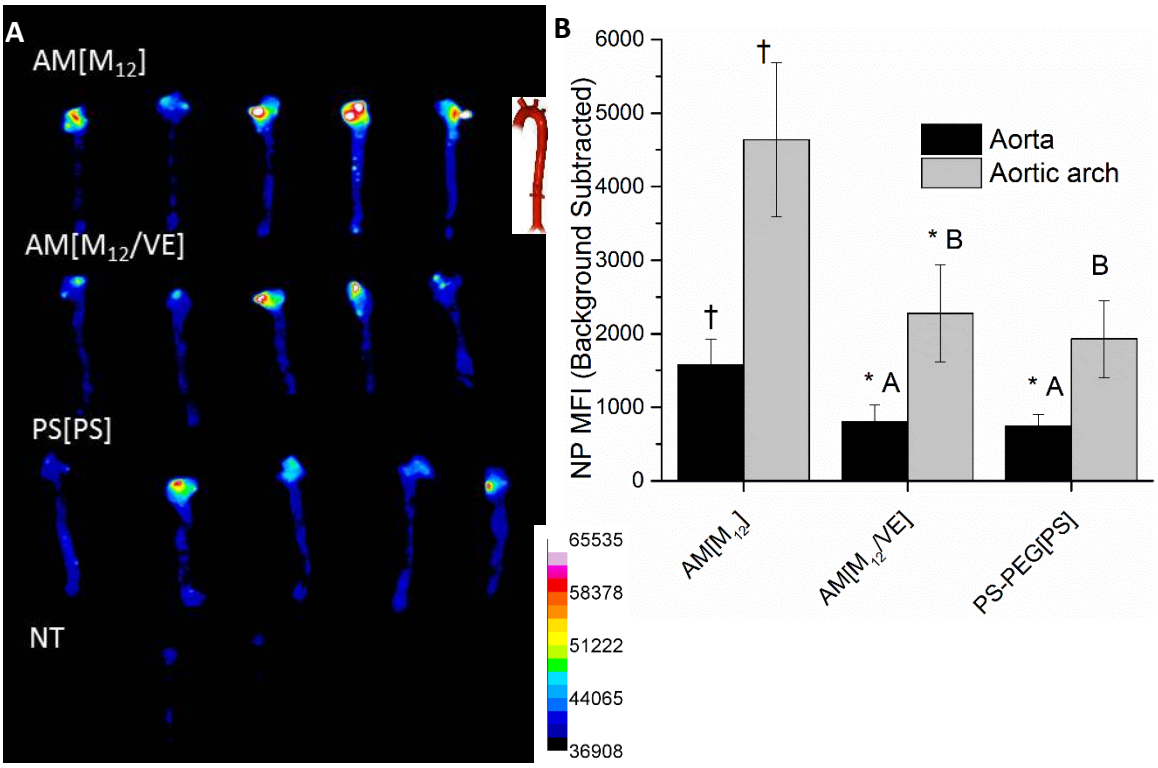
A
AM[M12]
AM[M12/VE]
PS[PS]
NT
65535
58378
51222
44065
36908
B
NP MFI (Background Subtracted)
6000
5000
4000
3000
2000
1000
0
Aorta
Aortic arch
†
†
* A
* B
* A
B
AM[M12]
AM[M12/VE]
PS-PEG[PS]

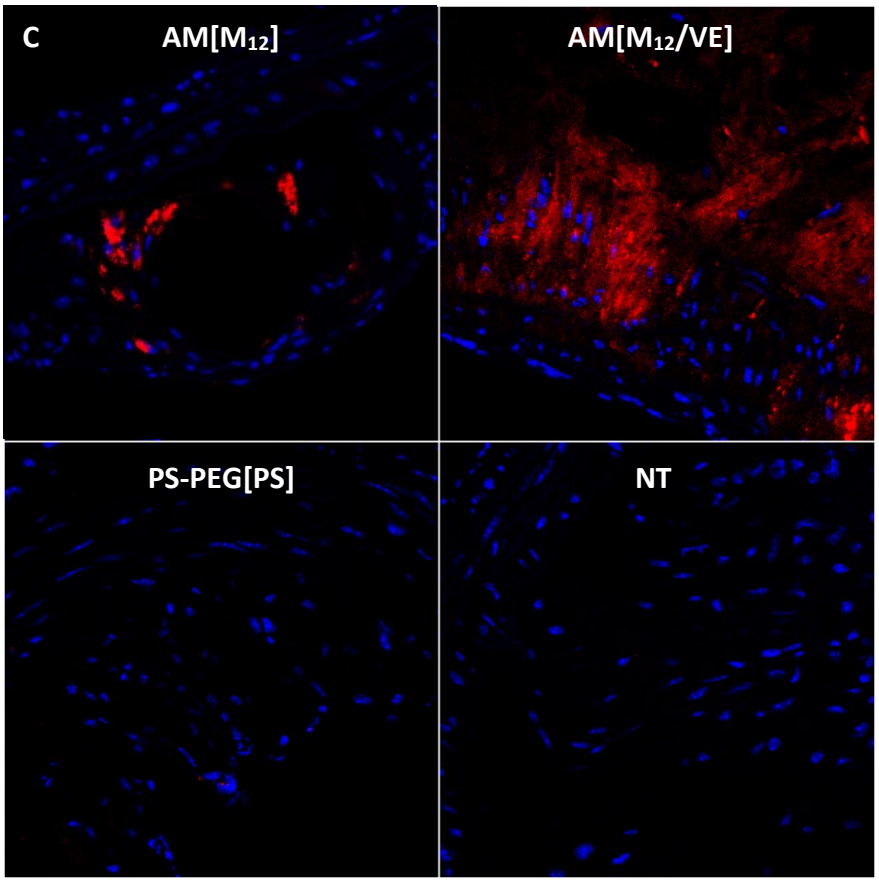
C
AM[M12]
AM[M12/VE]
PS-PEG[PS]
NT

Figure 4.6. NP localization to aortas. A) NP accumulation along the aortic tree. Aortas were excised from the ascending aorta from the left ventricle to the iliac branch point. B) Quantification of NP fluorescence showing higher levels of accumulation in the aortic arch, with preferential binding by AM[M_{12}] NPs. Error bars represent standard error of the mean (S.E.M.), Asterisk (*) indicates $p < .05$ from the control (NT), Dagger (†) indicates $p < .001$ from the control (NT), treatments with the same letter are not statistically significant from one another. C) Aortic cross sections showing NP fluorescence within artery walls and plaques.

NP cellular association and phenotypic changes in aortas

Utilizing flow cytometry it was found that AM NPs preferentially associate with activated endothelial cells (VCAM1 positive) within the aorta (**Figure 4.7A**). AM NPs also induced phenotypic changes relative to non-treated $ApoE^{-/-}$ mice and mice treated with PS NPs (**Figure 4.7B**). AM NP treated mice had lower levels of activated endothelial cells in aortic tissue. AM[M_{12}/VE] and PS-PEG[PS] also had lower relative levels of smooth muscle cells (SMCs).

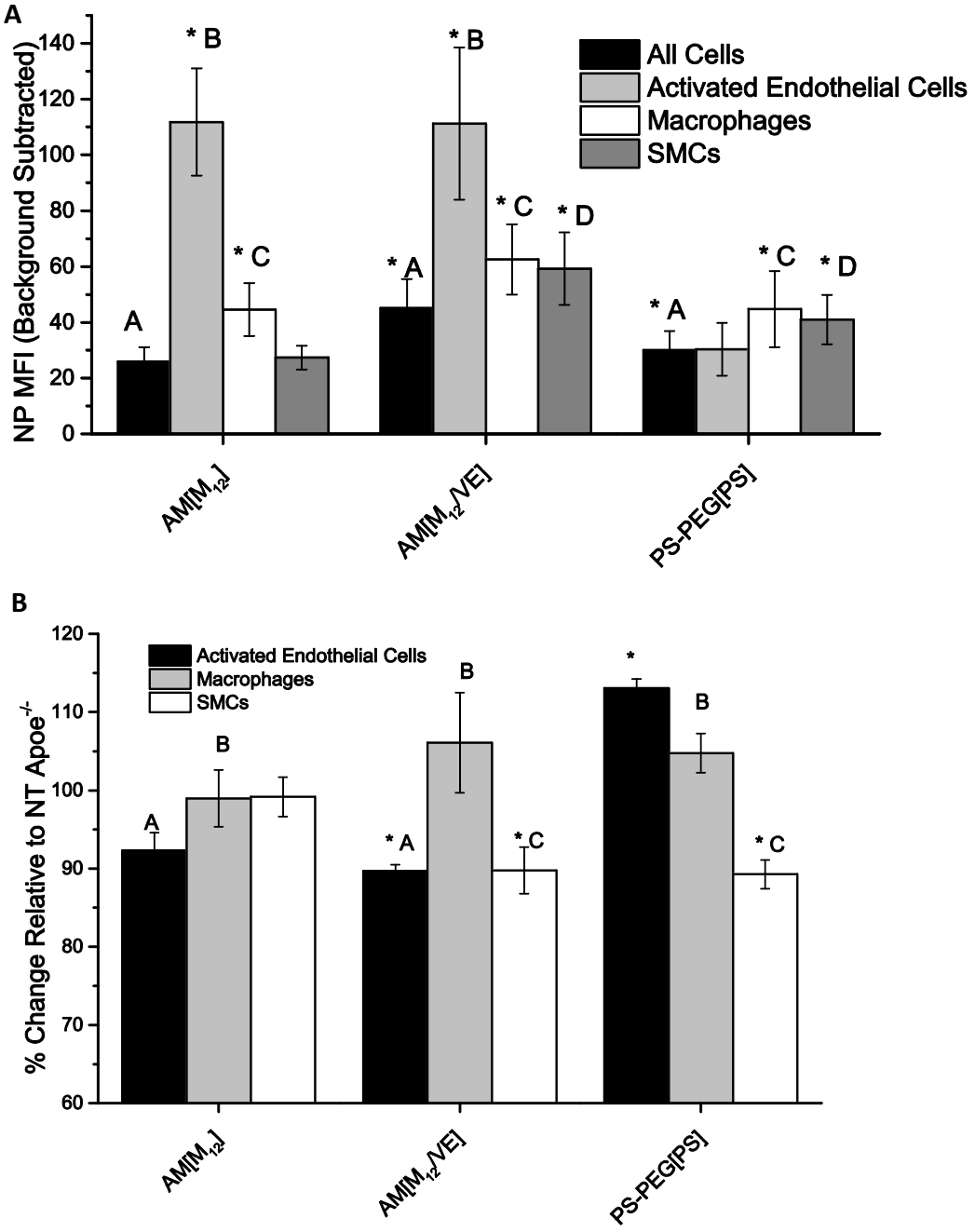

Figure 4.7. Cellular association of NPs. A) NP fluorescence in activated endothelial cells (VCAM expressing), macrophages (CD68 expressing) and smooth muscle cells (SMCs, α-actin expressing). AM NPs are internalized preferentially by activated endothelial cells. B) Change in cellular composition of aortas relative to untreated ApoE$^{-/-}$ (NT). AM NPs have lower levels of activated endothelial cells and AM[M_{12}/VE] and PS-PEG[PS] also have lower levels of SMCs. Error bars

represent standard error of the mean (S.E.M.). Asterisk (*) indicates $p < .05$ from the control (NT), , treatments with the same letter are not statistically significant from one another.

NP effect on gene expression

qRT-PCR was used to determine relative gene expression in the aorta for NP treated mice (**Figure 4.8**). All groups were normalized to untreated ApoE mice using two control genes (GAPDH and B2m) that did not change expression. AM[M_{12}/VE] NPs upregulated the cholesterol export genes ABCA1 and NR1H3 while downregulating the inflammatory cytokine gene, IL-6. AM [M_{12}/VE] NP treated mice had higher expression of the scavenger receptor CD36 than the untreated C57B/L6 control. PS NPs mildly upregulated the inflammation markers TNFα and MCP-1. Overall, AM[M_{12}/VE] treated mice had similar patterns of gene expression to untreated C57 B6 mice.

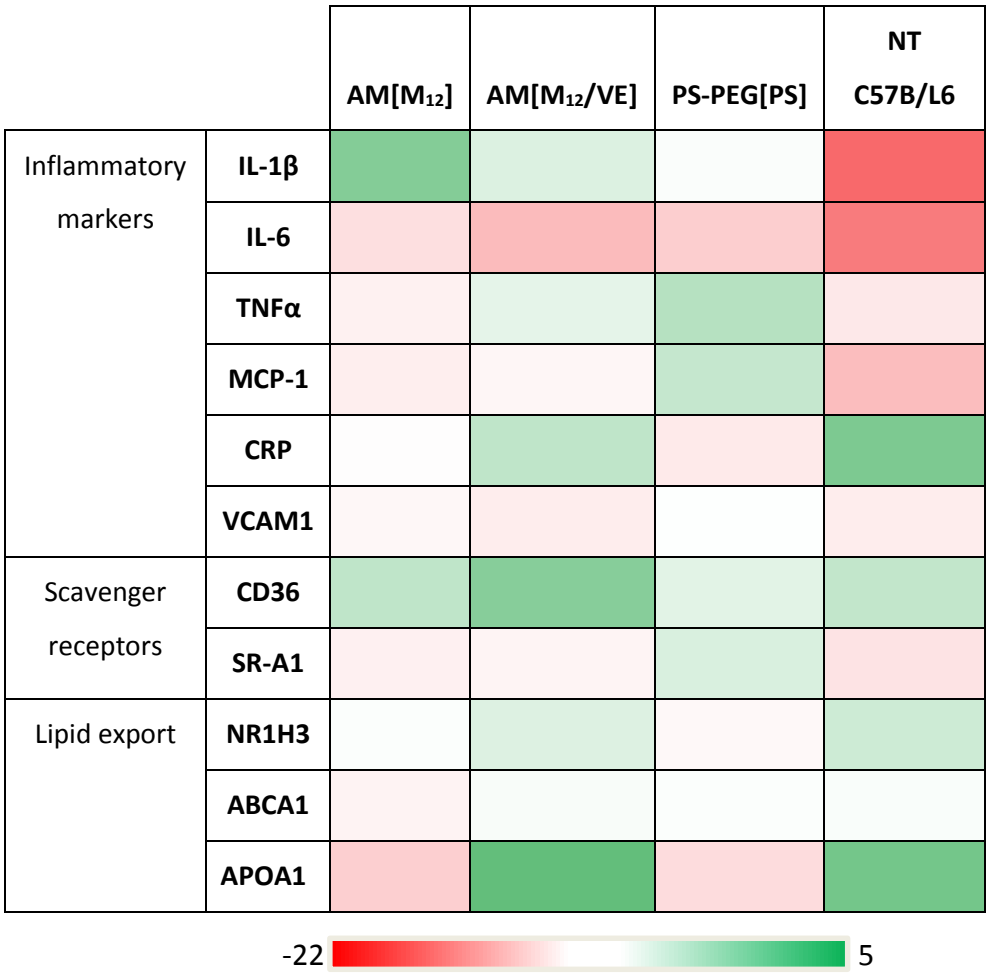

Figure 4.8. Gene expression relative to untreated ApoE$^{-/-}$ mice using qRT-PCR. Green represents gene upregulation and red represents gene downregulation.

Aorta plaque morphology

Untreated ApoE$^{-/-}$ mice had stage IV lesions along the ascending aorta and arch, characterized by the presence of large fibrous plaques with necrotic cores. **Figure 4.9** shows representative images for each treatment group after staining with Oil Red O (lipid burden), smooth muscle actin (neointimal formation) and COX-2 (inflammatory signaling). Plaques from AM NP treated mice had lower levels of COX-2 and smooth muscle actin expression. Additionally, mice treated with AM NPs had lower overall vessel occlusion by plaques, which was reflected by an overall lower lipid burden.

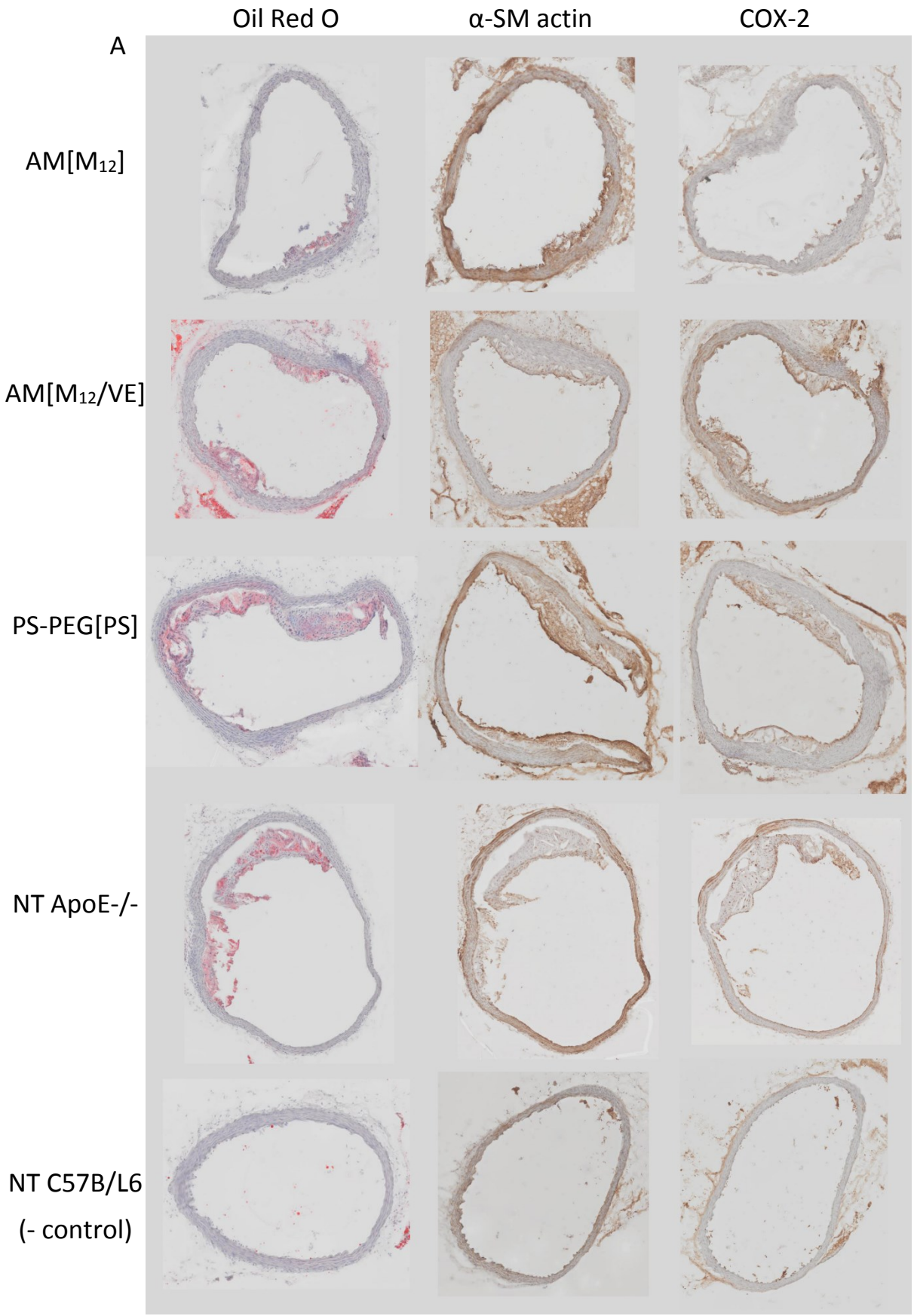
Oil Red O
α-SM actin
COX-2
A
AM[M12]
AM[M12/VE]
PS-PEG[PS]
NT ApoE-/-
NT C57B/L6
(- control)

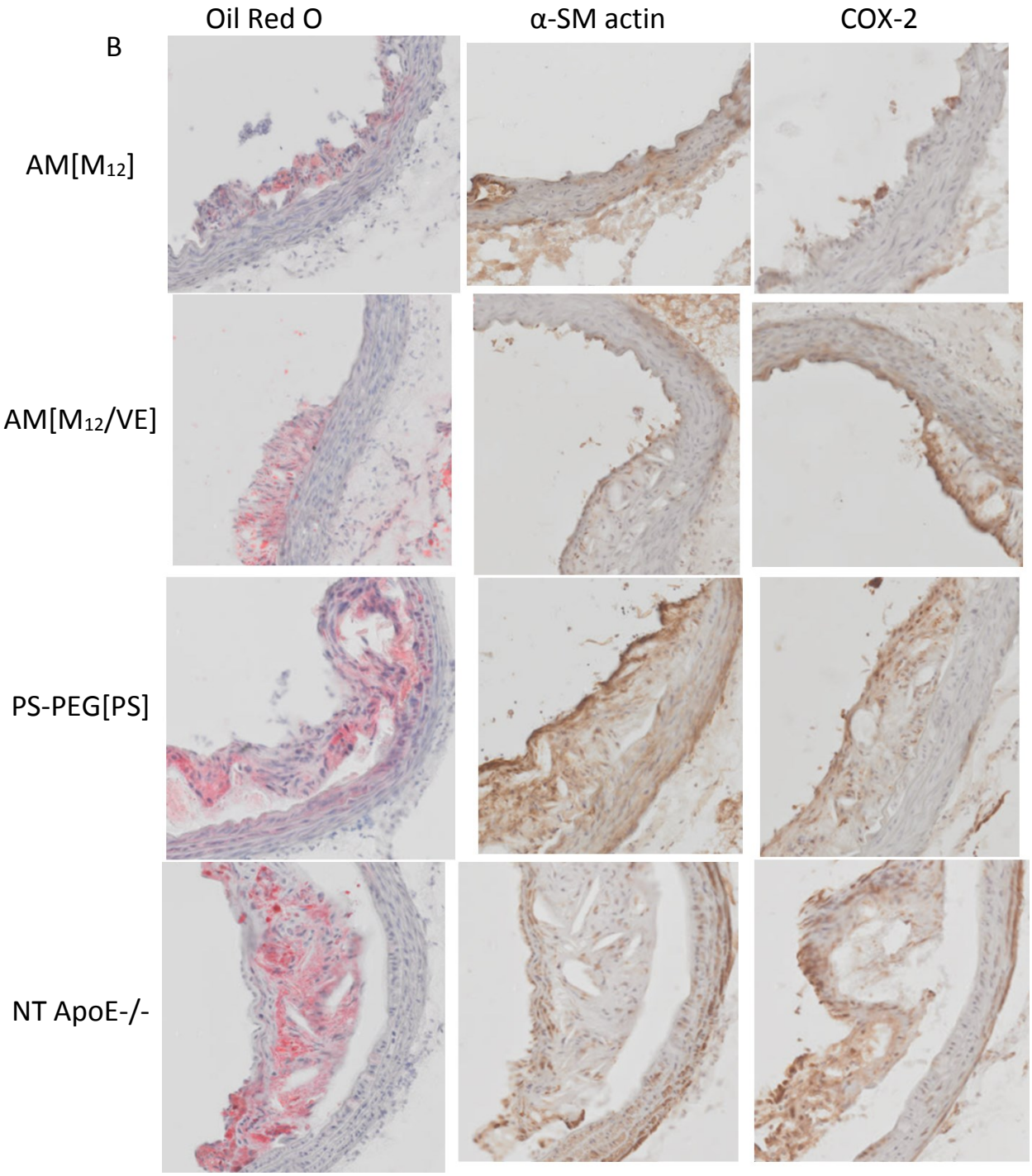

Figure 4.9. Aorta morphology. Representative images of aortic cross sections showing Oil Red O staining of lipid deposits, smooth muscle actin indicating neointimal formation, and COX-2 expression indicating inflammatory signaling. A) Complete aortic cross sections. B) Magnified images highlighting regions of plaque formation.

Discussion

The management of atherosclerosis will require site directed treatments with the ability to block local uptake of oxidized lipids and prevent the resulting inflammatory signaling in plaque macrophages. AMs have shown significant promise to mitigate these atherogenic endpoints *in vitro*. Creating kinetically stabilized NPs via flash nanoprecipitation makes the AMs a more viable therapeutic entity due to the reduced protein binding and extended *in vivo* half-life. AM NPs have shown significant promise at combating atherogenesis *in vitro*. However, *in vitro* studies cannot fully recapitulate the complexity of the disease, thus *in vivo* studies are required to fully characterize this nanosystem. In this work, second generation athero-protective NPs were evaluated for behavior and bioactivity *in vivo* with an atherosclerotic mouse model, ApoE$^{-/-}$.

ApoE$^{-/-}$ were chosen as an animal model as these mice develop normally, but exhibit five times higher normal serum plasma cholesterol and thus experience spontaneous development of atherosclerotic lesions [271]. Fed a high fat diet, ApoE$^{-/-}$ mice rapidly develop severe atherosclerotic lesions on the ascending aorta, aortic arch, and vascular tree. This model allowed the visualization of NP targeting of lesions in addition to the evaluation of the role of therapeutic interventions on atherogenic endpoints. Mice were fed a high fat diet for 8 weeks prior to the experiment to develop initial, stage II atherosclerotic lesions. Mice were then dosed with the NP therapeutics repeatedly over 4 weeks to evaluate the long term effects on plaque development. *In vivo* clearance and biodistribution of NPs involves the interplay of numerous biological processes and depends greatly on surface properties due to the high surface to volume ratio [244, 245]. AM NPs injected intravenously exhibited relatively long half-lives of ~28 h. This is considerably longer than similar micellar systems designed to target and treat atherosclerosis [125]. After injection, NPs distributed evenly throughout the body of mice as evidenced by the similar distribution profiles for chest, upper abdomen, and lower abdomen. PS-PEG[PS] NPs had

an even longer half-life of 78 hours, which was reflected in the detectable presence of NPs in serum at the termination of the experiment. This was most likely due to the lack of cellular interaction and degradation of PS NPs (Figure S4.x). The higher concentration levels for PS-PEG[PS] NPs whole body fluorescence remains at similar levels to AM NPs indicating lack of tissue accumulation.

AM NP tissue fluorescence at the terminal timepoint showed the highest concentration in the liver, indicating hepatic metabolism. The lack of fluorescence in the lungs demonstrates that the small and flexible AM do not agglomerate and become trapped in capillary beds [272]. AM NPs are expected to easily clear the lung capillary beds as they have a narrow size distribution with z-average size of 150-350 nm, which is much smaller than the mechanical filtration size of 4-10 μm. Additionally, they should have the ability to resist protein binding and agglomeration due to PEG shielding. AM are likely cleaved by esterases, enabling renal clearance of degradation products. The lack of accumulation in the spleen is also beneficial as AM will not interfere with filtration of red cells and not initiate an immune response or bind to unactivated reserve monocytes [273]. On the other hand, PS-PEG[PS] NPs accumulated in the spleen which may trigger an immune reaction although previous studies found that they do not initiate an immediate inflammatory response in macrophages. These particles also have a significant accumulation and persistence in the liver suggesting that they are not being cleared, degraded or metabolized.

AMs that detach from the NPs will probably be cleared renally due to unimer size and hepatically due to SR binding by kupffer cells, which is supported by *ex vivo* fluorescence in the kidney and liver. The larger size of intact NPs relative to micelles protects them from renal filtration, which has a size cutoff of ~8nm, enabling longer circulation times [255]. The conjugation of tracking fluorophores to AMs may potentially change the behavior of NPs and contribute to faster clearance from circulation relative to unlabeled NPs [93]. AF680 has a MW of over 1150 Da

and an overall negative charge, and may interact strongly with serum proteins, leading to opsonization and clearance from circulation [97]. Although PEG shielding creates a protective corona that protects micelles from opsonization, protein binding to the charged dye at the end of the PEG chain may pull unimers out, giving an artificially short half-life.

AM NPs exhibited preferential targeting to atherosclerotic lesions. This may be due to the affinity of AMs to scavenger receptors, which are overexpressed in plaques [274]. The most advanced lesions typically form on the ascending aorta close to the heart at the bifurcation of the carotid arteries [262, 268]. While lesions will form on other sites of the aortic tree, they will be less occlusive. The highest levels of AM NP accumulation are on the aortic arch, where the plaques are expected to be most pronounced and severely diseased. Differences in AM architecture and packaging have previously been shown to modulate SR binding interactions and inhibition of oxidized lipid uptake [222, 232]. Thus, in this work these difference were expected to affect the inherent affinity of AM NPs to the lesions. The presence of M_{12} in the core of NPs was found to be integral to scavenger receptor mediated uptake of NPs [256]. This correlated with the higher levels of NP binding to areas of plaque development seen with the AM[M_{12}] formulation. *In vitro* NP internalization by macrophages appears to be directly correlated with inhibition of oxLDL uptake and binding to areas of plaque formation.

When individual cell types within aortas were probed, it was found that AM NPs interact preferentially with activated endothelial cells expressing VCAM-1. Endothelial cells line the inside of the artery and are the initial mechanism for recruiting monocytes. When inflamed, they can also express high levels of the scavenger receptor, LOX-1, which may be interacting with NPs [167]. The phenotype switching of cells that AM NPs are associated with indicates a possible mechanism for arresting plaque growth. Our preliminary data indicates that AM NPs could prevent the uptake of oxLDL by endothelial scavenger receptors (data not shown), thus lowering

the number of cells with the activated phenotype and lowering the recruitment of additional lymphocytes to the site of the lesion. Additionally, VE has been shown to reduce adhesion molecule expression in endothelial cells, which could further explain the reduction in activated endothelial phenotype [253].

Examining the gene expression profile of aortas can give a prediction of the pathogenesis of the artery. Upregulation of the cholesterol export genes ABCA1 and NR1H3 by AM[M_{12}/VE] NPs indicates clearance of cellular lipids and potential reduction in the overall lipid burden of the plaque [275]. Additionally, downregulation of the inflammatory cytokine, IL-6, could reduce further monocyte recruitment [248]. This downregulation could be due to the fact that VE has been shown to inhibit cyclooxygenase (COX) activity in macrophages [252]. AM NP treated mice had higher expression of the scavenger receptor CD36, which is caused by the M_{12} core [256]. The similar gene expression pattern between ApoE$^{-/-}$ mice treated with AM[M_{12}/VE] and the untreated C57B/L6 mice indicates that this formulation may be able to prevent further arterial damage and disease progression.

Tissue histology of the aortic arch can give the best representation of disease progression. Macroscopically, lesions appear as white ingrowths in the intima of the aorta. After 16 weeks of diet, lesions in untreated mice were stage IV, with plaques showing remodeling (smooth muscle actin) and inflammation (COX-2) [188]. Smooth muscle cell proliferation into the artery occludes blood flow and is thought to be triggered by oxidized lipid induced inflammation [39]. The highest levels of SMC actin expression was on the surface of the plaque in the untreated ApoE$^{-/-}$ mouse group, indicating further growth into the artery. Plaques were also identified by morphology, specifically growth into the artery and presence of fibroblasts. Oil Red O lipid staining highlighted the lipid burden that exists in atherosclerotic lesions. AM NP treated mice had consistently less

occlusion than PS or untreated mice, which translated into accumulation lower lipid burden. Aortic lesions from AM NP treated mice also had lower levels of COX-2 and SMC actin.

Although AM NPs can reduce inflammatory signaling caused by oxidized lipids, shrinkage of accumulated plaques remains a challenge but is possible if reverse cholesterol transport is increased. Statins have recently been found to increase cholesterol export from cells but are primarily active in the liver when dosed traditionally. The hydrophobicity of this drug class imbues them with the ability to drive nucleation in flash nanoprecipitation and function as a NP core. Facilitated delivery of statins to lesions via AM NPs could have a dramatic increase in the trafficking of cholesterol away from plaques.

Conclusion

NPs fabricated from AMs display long circulation half-lives and localize to areas of growing atherosclerotic lesions. At lesion sites, AM[M_{12}/VE] NPs can lower inflammatory signaling and alter the cellular composition of plaques to have fewer activated endothelial and smooth muscle cells. This resulted in a decrease in lesion severity and size manifested by reduced lipid burden, lower levels of COX-2 inflammation and minimal smooth muscle proliferation. These outcomes hold promise that AM NPs may be able to locally address plaque development over the long time frames that the disease progresses.

Supplementary Data

In vitro efficacy of NPs

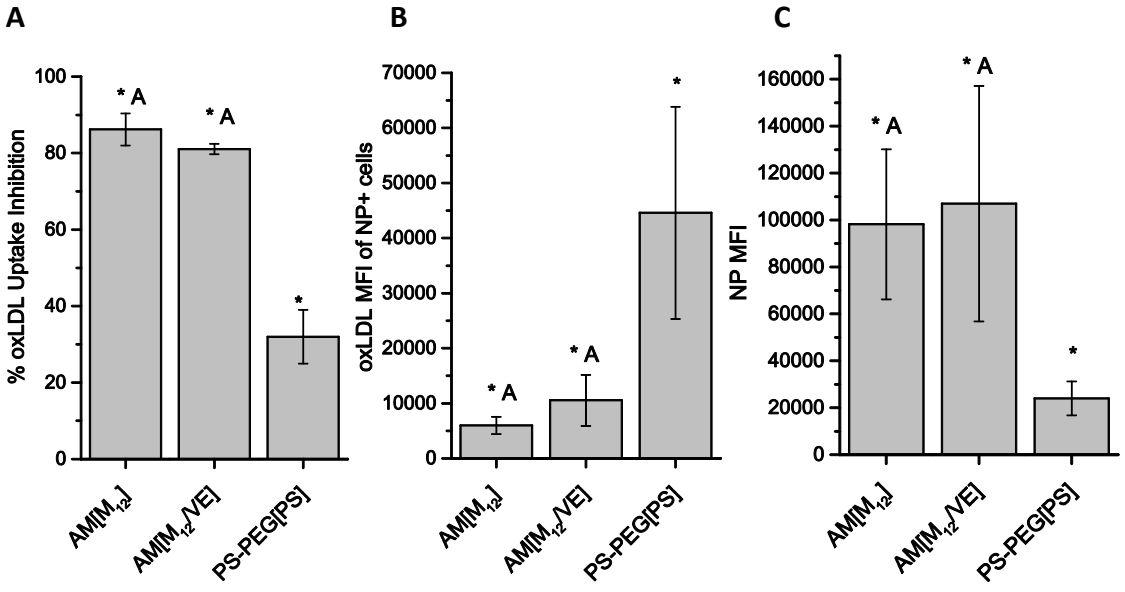

Figure S4.1. *In vitro* bioactivity of NPs. A) *In vitro* oxLDL uptake inhibition, B) oxLDL content of NP+ cells and C) cellular association of NPs in hMDMs. hMDMs were co-incubated with 5 μg/mL oxLDL and 10^{-5}M NPs for 24 h and analyzed by flow cytometry. AM NPs inhibited oxLDL uptake and displayed strong association with the hMDMs, while PS-PEG[PS] NPs minimally inhibited oxLDL uptake and were not internalized. Cells with internalized PS-PEG[PS] NPs had high levels of oxLDL in contrast to AM NPs, which exhibited very low oxLDL levels.

Primer sequences

Primer sequences were designed by Harvard Primer Bank and synthesized by Integrated DNA Technology. Primer efficiency was calculated using 4x dilution series of mouse liver cDNA. All primers used exhibited >95% efficiency with a single melting peak corresponding to a unique amplicon. Genomic DNA contamination was monitored by including a reverse transcription reaction without reverse transcriptase.

Table S4.1. Primer sequences used for qRT-PCR

Gene	Forward Primer	Reverse Primer
Murine TNFα	CCC TCA CAC TCA GAT CAT CTT CT	GCT ACG ACG TGG GCT ACA G
Murine IL-1β	GCA ACT GTT CCT GAA CTC AAC T	ATC TTT TGG GGT CCG TCA ACT
Murine GAPDH	AGG TCG GTG TGA ACG GAT TTG	TGT AGA CCA TGT AGT TGA GGT CA
Murine B2m	TTC TGG TGC TTG TCT CAC TGA	CAG TAT GTT CGG CTT CCC ATT C
Murine CRP	TTC CCA AGG AGT CAG ATA CTT CC	TCA GAG CAG TGT AGA AAT GGA GA
Murine IL-6	CTG CAA GAG ACT TCC ATC CAG	AGT GGT ATA GAC AGG TCT GTT GG
Murine CCL2	TTA AAA ACC TGG ATC GGA ACC AA	GCA TTA GCT TCA GAT TTA CGG GT
Murine VCAM1	TTG GGA GCC TCA ACG GTA CT	GCA ATC GTT TTG TAT TCA GGG GA
Murine CRP	TTC CCA AGG AGT CAG ATA CTT CC	TCA GAG CAG TGT AGA AAT GGA GA
Murine CD36	AGA TGA CGT GGC AAA GAA CAG	CCT TGG CTA GAT AAC GAA CTC TG
Murine MSR1	TGG AGG AGA GAA TCG AAA GCA	CTG GAC TGA CGA AAT CAA GGA A
Murine ABCA1	AAA ACC GCA GAC ATC CTT CAG	CAT ACC GAA ACT CGT TCA CCC
Murine NR1H3	CTC AAT GCC TGA TGT TTC TCC T	TCC AAC CCT ATC CCT AAA GCA A
Murine APOA1	GGC ACG TAT GGC AGC AAG AT	CCA AGG AGG AGG ATT CAA ACT G

NP/inflammation co-localization

Inflammation was monitored with the use of activatable inflammatory probe MMPSense 750 (Perkin Elmer). At 8 weeks post initiation of NP administration, mice were given a tail vein injection of MMPsense 750 and imaged live 6 h later using a MultiSpectral FX Pro to visualize areas of matrix metalloproteinase activity, indicating vascular remodeling.

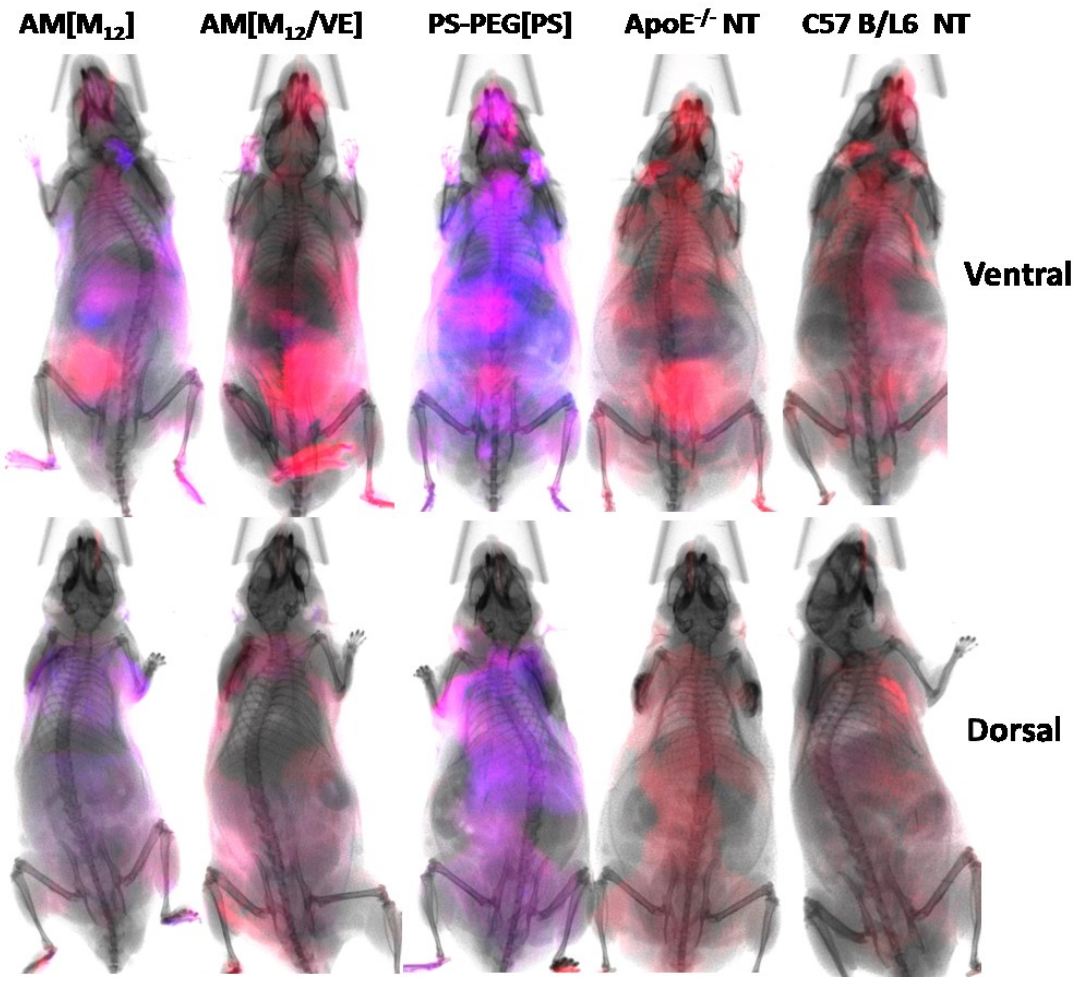

Figure S4.2 NP and inflammation co-localization. MMPsense 750 shows areas of matrix metalloproteinase activity as a marker of inflammation (red), NPs (blue) and co-localization (purple). AM[M_{12}] and PS NPs have high degrees of co-localization with MMP activity.

Chapter 5 – Summary and future directions

Note: Sections of this chapter have been reproduced from the following publication:

Lewis DR, Kamisoglu K, York AW, Moghe PV. *Polymer-based therapeutics: Nanoassemblies and nanoparticles for management of atherosclerosis*. Wiley Interdiscip Rev Nanomed Nanobiotechnol. 2011;3(4):400-420.

Summary and research impact

Atherosclerosis remains a challenging therapeutic target with significant health and economic burdens. The use of amphiphilic macromolecules (AMs) as a tool to manage atherosclerosis is a novel way of to address the disease and prevent its downstream consequences. This work elucidates critical features of AMs that are necessary for efficacy and advances AMs as a translational therapeutic. The goal of this project was to understand the structure-activity relationships of AM and develop a multifunctional targeted nanosystem as an atherosclerosis therapeutic.

Small changes in the architecture of AMs were found to have large effects on their bioactivity at inhibiting lipid accumulation. Quantitative structure-activity relationship models were generated using descriptors of the 3D configuration that predicted the efficacy of new AMs, which was dependent on the hydrophobic arms maintaining an extended conformation. Future development of AM variants can utilize this predictive capability to focus synthesis on compounds that will be most efficacious, accelerating research translation.

AMs were further advanced by formulating the AMs into nanoparticles (NPs) employing the hydrophobic antioxidant vitamin E (VE) in the core. Original compositions of NPs with M_{12} in the core were found to cause a significant increase in inflammatory signaling. Using flash nanoprecipitation with cytocompatible AMs and a VE core resulted in NPs that exhibited maintenance of bioactivity in the presence of serum with a minimal inflammatory response.

Bioactive AM NPs were then tested in an atherosclerotic mouse model for *in vivo* dynamics and efficacy. AM NPs exhibited slow clearance from circulation and did not accumulate in the lymphatic system. It was also found that AM NPs localized to atherosclerotic lesions, primarily binding to activated endothelial cells. There, they were able to reduce the level of

endothelial activation and NPs with the VE core were able to restore gene expression to basal levels. This resulted in smaller, less inflammatory atherosclerotic plaques that had less lipid accumulation.

Translating AM NPs into a viable therapeutic could add an additional tool to those currently in the clinic and help ameliorate the significant burden this disease places on society. AMs could act synergistically with approved therapies by reducing the local lipid burden.

Future Directions

This research has many future paths forward to develop AMs as a multimodal therapeutic or diagnostic agent. These can broadly fall into two main categories; basic science to understand further the mechanisms by which AMs work and translational research to bring the AMs closer to clinical use.

Composition-activity relationships

QSAR studies with AMs showed highly variable levels of bioactivity depending on AM conformations [222]. Similarly, AM NPs were found to have differences based on shell and core compositions [256]. Developing a guiding framework that can predict biological efficacy based on known parameters would accelerate optimization of AM NPs for *in vivo* studies.

Mitigating inflammation

Inflammatory signaling plays a key role in the intensification of atherosclerosis and is one of the most promising targets for future nanosystems [276]. The somewhat disparate fields of atherogenesis and inflammation need to be simultaneously addressed in order to design effective methods for inhibition of atheroinflammatory cascades that underlie the complex etiology of atherosclerosis. Designing nanoscale drug/polymer systems to interrupt the signaling cascade at multiple nodes would be an effective way to inhibit disease progression [60]. Non-inflammatory NPs were fabricated in this work but did not display an inherent lowering of inflammatory cytokine expression or secretion. Incorporation or conjugation of active anti-inflammatory agents could further lower inflammation signaling beyond basal levels.

RNA interference to knockdown pro-inflammatory gene expression could regulate the cytokine and monocyte recruitment proteins without compromising systemic immune responsiveness [277]. Cationic AM NPs could be a more effective way to bind siRNA and facilitate

its cellular delivery [278]. Cationic AM unimers are limited by the number of positively charged groups that can be covalently linked, but using cationic hydrophobes with flash nanoprecipitation could allow a higher charge density and thus more RNA loading capacity.

In addition to interfering with known mechanisms of inflammation, AMs could assist in the elucidation of intracellular signaling pathways, which parallels the identification of novel molecular targets for better disease targeting and cell-based delivery [37]. Determining the precise signals that are initiated by M_{12} core AM NPs could allow for the design of non-inflammatory NPs with higher bioactivity. It could also highlight a potential therapeutic target.

If anti-inflammatory AM NPs can be generated, the possibility arises of stabilizing vulnerable plaques [102]. Atherosclerotic lesions often exist harmlessly throughout an individual's life and only become a problem if the plaque ruptures, initiating a thrombus [9]. Rupture happens when the fibrous cap on the surface of the lesion is degraded by matrix metalloproteinases, which are upregulated in areas of inflammation. The use of *ex vivo* carotid artery plaques from patients who have undergone a carotid endarterectomy could allow for this screening [279]. After treatment of plaque sections with AM NPs, the cellular inflammatory response could be measured against the thickness of the fibrous cap protecting plaques, which would indicate whether the AM NP therapy could be effective.

Active targeting

Since atherosclerosis is a focal disease, it is especially important to have localized therapy in order to slow down and possibly reverse the disease progression. Specific targeting to growing lesions could avoid some of the increased susceptibility to infection seen with anti-cytokine therapies [280]. Advanced techniques, such as phage display, are leading to the rapid discovery of novel ligands that effectively bind to these targets [281]. Computer simulations of molecular

docking can also guide the mechanistic design of polymer-target receptor interactions, screen for optimal AM configurations and probe possible intervention of lesion development [204]. Utilizing highly specific, non-immunogenic and small size ligands, including peptides and peptidomimetics, on the surface of the AM NPs could allow for more selective and efficient therapeutic effect [282].

Stent coating and drug delivery

A relevant application for AMs that would not need inherent localization could be coating on the surface of a stent to reduce restenosis. SMC proliferation is stimulated by numerous inflammatory signals including oxidized lipids from the core of a plaque [39]. The inhibition of interaction between oxidized lipids and resident macrophages or endothelial cells could reduce the inflammatory response. If AMs can mitigate this inflammation, it could reduce SMC proliferation and thus vessel restenosis. If coating results show adequate release from stents and *in vitro* activity with SMC, this could be tested in a rabbit model of atherosclerosis with stent implantation.

With the advent of NPs that can prevent vascular remodeling and blood vessel occlusion, new alternatives could be envisioned that replace drug-eluting stents [178]. However several challenges will need to be overcome, including the barriers for intravascular administration and effective targeting that can evade premature clearance. AM NPs have key advantages: 1) increased circulation half-life and 2) resistance to clearance that allow widely spaced dosing while maintaining therapeutic efficacy.

These advantages could be leveraged with the incorporation of other drugs into AM NPs, which may provide expanded utility significantly beyond blocking oxidized lipid uptake. Reverse cholesterol transport could actually shrink accumulated lesions if the equilibrium of lipid trafficking is shifted. Some statins have been shown to upregulate this process yet primarily

localize to the liver [283]. As they are hydrophobic, incorporation into NPs is possible and could improve lesion localization and cellular internalization.

Translational animal studies

To further advance AM NPs as a viable therapeutic, larger scale studies need to be performed with more human disease relevant animal models. Additionally, safety studies are fundamentally critical prior to efficacy studies. ApoE$^{-/-}$ mice are the simplest atherosclerosis model available. Many drug candidates that are able to reduce lesion size are unable to replicate efficacy in human trials. Mice do not naturally develop atherosclerosis and only by knocking out a key lipid trafficker, do they develop lesions.

New Zealand rabbits can develop moderate atherosclerosis on a high fat diet but are primarily used for stent restenosis studies. Balloon catheterization and stent implantation can cause significant damage to arteries, specifically endothelial denudation and medial dissection, which initiates an inflammatory response. This can lead to vessel occlusion outcomes via two distinct mechanisms; platelet adhesion and thrombus formation, or smooth muscle cell proliferation leading to gradual restenosis [79]. However, this injury mechanism and response is significantly different than that which leads to slow vessel occlusion by plaque buildup in humans. Testing AM NPs in this disease model may not provide accurate information about their therapeutic potential due to the discrepancy in the mechanism of action of AM NPs and the root causes of vascular problems following catheterization.

It is supported in literature the one of the more accurate models for human coronary arterial disease is the porcine model on a high fat diet. They have very similar coronary anatomy and develop multi-focal atherosclerotic plaques along the aorta and coronary arteries [284]. Similar in size to human hearts, they can also be studied for stent implantation or drug efficacy

[285]. AM NPs need to be tested in a more rigorous disease model such as this to better evaluate their ability to block atherogenesis and inflammation.

Diagnostic applications

Fluorophores were utilized in this work due to the facile nature of conjugation with AM NPs and ease of detection with imaging modalities. However, large organic molecules of unknown biological reactivity are not suitable for clinical use. They also have limited utility as visible and near infrared light is highly absorbed by tissue, which prevents accurate quantification [190].

Further development of AM NPs can focus on diagnostic applications. If targeting is sufficiently specific, the potential for AMs to be used for diagnostic purposes when coupled with appropriate imaging agents arises. The diagnostic market for atherosclerosis is immature and there is currently no way of directly measuring plaque vulnerability [286]. Intravascular ultrasound (IVUS) is invasive and unable to predict impending plaque rupture [287]. Increased metabolic activity and scavenger receptor expression may signal a more vulnerable plaque, which would present an optimal target for AM NPs.

Multiple imaging modalities could readily be incorporated into AM nanoassemblies. The conjugation of gadolinium chelating agents to the PEG chain would allow MRI imaging of AM NPs as it is a well-studied contrast agent [146]. Radiolabeling AMs could allow for more precise tracking via PET-CT and exact quantification of AM NP trafficking and metabolism [247]. Upconverting rare earth nanocrystals are also an attractive candidate as they exhibit NIR fluorescence in a recently discovered biologic imaging window [288]. These could be coated with a hydrophobe to easily encapsulate inside AM NPs.

A diverse range of development paths can be taken to further explore the therapeutic and diagnostic options for AMs. By alleviating inflammation with structural modifications to AM

NPs or synergistic drug encapsulation and increasing the specificity of AM localization, the atherogenic cascade can be reversed. Coupled with improved imaging markers, these could be examined in a translational disease model for clinically relevant adverse endpoint reductions, bringing AMs closer to therapeutic use.

Publications

1. **Lewis DR**, Petersen LK, Zablocki KR, York AW, Uhrich KE, Prud'homme RK, et al. *Amphiphilic macromolecule nanoparticles mitigate atherosclerosis and inflammation in* ApoE$^{-/-}$ *mice.* PNAS. To be submitted.
2. Petersen LK, York AW, **Lewis DR**, Ahuja S, Bruzek MJ, et al. *The Rational Design of Bioactive Nanoparticle Therapeutics for Management of Atherosclerosis through Scavenger Receptor Intervention.* Biomaterials. To be submitted.
3. Haser PB, Petersen LK, Fan C, Zablocki K, York AW, **Lewis DR**, et al. *Nanolipoblockers: Ex vivo human plaque interaction for therapeutic management for atherosclerosis.* J Vasc Surg. 2013;58(4):1149.
4. **Lewis DR**, Kholodovych V, Tomasini MD, Abdelhamid D, Petersen LK, Welsh WJ, et al. *In silico design of anti-atherogenic biomaterials*. Biomaterials. 2013;34(32):7950-7959.
5. York AW, Zablocki KR, **Lewis DR**, Gu L, Uhrich KE, Prud'homme RK, et al. *Kinetically assembled nanoparticles of bioactive macromolecules exhibit enhanced stability and cell-targeted biological efficacy*. Adv Mater. 2012;24(6):733-739.
6. **Lewis DR**, Kamisoglu K, York AW, Moghe PV. *Polymer-based therapeutics: Nanoassemblies and nanoparticles for management of atherosclerosis*. Wiley Interdiscip Rev Nanomed Nanobiotechnol. 2011;3(4):400-420.
7. **Lewis DR**, Liu DJ. *Direct measurement of lipase inhibition by orlistat using a dissolution linked in vitro assay*. Clinic Pharmacol Biopharm. 2012;1(103).
8. Iverson NM, Plourde NM, Sparks SM, Wang J, Patel EN, Shah PS, **Lewis DR**, et al. *Dual use of amphiphilic macromolecules as cholesterol efflux triggers and inhibitors of macrophage athero-inflammation*. Biomaterials. 2011;32(32):8319-8327.
9. Pingali K, Mendez R, **Lewis DR**, Michniak-Kohn B, Cuitiño A, Muzzio F. *Evaluation of strain-induced hydrophobicity of pharmaceutical blends and its effect on drug release rate under multiple compression conditions*. Drug Dev Ind Pharm. 2011;37(4):428-435.
10. Pingali K, Mendez R**, Lewis DR**, Michniak-Kohn B, Cuitino A, Muzzio F. *Mixing order of glidant and lubricant – influence on powder and tablet properties*. Int J Pharm. 2011;409(1-2):269-277.

Chapter 6 – References

1. Heidenreich, P.A., et al., *Forecasting the Future of Cardiovascular Disease in the United States: A Policy Statement From the American Heart Association.* Circulation, 2011. **123**(8): p. 933-944.
2. Libby, P., *Inflammation in atherosclerosis.* Nature, 2002. **420**(6917): p. 868-74.
3. McGill, H.C. and C.A. McMahan, *Determinants of atherosclerosis in the young. Pathobiological Determinants of Atherosclerosis in Youth (PDAY) Research Group.* Am. J. Cardiol., 1998. **82**: p. 30T-36T.
4. Lloyd-Jones, D., et al., *Executive Summary: Heart Disease and Stroke Statistics--2010 Update: A Report From the American Heart Association.* Circulation, 2010. **121**(7): p. 948-954.
5. Lewis, D.R., et al., *Polymer-based therapeutics: nanoassemblies and nanoparticles for management of atherosclerosis.* Wiley Interdisciplinary Reviews: Nanomedicine and Nanobiotechnology, 2011. **3**(4): p. 400-420.
6. Sahoo, D. and V. Drover, *The Role of Scavenger Receptors in Signaling, Inflammation and Atherosclerosis*, in *Biochemistry of Atherosclerosis*, S. Cheema, Editor. 2006, Springer US. p. 70-91.
7. Berliner, J.A. and J.W. Heinecke, *The role of oxidized lipoproteins in atherogenesis.* Free Radic Biol Med, 1996. **20**(5): p. 707-27.
8. Libby, P., *Coronary artery injury and the biology of atherosclerosis: inflammation, thrombosis, and stabilization.* Am J Cardiol, 2000. **86**(8B): p. 3J-8J; discussion 8J-9J.
9. Boyle, J.J., *Macrophage Activation in Atherosclerosis: Pathogenesis and Pharmacology of Plaque Rupture.* Current Vascular Pharmacology, 2005. **3**: p. 63-68.
10. Saha, P., et al., *The monocyte/macrophage as a therapeutic target in atherosclerosis.* Current Opinion in Pharmacology, 2009. **9**(2): p. 109-118.
11. Waldo, S.W., et al., *Heterogeneity of Human Macrophages in Culture and in Atherosclerotic Plaques.* Am J Pathol, 2008. **172**(4): p. 1112-1126.
12. Gordon, S., *Alternative activation of macrophages.* Nat Rev Immunol, 2003. **3**(1): p. 23-35.
13. Mantovani, A., A. Sica, and M. Locati, *New vistas on macrophage differentiation and activation.* European Journal of Immunology, 2007. **37**(1): p. 14-16.
14. Mosser, D.M. and J.P. Edwards, *Exploring the full spectrum of macrophage activation.* Nat Rev Immunol, 2008. **8**(12): p. 958-969.
15. Mantovani, A., C. Garlanda, and M. Locati, *Macrophage Diversity and Polarization in Atherosclerosis: A Question of Balance.* Arteriosclerosis, Thrombosis & Vascular Biology, 2009. **29**(10): p. 1419-1423.
16. Stout, R.D., et al., *Macrophages sequentially change their functional phenotype in response to changes in microenvironmental influences.* J Immunol, 2005. **175**(1): p. 342-9.
17. Rajavashisth, T.B., et al., *Inflammatory Cytokines and Oxidized Low Density Lipoproteins Increase Endothelial Cell Expression of Membrane Type 1-Matrix Metalloproteinase.* Journal of Biological Chemistry, 1999. **274**(17): p. 11924-11929.
18. Saren, P., H.G. Welgus, and P.T. Kovanen, *TNF-alpha and IL-1beta selectively induce expression of 92-kDa gelatinase by human macrophages.* Journal of immunology, 1996. **157**(9): p. 4159-65.

19. Boisvert, W.A., et al., *A leukocyte homologue of the IL-8 receptor CXCR-2 mediates the accumulation of macrophages in atherosclerotic lesions of LDL receptor-deficient mice.* The Journal of Clinical Investigation, 1998. **101**(2): p. 353-63.
20. Gu, L., et al., *Absence of monocyte chemoattractant protein-1 reduces atherosclerosis in low density lipoprotein receptor-deficient mice.* Molecular cell, 1998. **2**(2): p. 275-81.
21. van Tits, L.J.H., et al., *Oxidized LDL enhances pro-inflammatory responses of alternatively activated M2 macrophages: A crucial role for Krüppel-like factor 2.* Atherosclerosis, 2011. **214**(2): p. 345-349.
22. Fuhrman, B., et al., *Ox-LDL induces monocyte-to-macrophage differentiation in vivo: Possible role for the macrophage colony stimulating factor receptor (M-CSF-R).* Atherosclerosis, 2008. **196**(2): p. 598-607.
23. Porcheray, F., et al., *Macrophage activation switching: an asset for the resolution of inflammation.* Clinical and experimental immunology, 2005. **142**(3): p. 481-9.
24. Kumar, V., et al., *Three-Dimensional cryoEM Reconstruction of Native LDL Particles to 16Å Resolution at Physiological Body Temperature.* PLoS One, 2011. **6**(5): p. e18841.
25. Hevonoja, T., et al., *Structure of low density lipoprotein (LDL) particles: Basis for understanding molecular changes in modified LDL.* Biochimica et Biophysica Acta (BBA) - Molecular and Cell Biology of Lipids, 2000. **1488**(3): p. 189-210.
26. Bijsterbosch, M.K. and T.J.C. van Berkel, *Native and modified lipoproteins as drug delivery systems.* Advanced Drug Delivery Reviews. **5**(3): p. 231-251.
27. Varadhachary, A.S., M. Monestier, and P. Salgame, *Reciprocal Induction of IL-10 and IL-12 from Macrophages by Low-Density Lipoprotein and Its Oxidized Forms.* Cellular Immunology, 2001. **213**(1): p. 45-51.
28. Murphy, J.E., et al., *Biochemistry and cell biology of mammalian scavenger receptors.* Atherosclerosis, 2005. **182**(1): p. 1-15.
29. Kunjathoor, V.V., et al., *Scavenger receptors class A-I/II and CD36 are the principal receptors responsible for the uptake of modified low density lipoprotein leading to lipid loading in macrophages.* J Biol Chem, 2002. **277**(51): p. 49982-8.
30. Silverstein, R.L., *Inflammation, atherosclerosis, and arterial thrombosis: role of the scavenger receptor CD36.* Cleve Clin J Med, 2009. **76 Suppl 2**: p. S27-30.
31. Janabi, M., et al., *Oxidized LDL-Induced NF-{kappa}B Activation and Subsequent Expression of Proinflammatory Genes Are Defective in Monocyte-Derived Macrophages From CD36-Deficient Patients.* Arterioscler Thromb Vasc Biol, 2000. **20**(8): p. 1953-1960.
32. Febbraio, M., et al., *Targeted disruption of the class B scavenger receptor CD36 protects against atherosclerotic lesion development in mice.* J Clin Invest, 2000. **105**(8): p. 1049-56.
33. Rahaman, S.O., et al., *A CD36-dependent signaling cascade is necessary for macrophage foam cell formation.* Cell Metabolism, 2006. **4**(3): p. 211-21.
34. Sun, B., et al., *Distinct mechanisms for OxLDL uptake and cellular trafficking by class B scavenger receptors CD36 and SR-BI.* J Lipid Res, 2007. **48**(12): p. 2560-70.
35. Zeng, Y., et al., *Endocytosis of oxidized low density lipoprotein through scavenger receptor CD36 utilizes a lipid raft pathway that does not require caveolin-1.* J Biol Chem, 2003. **278**(46): p. 45931-6.
36. Jones, N.L. and M.C. Willingham, *Modified LDLs are internalized by macrophages in part via macropinocytosis.* Anat Rec, 1999. **255**(1): p. 57-68.
37. Robbesyn, F., R. Salvayre, and A. Negre-Salvayre, *Dual role of oxidized LDL on the NF-kappaB signaling pathway.* Free Radic Res, 2004. **38**(6): p. 541-51.

38. Maziere, C., et al., *Oxidized low density lipoprotein induces activation of the transcription factor NF kappa B in fibroblasts, endothelial and smooth muscle cells.* Biochemistry and molecular biology international, 1996. **39**(6): p. 1201-7.
39. Auge, N., et al., *Oxidized LDL-induced smooth muscle cell proliferation involves the EGF receptor/PI-3 kinase/Akt and the sphingolipid signaling pathways.* Arteriosclerosis, Thrombosis, and Vascular Biology, 2002. **22**(12): p. 1990-5.
40. de Winther, M.P., et al., *Macrophage scavenger receptor class A: A multifunctional receptor in atherosclerosis.* Arteriosclerosis, Thrombosis, and Vascular Biology, 2000. **20**(2): p. 290-7.
41. Moore, K.J., et al., *Loss of receptor-mediated lipid uptake via scavenger receptor A or CD36 pathways does not ameliorate atherosclerosis in hyperlipidemic mice.* The Journal of Clinical Investigation, 2005. **115**(8): p. 2192-201.
42. Whitman, S.C., et al., *Macrophage-specific expression of class A scavenger receptors in LDL receptor(-/-) mice decreases atherosclerosis and changes spleen morphology.* Journal of Lipid Research, 2002. **43**(8): p. 1201-8.
43. Suzuki, H., et al., *A role for macrophage scavenger receptors in atherosclerosis and susceptibility to infection.* Nature, 1997. **386**(6622): p. 292-6.
44. Haworth, R., et al., *The macrophage scavenger receptor type A is expressed by activated macrophages and protects the host against lethal endotoxic shock.* The Journal of experimental medicine, 1997. **186**(9): p. 1431-9.
45. Ricci, R., et al., *Requirement of JNK2 for scavenger receptor A-mediated foam cell formation in atherogenesis.* Science, 2004. **306**(5701): p. 1558-61.
46. Kienast, J., et al., *Relation of urokinase-type plasminogen activator expression to presence and severity of atherosclerotic lesions in human coronary arteries.* Thrombosis and haemostasis, 1998. **79**(3): p. 579-86.
47. Hsu, H.Y., et al., *Ligand binding to macrophage scavenger receptor-A induces urokinase-type plasminogen activator expression by a protein kinase-dependent signaling pathway.* The Journal of biological chemistry, 1998. **273**(2): p. 1240-6.
48. Pollaud-Cherion, C., et al., *Involvement of calcium and arachidonate metabolism in acetylated-low-density-lipoprotein-stimulated tumor-necrosis-factor-alpha production by rat peritoneal macrophages.* European journal of biochemistry / FEBS, 1998. **253**(1): p. 345-53.
49. Ridker, P.M., et al., *Rosuvastatin to Prevent Vascular Events in Men and Women with Elevated C-Reactive Protein.* New England Journal of Medicine, 2008. **359**(21): p. 2195-2207.
50. Pai, J.K., et al., *Inflammatory Markers and the Risk of Coronary Heart Disease in Men and Women.* New England Journal of Medicine, 2004. **351**(25): p. 2599-2610.
51. Zacho, J., et al., *Genetically Elevated C-Reactive Protein and Ischemic Vascular Disease.* New England Journal of Medicine, 2008. **359**(18): p. 1897-1908.
52. Ikonen, E., *Mechanisms for Cellular Cholesterol Transport: Defects and Human Disease.* Physiological Reviews, 2006. **86**(4): p. 1237-1261.
53. Chinetti-Gbaguidi, G. and B. Staels, *Lipid ligand-activated transcription factors regulating lipid storage and release in human macrophages.* Biochimica et Biophysica Acta (BBA) - Molecular and Cell Biology of Lipids, 2009. **1791**(6): p. 486-493.
54. Spady, D.K., *Reverse Cholesterol Transport and Atherosclerosis Regression.* Circulation, 1999. **100**(6): p. 576-578.
55. Rubenstrunk, A., et al., *Safety issues and prospects for future generations of PPAR modulators.* Biochim Biophys Acta, 2007. **1771**(8): p. 1065-81.

56. Zinn, A., et al., *Reassessing the cardiovascular risks and benefits of thiazolidinediones.* Clinical Cardiology, 2008. **31**(9): p. 397-403.
57. Staels, B., *Fluid retention mediated by renal PPAR[gamma].* Cell Metabolism, 2005. **2**(2): p. 77-78.
58. Bucher, H.C., L.E. Griffith, and G.H. Guyatt, *Systematic Review on the Risk and Benefit of Different Cholesterol-Lowering Interventions.* Arterioscler Thromb Vasc Biol, 1999. **19**(2): p. 187-195.
59. Gotto, A.M., *Antioxidants, statins, and atherosclerosis.* Journal of the American College of Cardiology, 2003. **41**(7): p. 1205-1210.
60. Klingenberg, R. and G.r.K. Hansson, *Treating inflammation in atherosclerotic cardiovascular disease: emerging therapies.* European Heart Journal, 2009. **30**(23): p. 2838-2844.
61. Sheikine, Y.A. and G.K. Hansson, *Chemokines as Potential Therapeutic Targets in Atherosclerosis.* Current Drug Targets, 2006. **7**(1): p. 13-28.
62. Steinhubl, S.R., *Why Have Antioxidants Failed in Clinical Trials?* The American Journal of Cardiology, 2008. **101**(10, Supplement 1): p. S14-S19.
63. Krotz, F., H.Y. Sohn, and V. Klauss, *Antiplatelet drugs in cardiological practice: established strategies and new developments.* Vasc Health Risk Manag, 2008. **4**(3): p. 637-45.
64. Gonzalez, E.R., *Antiplatelet therapy in atherosclerotic cardiovascular disease.* Clin Ther, 1998. **20 Suppl B**: p. B18-41.
65. Siu, D., *A new way of targeting to treat coronary artery disease.* Journal of Cardiovascular Medicine, 2010. **11**(1): p. 1-6.
66. Kino, T. and G.P. Chrousos, *Combating atherosclerosis with LXR alpha and PPAR alpha agonists: is rational multitargeted polypharmacy the future of therapeutics in complex diseases?* Mol Interv, 2004. **4**(5): p. 254-7.
67. Joseph, S.B., et al., *Reciprocal regulation of inflammation and lipid metabolism by liver X receptors.* Nature Medicine, 2003. **9**(2): p. 213-219.
68. Rigamonti, E., et al., *Liver X receptor activation controls intracellular cholesterol trafficking and esterification in human macrophages.* Circulation Research, 2005. **97**(7): p. 682-9.
69. Joseph, S.B., et al., *Synthetic LXR ligand inhibits the development of atherosclerosis in mice.* Proc Natl Acad Sci U S A, 2002. **99**(11): p. 7604-9.
70. Niki, E., *Antioxidants and atherosclerosis.* Biochem. Soc. Trans., 2004. **32**(Pt 1): p. 156-159.
71. Landmesser, U. and D.G. Harrison, *Oxidant Stress as a Marker for Cardiovascular Events: Ox Marks the Spot.* Circulation, 2001. **104**(22): p. 2638-2640.
72. Saremi, A. and R. Arora, *Vitamin E and cardiovascular disease.* Am J Ther, 2010. **17**(3): p. e56-65.
73. Steinberg, D. and J.L. Witztum, *Is the Oxidative Modification Hypothesis Relevant to Human Atherosclerosis?: Do the Antioxidant Trials Conducted to Date Refute the Hypothesis?* Circulation, 2002. **105**(17): p. 2107-2111.
74. Kissner, R., et al., *Formation and Properties of Peroxynitrite as Studied by Laser Flash Photolysis, High-Pressure Stopped-Flow Technique, and Pulse Radiolysis.* Chemical Research in Toxicology, 1997. **10**(11): p. 1285-1292.
75. Drummond, G.R., et al., *Combating oxidative stress in vascular disease: NADPH oxidases as therapeutic targets.* Nat Rev Drug Discov, 2011. **10**(6): p. 453-471.
76. Moliterno, D.J., *Healing Achilles — Sirolimus versus Paclitaxel.* New England Journal of Medicine, 2005. **353**(7): p. 724-727.

77. Sousa, J.E., et al., *Lack of Neointimal Proliferation After Implantation of Sirolimus-Coated Stents in Human Coronary Arteries : A Quantitative Coronary Angiography and Three-Dimensional Intravascular Ultrasound Study.* Circulation, 2001. **103**(2): p. 192-195.
78. Grube, E., et al., *TAXUS I: Six- and Twelve-Month Results From a Randomized, Double-Blind Trial on a Slow-Release Paclitaxel-Eluting Stent for De Novo Coronary Lesions.* Circulation, 2003. **107**(1): p. 38-42.
79. Joner, M., et al., *Pathology of Drug-Eluting Stents in Humans: Delayed Healing and Late Thrombotic Risk.* J Am Coll Cardiol, 2006. **48**(1): p. 193-202.
80. Joner, M., et al., *Endothelial Cell Recovery Between Comparator Polymer-Based Drug-Eluting Stents.* Journal of the American College of Cardiology, 2008. **52**(5): p. 333-342.
81. Onuma, Y., et al., *The Everolimus-Eluting Stent in Real-World Patients: 6-Month Follow-Up of the X-SEARCH (Xience V Stent Evaluated at Rotterdam Cardiac Hospital) Registry.* Journal of the American College of Cardiology, 2009. **54**(3): p. 269-276.
82. Caruso, F., *Nanoengineering of Particle Surfaces.* Adv. Mater., 2001. **13**(1): p. 11-22.
83. Mailänder, V. and K. Landfester, *Interaction of Nanoparticles with Cells.* Biomacromolecules, 2009. **10**(9): p. 2379-2400.
84. Lowe, A.B., et al., *Facile preparation of transition metal nanoparticles stabilized by well-defined (co)polymers synthesized via aqueous reversible addition-fragmentation chain transfer polymerization.* J. Am. Chem. Soc., 2002. **124**: p. 11562-11563.
85. Sumerlin, B.S., et al., *Modification of gold surfaces with water-soluble (co)polymers prepared via aqueous reversible addition-fragmentation chain transfer (RAFT) polymerization.* Langmuir, 2003. **19**: p. 5559-5562.
86. Ranjan, R. and W.J. Brittain, *Combination of living radical polymerization and click chemistry for surface modification.* Macromolecules, 2007. **40**(17): p. 6217-6223.
87. Balazs, A.C., T. Emrick, and T.P. Russell, *Nanoparticle Polymer Composites: Where Two Small Worlds Meet.* Science, 2006. **314**(5802): p. 1107-1110.
88. Anton, N., J.-P. Benoit, and P. Saulnier, *Design and production of nanoparticles formulated from nano-emulsion templates--A review.* J. Control. Release, 2008. **128**(3): p. 185-199.
89. Hornig, S., et al., *Synthetic polymeric nanoparticles by nanoprecipitation.* J. Mater. Chem., 2009. **19**(23): p. 3838-3840.
90. Johnson, B.K. and R.K. Prud'homme, *Flash NanoPrecipitation of Organic Actives and Block Copolymers using a Confined Impinging Jets Mixer.* Aust. J. Chem., 2003. **56**(10): p. 1021-1024.
91. Fessi, H., et al., *Nanocapsule formation by interfacial polymer deposition following solvent displacement.* Int. J. Pharm., 1989. **55**(1): p. R1-R4.
92. Alexis, F., et al., *Factors affecting the clearance and biodistribution of polymeric nanoparticles.* Mol Pharm, 2008. **5**(4): p. 505-15.
93. Faraji, A.H. and P. Wipf, *Nanoparticles in cellular drug delivery.* Bioorganic & Medicinal Chemistry, 2009. **17**(8): p. 2950-2962.
94. Moghimi, S.M., A.C. Hunter, and J.C. Murray, *Long-Circulating and Target-Specific Nanoparticles: Theory to Practice.* Pharmacological Reviews, 2001. **53**(2): p. 283-318.
95. Aliabadi, H.M., et al., *Disposition of Drugs in Block Copolymer Micelle Delivery Systems: From Discovery to Recovery.* Clinical Pharmacokinetics, 2008. **47**(10): p. 619-634.
96. Chonn, A., S.C. Semple, and P.R. Cullis, *Association of blood proteins with large unilamellar liposomes in vivo. Relation to circulation lifetimes.* Journal of Biological Chemistry, 1992. **267**(26): p. 18759-18765.

97. Moghimi, S.M. and J. Szebeni, *Stealth liposomes and long circulating nanoparticles: critical issues in pharmacokinetics, opsonization and protein-binding properties.* Progress in Lipid Research, 2003. **42**(6): p. 463-478.
98. Sharma, G., et al., *Polymer particle shape independently influences binding and internalization by macrophages.* Journal of Controlled Release, 2010. **147**(3): p. 408-412.
99. Lehn, J.-M., *Supramolecular polymer chemistry—scope and perspectives.* Polym. Int., 2002. **51**(10): p. 825-839.
100. Haag, R., *Supramolecular Drug-Delivery Systems Based on Polymeric Core–Shell Architectures.* Angew. Chem. Int. Ed., 2004. **43**(3): p. 278-282.
101. Shimizu, T., M. Masuda, and H. Minamikawa, *Supramolecular Nanotube Architectures Based on Amphiphilic Molecules.* Chem. Rev., 2005. **105**(4): p. 1401-1444.
102. Broz, P., S. Marsch, and P. Hunzikel, *Targeting of vulnerable plaque macrophages with polymer-based nanostructures.* Trends in Cardiovascular Medicine, 2007. **17**(6): p. 190-196.
103. Chen, W., et al., *Nanoparticles as magnetic resonance imaging contrast agents for vascular and cardiac diseases.* WIREs Nanomed. Nanobiotechnol., 2010. **DOI: 10.1002/wnan.114**.
104. Mulder, W.J.M., et al., *Nanoparticulate Assemblies of Amphiphiles and Diagnostically Active Materials for Multimodality Imaging.* Acc. Chem. Res., 2009. **42**(7): p. 904-914.
105. Iverson, N.M., et al., *Controllable inhibition of cellular uptake of oxidized low-density lipoprotein: structure-function relationships for nanoscale amphiphilic polymers.* Acta Biomater, 2010. **6**(8): p. 3081-91.
106. Iverson, N., et al., *Convergence of nanotechnology and cardiovascular medicine: progress and emerging prospects.* BioDrugs, 2008. **22**(1): p. 1-10.
107. Chnari, E., et al., *Engineered polymeric nanoparticles for receptor-targeted blockage of oxidized low density lipoprotein uptake and atherogenesis in macrophages.* Biomacromolecules, 2006. **7**(6): p. 1796-1805.
108. Plourde, N.M., et al., *Structure-activity relations of nanolipoblockers with the atherogenic domain of human macrophage scavenger receptor A.* Biomacromolecules, 2009. **10**(6): p. 1381-91.
109. Kearney, A.S., *Prodrugs and targeted delivery.* Adv. Drug Deliv. Rev., 1996. **19**: p. 225-239.
110. Kabanov, A.V. and V.A. Kabanov, *Interpolyelectrolyte and block ionomer complexes for gene delivery: physico-chemical aspects.* Adv. Drug Deliv. Rev., 1998. **30**(1-3): p. 49-60.
111. Christie, R.J. and D.W. Grainger, *Design strategies to improve soluble macromolecular delivery constructs.* Adv. Drug Delivery Rev., 2003. **55**: p. 421-437.
112. Pack, D.W., et al., *Design and development of polymers for gene delivery.* Nat. Rev. Drug Discovery, 2005. **4**(7): p. 581-593.
113. D'Emanuele, A. and D. Attwood, *Dendrimer–drug interactions.* Adv. Drug Delivery Rev., 2005. **57**: p. 2147-2162.
114. Nori, A. and J. Kopecek, *Intracellular targeting of polymer-bound drugs for cancer chemotherapy.* Adv. Drug Delivery Rev., 2005. **57**: p. 609-636.
115. Svenson, S. and D.A. Tomalia, *Dendrimers in biomedical applications—reflections on the field.* Adv. Drug Delivery Rev., 2005. **57**: p. 2106-2129.
116. Wong, S.Y., J.M. Pelet, and D. Putnam, *Polymer systems for gene delivery - Past, present, and future.* Prog. Polym. Sci., 2007. **32**: p. 799-837.
117. York, A.W., S.E. Kirkland, and C.L. McCormick, *Advances in the synthesis of amphiphilic block copolymers via RAFT polymerization: Stimuli-responsive drug and gene delivery.* Adv. Drug Deliv. Rev., 2008. **60**(9): p. 1018-1036.

118. Lutz, J.-F. and H.G. Börner, *Modern trends in polymer bioconjugates design.* Prog. Polym. Sci., 2008. **33**: p. 1-39.
119. Lusis, A.J., *Atherosclerosis.* Nature, 2000. **407**(6801): p. 233-241.
120. Goldstein, J.L., et al., *Binding site on macrophages that mediates uptake and degradation of acetylated low density lipoprotein, producing massive cholesterol deposition.* P. Natl. Acad. Sci. USA, 1979. **76**(1): p. 333-337.
121. Mulder, W.J.M., et al., *Molecular imaging of macrophages in atherosclerotic plaques using bimodal PEG-micelles.* Magnetic Resonance in Medicine, 2007. **58**(6): p. 1164-1170.
122. Broz, P., et al., *Inhibition of Macrophage Phagocytotic Activity by a Receptor-targeted Polymer Vesicle-based Drug Delivery Formulation of Pravastatin.* Journal of Cardiovascular Pharmacology, 2008. **51**(3): p. 246-252 10.1097/FJC.0b013e3181624aed.
123. Amirbekian, V., et al., *Detecting and assessing macrophages in vivo to evaluate atherosclerosis noninvasively using molecular MRI.* Proceedings of the National Academy of Sciences, 2007. **104**(3): p. 961-966.
124. van Tilborg, G.A.F., et al., *Annexin A5-Functionalized Bimodal Nanoparticles for MRI and Fluorescence Imaging of Atherosclerotic Plaques.* Bioconjugate Chemistry, 2010: p. null-null.
125. Peters, D., et al., *Targeting atherosclerosis by using modular, multifunctional micelles.* Proceedings of the National Academy of Sciences, 2009. **106**(24): p. 9815-9819.
126. Chnari, E., et al., *Engineered polymeric nanoparticles for receptor-targeted blockage of oxidized low density lipoprotein uptake and atherogenesis in macrophages.* Biomacromolecules, 2006. **7**(6): p. 1796-1805.
127. Chnari, E., et al., *Nanoscale anionic macromolecules for selective retention of low-density lipoproteins.* Biomaterials, 2005. **26**(17): p. 3749-3758.
128. Jones, M.-C. and J.-C. Leroux, *Polymeric micelles - a new generation of colloidal drug carriers.* European Journal of Pharmaceutics and Biopharmaceutics, 1999. **48**(2): p. 101-111.
129. Discher, D.E. and A. Eisenberg, *Polymer Vesicles.* Science, 2002. **297**(5583): p. 967-973.
130. Discher, B.M., et al., *Polymersomes: Tough Vesicles Made from Diblock Copolymers.* Science, 1999. **284**(5417): p. 1143-1146.
131. Kwon, G.S. and T. Okano, *Polymeric micelles as new drug carriers.* Adv. Drug Deliv. Rev., 1996. **21**(2): p. 107-116.
132. Riess, G., *Micellization of block copolymers.* Prog. Polym. Sci., 2003. **28**(7): p. 1107-1170.
133. Discher, D.E. and F. Ahmed, *Polymersomes.* Annu. Rev. Biomed. Eng., 2006. **8**: p. 323–341.
134. Morishima, Y., et al., *Characterization of Unimolecular Micelles of Random Copolymers of Sodium 2-(Acrylamido)-2-methylpropanesulfonate and Methacrylamides Bearing Bulky Hydrophobic Substituents.* Macromolecules, 1995. **28**(8): p. 2874-2881.
135. Lukyanov, A.N. and V.P. Torchilin, *Micelles from lipid derivatives of water-soluble polymers as delivery systems for poorly soluble drugs.* Adv. Drug Deliv. Rev., 2004. **56**(9): p. 1273-1289.
136. Li, F., M. Danquah, and R.I. Mahato, *Synthesis and Characterization of Amphiphilic Lipopolymers for Micellar Drug Delivery.* Biomacromolecules, 2010. **11**(10): p. 2610-2620.
137. Nishiyama, N. and K. Kataoka, *Current state, achievements, and future prospects of polymeric micelles as nanocarriers for drug and gene delivery.* Pharmacol. Therapeut., 2006. **112**(3): p. 630-648.
138. Dash, P.R., et al., *Factors affecting blood clearance and in vivo distribution of polyelectrolyte complexes for gene delivery.* Gene Ther., 1999. **6**: p. 643-650.

139. Li, Y., et al., *Synthesis of reversible shell cross-linked micelles for controlled release of bioactive agents.* Macromolecules, 2006. **39**(8): p. 2726-2728.
140. Wooley, K.L., *Shell crosslinked polymer assemblies: Nanoscale constructs inspired from biological systems.* J. Polym. Sci., Part A: Polym. Chem., 2000. **38**(9): p. 1397-1407.
141. Read, E.S. and S.P. Armes, *Recent advances in shell cross-linked micelles.* Chem. Commun., 2007: p. 3021-3035.
142. Torchilin, V.P., *Lipid-Core Micelles for Targeted Drug Delivery.* Current Drug Delivery, 2005. **2**: p. 319-327.
143. Tian, L., et al., *Amphiphilic Scorpion-like Macromolecules: Design, Synthesis, and Characterization.* Macromolecules, 2004. **37**(2): p. 538-543.
144. Chnari, E., et al., *Nanoscale Anionic Macromolecules Can Inhibit Cellular Uptake of Differentially Oxidized LDL.* Biomacromolecules, 2006. **7**(2): p. 597-603.
145. Briley-Saebo, K.C., et al., *Targeted Molecular Probes for Imaging Atherosclerotic Lesions With Magnetic Resonance Using Antibodies That Recognize Oxidation-Specific Epitopes.* Circulation, 2008. **117**(25): p. 3206-3215.
146. Beilvert, A., et al., *Tyrosine polyethylene glycol (PEG)-micelle magnetic resonance contrast agent for the detection of lipid rich areas in atherosclerotic plaque.* Magnetic Resonance in Medicine, 2009. **62**(5): p. 1195-1201.
147. McCormick, C.L., et al., *RAFT-synthesized diblock and triblock copolymers: thermally-induced supramolecular assembly in aqueous media.* Soft Matter, 2008. **4**: p. 1760-1773.
148. McCormick, C.L., A.W. York, and S.E. Kirkland, *Synthetic routes to stimuli-responsive micelles, vesicles, and surfaces via controlled/living radical polymerization.* Poly. Rev., 2006. **46**: p. 421-443.
149. Yokoyama, M., *Drug targeting with nano-sized carrier systems.* J. Artif. Organs, 2005. **8**: p. 77-84.
150. Vasir, J.K., M.K. Reddy, and V.D. Labhasetwar, *Nanosystems in drug targeting: Opportunities and challenges.* Current Nanoscience, 2005. **1**(1): p. 47-64.
151. Uwatoku, T., et al., *Application of Nanoparticle Technology for the Prevention of Restenosis After Balloon Injury in Rats.* Circ Res, 2003. **92**(7): p. e62-69.
152. Ding, B.S., et al., *Advanced drug delivery systems that target the vascular endothelium.* Molecular Interventions, 2006. **6**(2): p. 98-112.
153. Muro, S., et al., *A novel endocytic pathway induced by clustering endothelial ICAM-1 or PECAM-1.* Journal of Cell Science, 2003. **116**(8): p. 1599-1609.
154. Muro, S., et al., *Slow intracellular trafficking of catalase nanoparticles targeted to ICAM-1 protects endothelial cells from oxidative stress.* American Journal of Physiology-Cell Physiology, 2003. **285**(5): p. C1339-C1347.
155. Poston, R.N., Haskard, D. O., Coucher, J. R., Gall, N. P., Johnson-Tidey, R. R., *Expression of intercellular adhesion molecule-1 in atherosclerotic plaques.* Am J Pathol, 1992. **140**(3): p. 665-673.
156. Garnacho, C., et al., *Delivery of acid sphingomyelinase in normal and Niemann-Pick disease mice using intercellular adhesion molecule-1-targeted polymer nanocarriers.* Journal of Pharmacology and Experimental Therapeutics, 2008. **325**(2): p. 400-408.
157. Muro, S., et al., *Endothelial targeting of high-affinity multivalent polymer nanocarriers directed to intercellular adhesion molecule 1.* Journal of Pharmacology and Experimental Therapeutics, 2006. **317**(3): p. 1161-1169.
158. Murciano, J.C., et al., *ICAM-directed vascular immunotargeting of antithrombotic agents to the endothelial luminal surface.* Blood, 2003. **101**(10): p. 3977-3984.

159. Muro, S., et al., *Control of Endothelial Targeting and Intracellular Delivery of Therapeutic Enzymes by Modulating the Size and Shape of ICAM-1-targeted Carriers.* Molecular Therapy, 2008. **16**(8): p. 1450-1458.
160. Zhang, N., et al., *PLGA nanoparticle-peptide conjugate effectively targets intercellular cell-adhesion molecule-1.* Bioconjugate Chemistry, 2008. **19**(1): p. 145-152.
161. Tibbetts, S.A., et al., *Linear and cyclic LFA-1 and ICAM-1 peptides inhibit T cell adhesion and function.* Peptides, 2000. **21**(8): p. 1161-1167.
162. Yusuf-Makagiansar, H. and T.J. Siahaan, *Binding and internalization of an LFA-1-derived cyclic peptide by ICAM receptors on activated lymphocyte: A potential ligand for drug targeting to ICAM-1-expressing cells.* Pharmaceutical Research, 2001. **18**(3): p. 329-335.
163. Simone, E., B.S. Ding, and V. Muzykantov, *Targeted delivery of therapeutics to endothelium.* Cell and Tissue Research, 2009. **335**(1): p. 283-300.
164. Kelly, K.A., et al., *Detection of vascular adhesion molecule-1 expression using a novel multimodal nanoparticle.* Circ Res, 2005. **96**(3): p. 327-36.
165. Nahrendorf, M., et al., *Noninvasive vascular cell adhesion molecule-1 imaging identifies inflammatory activation of cells in atherosclerosis.* Circulation, 2006. **114**(14): p. 1504-1511.
166. Moore, K.J. and M.W. Freeman, *Scavenger Receptors in Atherosclerosis: Beyond Lipid Uptake.* Arterioscler Thromb Vasc Biol, 2006. **26**(8): p. 1702-1711.
167. Ogura, S., et al., *LOX-1: The Multifunctional Receptor Underlying Cardiovascular Dysfunction.* Circulation Journal, 2009. **73**(11): p. 1993-1999.
168. Wang, J., et al., *Nanoscale amphiphilic macromolecules as lipoprotein inhibitors: the role of charge and architecture.* Int J Nanomedicine, 2007. **2**(4): p. 697-705.
169. Plourde, N.M., et al., *Structure−Activity Relations of Nanolipoblockers with the Atherogenic Domain of Human Macrophage Scavenger Receptor A.* Biomacromolecules, 2009. **10**(6): p. 1381-1391.
170. Azzazy, H.M.E. and W.E. Highsmith, *Phage display technology: clinical applications and recent innovations.* Clinical Biochemistry, 2002. **35**(6): p. 425-445.
171. Flacke, S., et al., *Novel MRI Contrast Agent for Molecular Imaging of Fibrin: Implications for Detecting Vulnerable Plaques.* Circulation, 2001. **104**(11): p. 1280-1285.
172. Winter, P.M., et al., *Molecular Imaging of Angiogenesis in Early-Stage Atherosclerosis With {alpha}v{beta}3-Integrin-Targeted Nanoparticles.* Circulation, 2003. **108**(18): p. 2270-2274.
173. Winter, P.M., et al., *Endothelial {alpha}{nu}{beta}3 Integrin-Targeted Fumagillin Nanoparticles Inhibit Angiogenesis in Atherosclerosis.* Arterioscler Thromb Vasc Biol, 2006. **26**(9): p. 2103-2109.
174. Ikuta, K., et al., *Development of polymeric drug delivery system for recognizing vascular endothelial dysfunction.* Bioorganic & Medicinal Chemistry, 2008. **16**(6): p. 2811-2818.
175. McCarthy, J., F. Jaffer, and R. Weissleder, *A Macrophage-Targeted Theranostic Nanoparticle for Biomedical Applications.* Small, 2006. **2**(8-9): p. 983-987.
176. Nahrendorf, M., et al., *Nanoparticle PET-CT imaging of macrophages in inflammatory atherosclerosis.* Circulation, 2008. **117**(3): p. 379-387.
177. Chan, J.M., et al., *Spatiotemporal controlled delivery of nanoparticles to injured vasculature.* Proceedings of the National Academy of Sciences, 2010. **107**(5): p. 2213-2218.
178. Joner, M., et al., *Site-Specific Targeting of Nanoparticle Prednisolone Reduces In-Stent Restenosis in a Rabbit Model of Established Atheroma.* Arterioscler Thromb Vasc Biol, 2008. **28**(11): p. 1960-1966.

179. Lanza, G., et al., *Theragnostics for tumor and plaque angiogenesis with perfluorocarbon nanoemulsions.* Angiogenesis, 2010. **13**(2): p. 189-202.
180. Winter, P.M., et al., *Antiangiogenic Synergism of Integrin-Targeted Fumagillin Nanoparticles and Atorvastatin in Atherosclerosis.* J Am Coll Cardiol Img, 2008. **1**(5): p. 624-634.
181. Bai, S. and F. Ahsan, *Synthesis and evaluation of pegylated dendrimeric nanocarrier for pulmonary delivery of low molecular weight heparin.* Pharm Res, 2009. **26**(3): p. 539-48.
182. Padoveze, A.F., et al., *Effect of a cholesterol-rich diet on the metabolism of the free and esterified cholesterol components of a nanoemulsion that resembles LDL in rabbits.* Brazilian Journal of Medical and Biological Research, 2009. **42**: p. 172-178.
183. Mackiewicz, M.R., H.L. Hodges, and S.M. Reed, *C-Reactive Protein Induced Rearrangement of Phosphatidylcholine on Nanoparticle Mimics of Lipoprotein Particles.* The Journal of Physical Chemistry B, 2010. **114**(16): p. 5556-5562.
184. Buono, C., et al., *Fluorescent pegylated nanoparticles demonstrate fluid-phase pinocytosis by macrophages in mouse atherosclerotic lesions.* The Journal of Clinical Investigation, 2009. **119**(5): p. 1373-1381.
185. Choudhury, R.P., V. Fuster, and Z.A. Fayad, *Molecular, cellular and functional imaging of atherothrombosis.* Nat Rev Drug Discov, 2004. **3**(11): p. 913-25.
186. Caravan, P., et al., *Gadolinium(III) Chelates as MRI Contrast Agents: Structure, Dynamics, and Applications.* Chemical Reviews, 1999. **99**(9): p. 2293-2352.
187. SCHMITZ, S.A., et al., *Superparamagnetic Iron Oxide-Enhanced MRI of Atherosclerotic Plaques in Watanabe Hereditable Hyperlipidemic Rabbits.* Investigative Radiology, 2000. **35**(8): p. 460-471.
188. Fayad, Z.A., et al., *Iron Oxide Magnetic Resonance Imaging for Atherosclerosis Therapeutic Evaluation: Still "Rusty?".* J Am Coll Cardiol, 2009. **53**(22): p. 2051-2052.
189. Hyafil, F., et al., *Noninvasive detection of macrophages using a nanoparticulate contrast agent for computed tomography.* Nat Med, 2007. **13**(5): p. 636-41.
190. Smith, A.M., M.C. Mancini, and S. Nie, *Bioimaging: second window for in vivo imaging.* Nat Nanotechnol, 2009. **4**(11): p. 710-1.
191. Bijsterbosch, M.K. and T.J.C. van Berkel, *Native and modified lipoproteins as drug delivery systems.* Advanced Drug Delivery Reviews, 1990. **5**(3): p. 231-251.
192. Libby, P., P.M. Ridker, and A. Maseri, *Inflammation and atherosclerosis.* Circulation, 2002. **105**(9): p. 1135-43.
193. Hehir, S., et al., *Carbohydrate composition of amphiphilic macromolecules influences physicochemical properties and binding to atherogenic scavenger receptor A.* Acta Biomaterialia, 2012. **8**(11): p. 3956-3962.
194. Iverson, N.M., et al., *Dual use of amphiphilic macromolecules as cholesterol efflux triggers and inhibitors of macrophage athero-inflammation.* Biomaterials, 2011. **32**(32): p. 8319-8327.
195. Wang, J., et al., *Nanoscale amphiphilic macromolecules as lipoprotein inhibitors: the role of charge and architecture.* International Journal of Nanomedicine, 2007. **2**(4): p. 697-705.
196. Mayr, L.M. and D. Bojanic, *Novel trends in high-throughput screening.* Current Opinion in Pharmacology, 2009. **9**(5): p. 580-588.
197. Wang, C.Y., et al., *Identification of Previously Unrecognized Antiestrogenic Chemicals Using a Novel Virtual Screening Approach.* Chemical Research in Toxicology, 2006. **19**(12): p. 1595-1601.

198. Chekmarev, D., et al., *Predicting Inhibitors of Acetylcholinesterase by Regression and Classification Machine Learning Approaches with Combinations of Molecular Descriptors.* Pharmaceutical Research, 2009. **26**(9): p. 2216-2224.
199. Paranjpe, P.V., et al., *Tumor-targeted bioconjugate based delivery of camptothecin: design, synthesis and in vitro evaluation.* Journal of Controlled Release, 2004. **100**(2): p. 275-292.
200. Passic, S.R., et al., *Structure-activity relationships of polybiguanides with activity against human immunodeficiency virus type 1.* Biomedicine & Pharmacotherapy, 2010. **64**(10): p. 723-732.
201. Kortagere, S. and W. Welsh, *Development and application of hybrid structure based method for efficient screening of ligands binding to G-protein coupled receptors.* Journal of Computer-Aided Molecular Design, 2006. **20**(12): p. 789-802.
202. Aparoy, P., K. Kumar Reddy, and P. Reddanna, *Structure and Ligand Based Drug Design Strategies in the Development of Novel 5- LOX Inhibitors.* Current Medicinal Chemistry, 2012. **19**(22): p. 3763-3778.
203. Hsieh, J.-H., et al., *Cheminformatics Meets Molecular Mechanics: A Combined Application of Knowledge-Based Pose Scoring and Physical Force Field-Based Hit Scoring Functions Improves the Accuracy of Structure-Based Virtual Screening.* Journal of Chemical Information and Modeling, 2011. **52**(1): p. 16-28.
204. Mize, C.D., et al., *Ligand-based autotaxin pharmacophore models reflect structure-based docking results.* Journal of Molecular Graphics and Modelling, 2011. **31**(0): p. 76-86.
205. Bhatt, H.G. and P.K. Patel, *Pharmacophore modeling, virtual screening and 3D-QSAR studies of 5-tetrahydroquinolinylidine aminoguanidine derivatives as sodium hydrogen exchanger inhibitors.* Bioorganic & Medicinal Chemistry Letters, 2012. **22**(11): p. 3758-3765.
206. Sushko, I., et al., *Online chemical modeling environment (OCHEM): web platform for data storage, model development and publishing of chemical information.* Journal of Computer-Aided Molecular Design, 2011. **25**(6): p. 533-554.
207. Dube, D., et al., *3D-QSAR based pharmacophore modeling and virtual screening for identification of novel pteridine reductase inhibitors.* Journal of Molecular Modeling, 2012. **18**(5): p. 1701-1711.
208. Dong, X., et al., *Receptor-Based Pharmacophore and Pharmacophore Key Descriptors for Virtual Screening and QSAR Modeling.* Current Computer - Aided Drug Design, 2011. **7**(3): p. 181-189.
209. Ebalunode, J., W. Zheng, and A. Tropsha, *Application of QSAR and Shape Pharmacophore Modeling Approaches for Targeted Chemical Library Design*, in *Chemical Library Design*, J.Z. Zhou, Editor. 2011, Humana Press. p. 111-133.
210. Kooistra, A.J., et al., *From heptahelical bundle to hits from the Haystack: structure-based virtual screening for GPCR ligands.* Methods in enzymology, 2013. **522**: p. 279-336.
211. Kamal, A., M. Kashi Reddy, and A. Viswanath, *The design and development of imidazothiazole–chalcone derivatives as potential anticancer drugs.* Expert Opinion on Drug Discovery, 2013. **8**(3): p. 289-304.
212. Krasowski, M.D. and A.J. Hopfinger, *The discovery of new anesthetics by targeting GABAA receptors.* Expert Opinion on Drug Discovery, 2011. **6**(11): p. 1187-1201.
213. Martin, T.M., et al., *Does Rational Selection of Training and Test Sets Improve the Outcome of QSAR Modeling?* Journal of Chemical Information and Modeling, 2012. **52**(10): p. 2570-2578.

214. Ertl, P. and R. Lewis, *IADE: a system for intelligent automatic design of bioisosteric analogs.* Journal of Computer-Aided Molecular Design, 2012. **26**(11): p. 1207-1215.
215. Gubskaya, A.V., et al., *Prediction of fibrinogen adsorption for biodegradable polymers: Integration of molecular dynamics and surrogate modeling.* Polymer, 2007. **48**(19): p. 5788-5801.
216. Smith, J.R., et al., *Using Surrogate Modeling in the Prediction of Fibrinogen Adsorption onto Polymer Surfaces.* Journal of Chemical Information and Computer Sciences, 2004. **44**(3): p. 1088-1097.
217. Duan, P., et al., *Potent Inhibitors of Human Organic Anion Transporters 1 and 3 from Clinical Drug Libraries: Discovery and Molecular Characterization.* Molecular Pharmaceutics, 2012. **9**(11): p. 3340-3346.
218. Fomovska, A., et al., *Salicylanilide Inhibitors of Toxoplasma gondii.* Journal of Medicinal Chemistry, 2012. **55**(19): p. 8375-8391.
219. Tian, L., et al., *Amphiphilic Scorpion-like Macromolecules:Design, Synthesis, and Characterization.* Macromolecules, 2004. **37**(2): p. 538-543.
220. Djordjevic, J., et al., *Amphiphilic scorpion-like macromolecules as micellar nanocarriers.* J. Bioact. Compat. Polym., 2008. **2008**(23): p. 532-551.
221. Wang, J., et al., *Comparison of PEG chain length and density on amphiphilic macromolecular nanocarriers: self-assembled and unimolecular micelles.* Acta Biomater, 2009. **5**: p. 883-92.
222. Lewis, D.R., et al., *In silico design of anti-atherogenic biomaterials.* Biomaterials, 2013. **34**(32): p. 7950-7959.
223. Case, D.A., et al., *AMBER 12.* University of California, San Francisco, 2012.
224. Marrink, S.J., et al., *The MARTINI Force Field: Coarse Grained Model for Biomolecular Simulations.* The Journal of Physical Chemistry B, 2007. **111**(27): p. 7812-7824.
225. Monticelli, L., et al., *The MARTINI Coarse-Grained Force Field: Extension to Proteins.* Journal of Chemical Theory and Computation, 2008. **4**(5): p. 819-834.
226. Lee, H., et al., *A Coarse-Grained Model for Polyethylene Oxide and Polyethylene Glycol: Conformation and Hydrodynamics.* The Journal of Physical Chemistry B, 2009. **113**(40): p. 13186-13194.
227. Marrink, S.J., A.H. de Vries, and A.E. Mark, *Coarse Grained Model for Semiquantitative Lipid Simulations.* The Journal of Physical Chemistry B, 2003. **108**(2): p. 750-760.
228. Hess, B., et al., *GROMACS 4: Algorithms for Highly Efficient, Load-Balanced, and Scalable Molecular Simulation.* Journal of Chemical Theory and Computation, 2008. **4**(3): p. 435-447.
229. Rzepiela, A.J., et al., *Reconstruction of atomistic details from coarse-grained structures.* Journal of Computational Chemistry, 2010. **31**(6): p. 1333-1343.
230. Sousa da Silva, A. and W. Vranken, *ACPYPE - AnteChamber PYthon Parser interfacE.* BMC Research Notes, 2012. **5**(1): p. 367.
231. Iverson, N., et al., *Convergence of nanotechnology and cardiovascular medicine.* Biodrugs, 2008. **22**(1): p. 1-10.
232. York, A.W., et al., *Kinetically Assembled Nanoparticles of Bioactive Macromolecules Exhibit Enhanced Stability and Cell-Targeted Biological Efficacy.* Advanced Materials, 2012. **24**(6): p. 733-739.
233. Kou, P.M., et al., *Predicting biomaterial property-dendritic cell phenotype relationships from the multivariate analysis of responses to polymethacrylates.* Biomaterials, 2012. **33**(6): p. 1699-1713.

234. Petersen, L.K., et al., *Activation of innate immune responses in a pathogen-mimicking manner by amphiphilic polyanhydride nanoparticle adjuvants.* Biomaterials, 2011. **32**(28): p. 6815-6822.
235. Todeschini, R., M. Lasagni, and E. Marengo, *New molecular descriptors for 2D and 3D structures. Theory.* Journal of Chemometrics, 1994. **8**(4): p. 263-272.
236. Consonni, V., R. Todeschini, and M. Pavan, *Structure/Response Correlations and Similarity/Diversity Analysis by GETAWAY Descriptors. 1. Theory of the Novel 3D Molecular Descriptors.* Journal of Chemical Information and Computer Sciences, 2002. **42**(3): p. 682-692.
237. Consonni, V., et al., *Structure/Response Correlations and Similarity/Diversity Analysis by GETAWAY Descriptors. 2. Application of the Novel 3D Molecular Descriptors to QSAR/QSPR Studies.* Journal of Chemical Information and Computer Sciences, 2002. **42**(3): p. 693-705.
238. H.Kubinyi, G.F., Y.C.Martin, ed. *3D QSAR in Drug Design*. Vol. 2. 1998, Kluwer/ESCOM: Dordrecht (The Netherlands). 355-380.
239. Boullier, A., et al., *Scavenger Receptors, Oxidized LDL, and Atherosclerosis.* Annals of the New York Academy of Sciences, 2001. **947**(1): p. 214-223.
240. Ross, R., *Atherosclerosis--an inflammatory disease.* N Engl J Med, 1999. **340**(2): p. 115-26.
241. Kumar, V., et al., *Formulation and Stability of Itraconazole and Odanacatib Nanoparticles: Governing Physical Parameters.* Mol. Pharmaceutics, 2009. **6**.
242. Gindy, M.E., A.Z. Panagiotopoulos, and R.K. Prud'homme, *Composite Block Copolymer Stabilized Nanoparticles: Simultaneous Encapsulation of Organic Actives and Inorganic Nanostructures.* Langmuir, 2007. **24**(1): p. 83-90.
243. Stevenson, R., et al., *Nanoparticles and Inflammation.* TheScientificWorldJOURNAL, 2011. **11**: p. 1300-1312.
244. Clift, M.J.D., et al., *The impact of different nanoparticle surface chemistry and size on uptake and toxicity in a murine macrophage cell line.* Toxicology and Applied Pharmacology, 2008. **232**(3): p. 418-427.
245. Brown, D.M., et al., *Size-Dependent Proinflammatory Effects of Ultrafine Polystyrene Particles: A Role for Surface Area and Oxidative Stress in the Enhanced Activity of Ultrafines.* Toxicology and Applied Pharmacology, 2001. **175**(3): p. 191-199.
246. Metz, S., et al., *Capacity of human monocytes to phagocytose approved iron oxide MR contrast agents in vitro.* European Radiology, 2004. **14**(10): p. 1851-1858.
247. Nahrendorf, M., et al., *Nanoparticle PET-CT Imaging of Macrophages in Inflammatory Atherosclerosis.* Circulation, 2008. **117**(3): p. 379-387.
248. Tedgui, A. and Z. Mallat, *Cytokines in Atherosclerosis: Pathogenic and Regulatory Pathways.* Physiol. Rev., 2006. **86**(2): p. 515-581.
249. Monteiro-Riviere, N.A. and C.L. Tran, *Nanotoxicology : characterization, dosing and health effects*. 2007, New York: Informa Healthcare. xiv, 434 p.
250. Vega-Villa, K.R., et al., *Clinical toxicities of nanocarrier systems.* Advanced Drug Delivery Reviews, 2008. **60**(8): p. 929-938.
251. Esterbauer, H., et al., *Role of vitamin E in preventing the oxidation of low-density lipoprotein.* The American Journal of Clinical Nutrition, 1991. **53**(1): p. 314S-321S.
252. Beharka, A.A., et al., *Mechanism of vitamin E inhibition of cyclooxygenase activity in macrophages from old mice: role of peroxynitrite.* Free Radical Biology and Medicine, 2002. **32**(6): p. 503-511.

253. Koga, T., et al., *Vitamin E supplementation suppresses macrophage accumulation and endothelial cell expression of adhesion molecules in the aorta of hypercholesterolemic rabbits.* Atherosclerosis, 2004. **176**(2): p. 265-272.
254. Liu, Y., et al., *Mixing in a multi-inlet vortex mixer (MIVM) for flash nano-precipitation.* Chem. Eng. Sci., 2008. **63**(11): p. 2829-2842.
255. Choi, H.S., et al., *Renal clearance of quantum dots.* Nat Biotechnol, 2007. **25**(10): p. 1165-70.
256. Petersen, L.K., et al., *The Rational Design of Bioactive Nanoparticle Therapeutics for Management of Atherosclerosis through Scavenger Receptor Intervention.* Biomaterials (in preparation), 2013.
257. FDA. *Guidance for Industry: Single Dose Acute Toxicity Testing for Pharmaceuticals*. Available from: http://www.fda.gov/downloads/Drugs/GuidanceComplianceRegulatoryInformation/Guidances/ucm079270.pdf.
258. Roger, V.L., et al., *Heart Disease and Stroke Statistics—2012 Update: A Report From the American Heart Association.* Circulation, 2011.
259. Gindy, M.E., A.Z. Panagiotopoulos, and R.K. Prud'homme, *Composite Block Copolymer Stabilized Nanoparticles: Simultaneous Encapsulation of Organic Actives and Inorganic Nanostructures.* Langmuir 2008. **24**: p. 83-90.
260. Parthasarathy, S. and N. Santanam, *Mechanisms of oxidation, antioxidants, and atherosclerosis.* Curr Opin Lipidol, 1994. **5**(5): p. 371-5.
261. Nakashima, Y., et al., *ApoE-deficient mice develop lesions of all phases of atherosclerosis throughout the arterial tree.* Arteriosclerosis, Thrombosis, and Vascular Biology, 1994. **14**(1): p. 133-140.
262. Fazio, S. and M.F. Linton, *Mouse models of hyperlipidemia and atherosclerosis.* Front Biosci, 2001. **6**: p. D515-25.
263. Meir, K.S. and E. Leitersdorf, *Atherosclerosis in the Apolipoprotein E–Deficient Mouse.* Arteriosclerosis, Thrombosis, and Vascular Biology, 2004. **24**(6): p. 1006-1014.
264. Zaragoza, C., et al., *Animal models of cardiovascular diseases.* J Biomed Biotechnol, 2011. **2011**: p. 497841.
265. Giddens, D.P., C.K. Zarins, and S. Glagov, *The role of fluid mechanics in the localization and detection of atherosclerosis.* J Biomech Eng, 1993. **115**(4b): p. 588-94.
266. Gimbrone, M.A., *Vascular Endothelium, Hemodynamic Forces, and Atherogenesis.* The American journal of pathology, 1999. **155**(1): p. 1-5.
267. Thubrikar, M.J. and F. Robicsek, *Pressure-induced arterial wall stress and atherosclerosis.* The Annals of thoracic surgery, 1995. **59**(6): p. 1594-1603.
268. Knowles, J.W. and N. Maeda, *Genetic Modifiers of Atherosclerosis in Mice.* Arteriosclerosis, Thrombosis, and Vascular Biology, 2000. **20**(11): p. 2336-2345.
269. De Meyer, G.R.Y., et al., *Possible Mechanisms of Collar-Induced Intimal Thickening.* Arterioscler Thromb Vasc Biol, 1997. **17**(10): p. 1924-1930.
270. Whitman, S.C., *A practical approach to using mice in atherosclerosis research.* Clin Biochem Rev, 2004. **25**(1): p. 81-93.
271. MOGHADASIAN, M.H., et al., *Pathophysiology of apolipoprotein E deficiency in mice: relevance to apo E-related disorders in humans.* The FASEB Journal, 2001. **15**(14): p. 2623-2630.
272. Kreuter, J., *Nanoparticles and microparticles for drug and vaccine delivery.* J Anat, 1996. **189 (Pt 3)**(Pt 3): p. 503-5.

273. Swirski, F.K., et al., *Identification of Splenic Reservoir Monocytes and Their Deployment to Inflammatory Sites.* Science, 2009. **325**(5940): p. 612-616.
274. Matsumoto, A., et al., *Human macrophage scavenger receptors: primary structure, expression, and localization in atherosclerotic lesions.* Proc Natl Acad Sci U S A, 1990. **87**(23): p. 9133-7.
275. Singaraja, R.R., et al., *Increased expression of ABCA1 provides significant protection against atherosclerosis.* Circulation, 2005. **112**(17): p. U158-U158.
276. Packard, R.R. and P. Libby, *Inflammation in atherosclerosis: from vascular biology to biomarker discovery and risk prediction.* Clin Chem, 2008. **54**(1): p. 24-38.
277. Wang, B., et al., *Regression of atherosclerosis plaques in apolipoprotein E−/− mice after lentivirus-mediated RNA interference of CD40.* International journal of cardiology, 2013. **163**(1): p. 34-39.
278. Aagaard, L. and J.J. Rossi, *RNAi therapeutics: Principles, prospects and challenges.* Advanced Drug Delivery Reviews, 2007. **59**(2-3): p. 75-86.
279. Haser, P.B., et al., *Nanolipoblockers: Ex Vivo Human Plaque Interaction for Therapeutic Management for Atherosclerosis.* Journal of vascular surgery, 2013. **58**(4): p. 1149.
280. Hansel, T.T., et al., *The safety and side effects of monoclonal antibodies.* Nat Rev Drug Discov, 2010. **9**(4): p. 325-338.
281. Hong, H.Y., et al., *Phage display selection of peptides that home to atherosclerotic plaques: IL-4 receptor as a candidate target in atherosclerosis.* Journal of Cellular and Molecular Medicine, 2008. **12**(5B): p. 2003-2014.
282. Chacko, A.-M., et al., *Targeted nanocarriers for imaging and therapy of vascular inflammation.* Current Opinion in Colloid & Interface Science, 2011. **16**(3): p. 215-227.
283. Cerda, A., H. Hirata Mario, and C. Hirata Rosario Dominguez, *Molecular mechanisms underlying statin effects on genes involved in the reverse cholesterol transport*. 2012. p. 101.
284. Fuster, V., et al., *Spontaneous and diet-induced coronary atherosclerosis in normal swine and swine with von Willebrand disease.* Arteriosclerosis, Thrombosis, and Vascular Biology, 1985. **5**(1): p. 67-73.
285. Touchard, A.G. and R.S. Schwartz, *Preclinical Restenosis Models: Challenges and Successes.* Toxicologic Pathology, 2006. **34**(1): p. 11-18.
286. Rudd, J.H., J.R. Davies, and P.L. Weissberg, *Imaging of atherosclerosis -- can we predict plaque rupture?* Trends Cardiovasc Med, 2005. **15**(1): p. 17-24.
287. Tanaka, A., et al., *Multiple plaque rupture and c-reactive protein in acute myocardial infarction.* Journal of the American College of Cardiology, 2005. **45**(10): p. 1594-1599.
288. Naczynski, D.J., et al., *Albumin Nanoshell Encapsulation of Near-Infrared-Excitable Rare-Earth Nanoparticles Enhances Biocompatibility and Enables Targeted Cell Imaging.* Small, 2010. **9999**(9999): p. NA.